UNIVERSIDADE FEDERAL DE MINAS GERAIS
Escola de Engenharia
Programa de Pós-graduação em Engenharia Elétrica

Control Techniques for Uncertain Second Order Systems: An LMI Approach

Danielle Silva Gontijo

Belo Horizonte
2023

Danielle Silva Gontijo

Control Techniques for Uncertain Second Order Systems: An LMI Approach

A thesis presented to the Graduate Program in Electrical Engineering (PPGEE) of the Federal University of Minas Gerais (UFMG) in partial fulfillment of the requirements to obtain the degree of Doctor in Electrical Engineering.

Advisor: Prof. Dr. Fernando de Oliveira Souza

Co-Advisor: Prof. Dr. José Mário Araújo

Belo Horizonte
2023

Gontijo, Danielle Silva.
G641c Control techniques for uncertain second order systems [recurso eletrônico] : an LMI approach / Danielle Silva Gontijo. - 2023.
1 recurso online (90 f. : il., color.) : pdf.

Orientador: Fernando de Oliveira Souza.
Coorientador: José Mário Araújo.

Tese (doutorado) - Universidade Federal de Minas Gerais, Escola de Engenharia.

Apêndices: f. 86-90.

Bibliografia: f. 79-85.
Exigências do sistema: Adobe Acrobat Reader.

1. Engenharia elétrica - Teses. 2. Controle robusto - Teses. 3. Desigualdades matriciais lineares - Teses. 4. Controladores PID - Teses. I. Souza, Fernando de Oliveira. II. Araújo, José Mário. III. Universidade Federal de Minas Gerais. Escola de Engenharia. IV. Título.

CDU: 621.3(043)

Ficha catalográfica elaborada pelo bibliotecário Reginaldo César Vital dos Santos CRB/6 2165
Biblioteca Prof. Mário Werneck, Escola de Engenharia da UFMG

UNIVERSIDADE FEDERAL DE MINAS GERAIS
ESCOLA DE ENGENHARIA
PROGRAMA DE PÓS-GRADUAÇÃO EM ENGENHARIA ELÉTRICA

FOLHA DE APROVAÇÃO

"CONTROL TECHNIQUES FOR UNCERTAIN SECOND ORDER SYSTEMS: AN LMI APPROACH"

DANIELLE SILVA GONTIJO

Tese de Doutorado submetida à Banca Examinadora designada pelo Colegiado do Programa de Pós-Graduação em Engenharia Elétrica da Escola de Engenharia da Universidade Federal de Minas Gerais, como requisito para obtenção do grau de Doutor em Engenharia Elétrica. Aprovada em 25 de agosto de 2023. Por:

Prof. Dr. Fernando de Oliveira Souza
DELT (UFMG) - Orientador

Prof. Dr. José Mário Araújo
DAS (IFBA) - Coorientador

Prof. Dr. Carlos Eduardo Trabuco Dórea
DCA (UFRN)

Prof. Dr. Tito Luis Maia Santos
DEE (UFBA)

Prof. Dr. Leonardo Amaral Mozelli
DELT (UFMG)

Prof. Dr. Víctor Costa da Silva Campos
DELT (UFMG)

Documento assinado eletronicamente por **Leonardo Amaral Mozelli**, **Professor do Magistério Superior**, em 25/08/2023, às 16:48, conforme horário oficial de Brasília, com fundamento no art. 5º do Decreto nº 10.543, de 13 de novembro de 2020.

Documento assinado eletronicamente por **Victor Costa da Silva Campos**, **Professor do Magistério Superior**, em 25/08/2023, às 16:48, conforme horário oficial de Brasília, com fundamento no art. 5º do Decreto nº 10.543, de 13 de novembro de 2020.

Documento assinado eletronicamente por **Fernando de Oliveira Souza**, **Professor do Magistério Superior**, em 25/08/2023, às 17:10, conforme horário oficial de Brasília, com fundamento no art. 5º do Decreto nº 10.543, de 13 de novembro de 2020.

Documento assinado eletronicamente por **José Mário Araújo**, **Usuário Externo**, em 29/08/2023, às 11:42, conforme horário oficial de Brasília, com fundamento no art. 5º do Decreto nº 10.543, de 13 de novembro de 2020.

Documento assinado eletronicamente por **Carlos Eduardo Trabuco Dórea**, **Usuário Externo**, em 29/08/2023, às 13:53, conforme horário oficial de Brasília, com fundamento no art. 5º do Decreto nº 10.543, de 13 de novembro de 2020.

Documento assinado eletronicamente por **Tito Luís Maia Santos**, **Usuário Externo**, em 29/08/2023, às 17:22, conforme horário oficial de Brasília, com fundamento no art. 5º do Decreto nº 10.543, de 13 de novembro de 2020.

A autenticidade deste documento pode ser conferida no site https://sei.ufmg.br/sei/controlador_externo.php?acao=documento_conferir&id_orgao_acesso_externo=0, informando o código verificador **2566027** e o código CRC **2764DFFC**.

To my parents, Maria e Djalma. In memory of my grandfather, José do Pedro.

Acknowledgments

First of all, I would like to thank God for illuminating my path and giving me the strength and courage to complete this stage of my life.

I thank my advisor Prof. Fernando Souza for his patience, guidance, and encouragement throughout my doctoral years. I am also grateful to my co-supervisor Prof. José Mário for his guidance and suggestions. It has been a privilege to work with them. Thanks to Prof. Eduardo Nunes, for having supported me in the initiation of my doctorate. Thanks also to Prof. Tito Santos, for his collaboration in the article. I would like to extend my gratitude to all PPGEE professors for sharing their knowledge.

I thank my dear parents Maria and Djalma and my brother Disley, my foundations, who never measured their efforts to help me realize my dreams, who always supported me, and who taught me that I can and should pursue my goals. To my husband Emmanuel, for always walking by my side and supporting me in all my decisions. And to all the people who contributed directly and indirectly to the completion of this stage of my life. Finally, I would like to thank CAPES for its financial support.

"Life is like riding a bicycle. To keep your balance, you must keep moving." (Albert Einstein)

Resumo

Sistemas de segunda ordem são uma classe importante de sistemas dinâmicos amplamente utilizados na engenharia para modelar uma variedade de fenômenos físicos. Caracterizados por seu comportamento dinâmico, os sistemas de segunda ordem requerem estratégias de controle eficazes para atingir o desempenho desejado. Este trabalho apresenta uma estrutura de projeto para obter um controlador robusto multivariável Proporcional-Integral-Derivativo (PID) para sistemas lineares de segunda ordem, e um controlador Proporcional-Integral-Derivativo mais Aceleração (PIDA), para lidar com o problema de regularização do modelo. Desafios de controle relevantes, como erro de modelagem, otimização de desempenho regulatório, alocação regional de polos, prevenção de saturação, atraso de entrada, função de custo LQR e controle baseado no observador, são tratados dentro da abordagem de projeto via desigualdade matricial linear (LMI). A estratégia de projeto proposta baseia-se em rescrever o modelo do sistema de uma maneira apropriada de forma que o projeto do controlador PID/PIDA seja equivalente a de um controlador por realimentação de estados. Primeiramente, uma metodologia é proposta para a obtenção de um controlador PID/PIDA, fundamentada na alocação regional de polos, desempenho H_∞, problema de regularização e prevenção de saturação, tratados simultaneamente. Uma metodologia para obter um controlador multivariável Proporcional-Integral-Derivativo (PID) robusto para sistemas de segunda ordem com atraso de entrada variante no tempo também é proposta. Ademais, é apresentada uma metodologia para obter um controlador PD/PID por meio da estratégia de controle do Regulador Quadrático Linear (LQR). Por fim, uma formulação para o projeto de controladores baseado em observador também é proposta, e em seguida uma metodologia baseada em formulações LMI para obter um controlador baseado em observador para sistemas de segunda ordem incertos. Para ilustrar a eficácia das metodologias de controle propostas são realizadas simulações, com exemplos numéricos, e um experimento prático, utilizando um pêndulo invertido móvel, destacando os benefícios de cada método.

Palavras chave: sistemas de segunda ordem; controle robusto; desigualdades matriciais lineares; sistemas incertos.

Abstract

Second-order systems constitute an important class of dynamic systems that are widely employed in engineering to model a variety of physical phenomena. Characterized by their dynamic behavior, second-order systems require effective control strategies to achieve the desired performance. This work presents a design framework for obtaining a robust multivariable Proportional-Integral-Derivative (PID) controller for linear second-order systems. Additionally, a Proportional-Integral-Derivative with Acceleration (PIDA) controller is proposed to address the model regularization problem. Relevant control challenges, such as modeling errors, regulatory performance optimization, regional pole placement, saturation prevention, input delay, LQR cost function, and observer-based control, are addressed within the framework of control design via Linear Matrix Inequality (LMI). The proposed design strategy is based on rewriting the system model in an appropriate way so that the design of the PID/PIDA controller is equivalent to that of a state feedback controller. Firstly, a methodology is proposed for obtaining a PID/PIDA controller, grounded in regional pole placement, H_∞ performance, regularization problem, and saturation prevention, all simultaneously addressed. Additionally, a methodology to obtain a robust multivariable Proportional-Integral-Derivative (PID) controller for second-order systems with time-varying input delay is also proposed. Furthermore, a methodology is introduced to obtain a PD/PID controller using the Linear Quadratic Regulator (LQR) control strategy. Finally, a formulation for observer-based controller design is proposed. This is followed by a methodology based on LMI formulations to obtain an observer-based controller for uncertain second-order systems. To demonstrate the efficacy of the proposed control methodologies, simulations with numerical examples and a practical experiment using an inverted pendulum mobile system were conducted. These experiments effectively showcase the advantages of each method.

Keywords: second-order systems; robust control; linear matrix inequalities; uncertain systems.

List of Figures

2.1 D-region for pole placement where s is a complex number. 30

3.1 The left-hand figure shows the system finite open-loop poles and the right-hand one its closed-loop poles. The shaded area indicates the desired D-region for the system closed-loop pole placement. Example 1. 43

3.2 The system closed-loop response to a unity set point and to an exogenous sinusoidal disturbance signal $w(t) = 5\sin(10t) + 5$ for $t \in [10, 20]$sec. Example 1. 44

3.3 Closed-loop response error vector $e(t)$ and control signal $u(t)$ to a unity set point and to an exogenous sinusoidal disturbance signal $w(t) = 5\sin(10t) + 5$ for $t \in [10, 20]$sec. Example 1. 44

3.4 The quarter–vehicle model of active suspension system. Example 2. 45

3.5 The left-hand figure shows the system open-loop poles and the right-hand one its closed-loop poles for all integer values of m_s. The shaded area indicates the desired D-region for the system closed-loop pole placement. Example 2. 46

3.6 The system closed-loop response to a unity set point and to an exogenous sinusoidal disturbance signal $w(t) = 1000\sin(5t)$ +1000 for $t \in [7, 12]$sec. Example 2. 46

3.7 Close views of the closed-loop system states, $z_1(t)$ and $\dot{z}_1(t)$, where the shaded area indicates where the signal may takes place for integer values of m_s. Example 2. . . 47

3.8 Closed-loop error response on the state $e(t)$ and control signal $u(t)$ to a unity set point and to an exogenous sinusoidal disturbance signal $w(t) = 1000\sin(5t) + 1000$ for $t \in [7, 12]$sec, for $m_s = 100$kg. Example 2. 47

3.9 Mechanical system. Example 3. 48

3.10 The left-hand figure shows the system finite open-loop poles and the right-hand one its closed-loop poles. The shaded area indicates the desired D-region for the system closed-loop pole placement. Example 3. 49

3.11 The system closed-loop response to a unity set point and to an exogenous sinusoidal disturbance signal $w(t) = \sin(5t) + 1$ for $t \in [10, 20]$sec. Example 3. 50

3.12 Closed-loop error response, and control signal $u(t)$ to a unity set point and to an exogenous sinusoidal disturbance signal $w(t) = \sin(5t) + 1$ for $t \in [10, 20]$sec. Example 3. 50
3.13 Flexible rotor coupled to an arm link. Example 4. 51
3.14 The left-hand figure shows the system finite open-loop poles and the right-hand one its closed-loop poles. The shaded area indicates the desired D-region for the system closed-loop pole placement. Example 4. 52
3.15 The system closed-loop response to a piece-wise constant set-point. Example 4. . . 53
3.16 Closed-loop error response, and control signal $u(t)$. Example 4. 53
3.17 The system closed-loop response. Example 1. 54
3.18 Closed-loop error response, and control signal $u(t)$. Example 1. 54
3.19 The system closed-loop response. Example 2. 55
3.20 Closed-loop error response, and control signal $u(t)$. Example 2. 55

4.1 EduMIP 57
4.2 MIP system sketch 58
4.3 Experiment with body angle θ 63
4.4 Bode diagram $H(s)_{\dot{\theta}}$ 64
4.5 Close look at the Bode diagram, the blue line is the $H(s)_{\dot{\theta}}$, and the red and yellow lines are the transfer function with an uncertainty of $\pm 4\%$. 65
4.6 Experiment with wheels angle ϕ 65
4.7 Wheel angle experiment ϕ, where the blue line is the input voltage and the red and green lines represent the speed of wheels 1 and 2, respectively. The red and green lines almost overlap as the speed data collected for both wheels was very close. . . 66
4.8 Response of body position (θ) and voltage, with PD controller, for $R = 1$, $R = 2$ and $R = 5$, blue, red and green line, respectively. 69
4.9 Response of body position (θ) and voltage, with PID controller, for $R = 2$ and $R = 5$, blue and red line, respectively. 70
4.10 Response of body position (θ) and voltage, with PID controller (blue line), and PD controller (red line) for $R = 5$. 71
4.11 Response of wheel position and control signal V(t), with PID controller (blue line), and PD controller (red line) for $R = 5$. 71
4.12 Bode Diagram: Controller Order Comparison 73
4.13 Response of body position (θ) and voltage, with PD/LQE controller, for $R = 1$ and $R = 2$, blue and red line, respectively. 74
4.14 Response of body position (θ), with PID controller (blue line) for $R = 5$, and PD/LQE controller (red line) for $R = 2$. 75
4.15 Control signal, with PID controller (blue line) for $R = 5$, and PD/LQE controller (red line) for $R = 2$. 75

4.16 Response of wheel position and speed, with PID controller (blue line) for $R = 5$, and PD/LQE controller (red line) for $R = 2$. 76

B.1 Diagram: PID discretization 90

List of Tables

3.1 Open-loop and closed-loop system poles in the Example 1. 43
3.2 Open-loop and closed-loop system poles in the Example 3. 49
3.3 Open-loop and closed-loop system poles at its vertices, Example 4. 52

4.1 PD controller gains, varying the weighting variable R. 68
4.2 PID controller gains, varying the weighting variable R. 69
4.3 PD/LQE gains, varying the weighting variable R. 72

List of Acronyms

LMI Linear Matrix Inequality

PD Proportional Derivative

PID Proportional Integral Derivative

PIDA Proportional Integral Derivative Acceleration

FEM Finite Element Models

LQR Linear Quadratic Regulator

LQE Linear Quadratic Estimator

Notation

$\mathbb{R}^n$	The n-dimensional Euclidean space
$\mathbb{R}^{n\times m}$	The set of $n \times m$ real matrix
j	$\sqrt{-1}$
$Re(s)$	Real part, being s a complex number
$Im(s)$	Imaginary part, being s a complex number
0	Null matrix of appropriate dimension
0_n	Null matrix of n-th order
I	Identity matrix of appropriate dimension
I_n	Identity matrix of n-th order
$\text{diag}\{\ldots\}$	Block-diagonal matrix
A	Matrix $A = [a_{ij}]$
$A^\top$	Transpose of matrix A
A^{-1}	Inverse of matrix A
$X > 0$ $(X \geq 0)$	X is positive (semi) definite
$X < 0$ $(X \leq 0)$	X is negative (semi) definite
$\text{sm}\{X\}$	$X + X^T$
$*$	Transpose element inside of a symmetric matrix
$\text{cov}\{A\}$	Convex envelope with vertices A
$\mathcal{E}$	Mathematical expectation

Contents

1 Introduction **18**

1.1 Second-Order Systems 18
1.2 Motivation 19
1.3 Related Works 20
1.4 Objectives 22
1.5 Outline of the chapters 23

2 Problem Formulation **24**

2.1 Representation of second order linear systems as linear descriptor systems 24
2.2 Rewriting PID/PIDA controller as state-feedback controller 25
2.3 Singulary on mass matrix, M, design the A control action 27
2.4 PID/PIDA controller for second order linear systems 28
2.4.1 H_∞ performance 29
2.4.2 PID control via pole placement 31
2.4.3 Saturation on the control input 32
2.4.4 Delayed control input 32
2.4.5 PD/PID via LQR cost function 34
Disturbance Response 34
2.4.6 Observer control design 38

3 Numerical Examples **42**

3.1 Second order systems free of time delay 42
3.2 Second order systems subject to time delay 52

4 Practical Experiment: Mobile Inverted Pendulum **57**

4.1 Modeling 58
4.1.1 Linearization 61
4.2 System Identification 62

4.2.1 Body angle θ experiment 62
4.2.2 Wheels angle ϕ experiment 65
4.3 Controller Design 68
4.3.1 Design of PD/PID-LQR controllers 68
4.3.2 Observer-based controller 70

5 Concluding Remarks **77**
5.1 Publications 78

Bibliography **79**

Appendix A Appendix **86**

Appendix B Appendix **90**

1 Introduction

This chapter describes various aspects related to the control of second-order systems. It discusses the motivations for studying this subject, provides a brief literature review, and presents the proposed objectives. At the end of the chapter, the research contributions and the organization of the work will be presented.

1.1 Second-Order Systems

Second-order differential equations can be used to represent various systems, such as electrical, electromechanical, and mechanical systems. They are commonly used in examples of vibration control and robotic control (Abdelaziz 2014a; Zhang et al. 2019a).

The study of the control of second-order systems in flexible structures has gained significant interest, primarily because of the performance demands of mechanical systems. These include active suspension systems for vehicles, aircraft, and aerospace structures, and robotic manipulators (Patel and Mehta 2017; Sun et al. 2015; Wei et al. 2019). Control strategies play a crucial role in achieving the desired control forces in dynamic environments. In these environments, sensors detect states, computers calculate control forces in real-time, and actuators generate the necessary forces. These strategies have been extensively employed to effectively control of second-order systems under various dynamic operating conditions (Pratt et al. 2009).

To apply control strategies to second-order systems, which are typically described in classical theory by ordinary differential equations and classical state-space systems, it is common practice to transform these systems into first-order systems by introducing new variables for the first derivative (Zhang and Yu 2018). This transformation into first-order systems is a well-established theory, which makes it possible to use several consolidated techniques to control these systems (Abdelaziz 2014a; Chu and Datta 1996; Zhao et al. 2016).

This work presents a new robust control structure based on Proportional-Integral-Derivative (PID) / Proportional-Integral-Derivative with Acceleration (PIDA) controllers that improve the robustness characteristics and the performance of systems even in the presence of model

constraints. Subsequently, the motivation behind the development of these control techniques is presented.

1.2 Motivation

Second-order systems control is widely applied in mechanical systems, from the stabilization of flexible structures to aircraft and the active suspension of vehicles or seats (Alfadhli et al. 2018; Hayati et al. 2020; Singh et al. 2019).

In these problems, the success of the designed system depends on a series of requirements, for instance, the robustness of the controlled system against a model mismatch, unavailability of states for feedback, disturbance rejection in track control problems, saturation avoidance of the control effort, and treatment of the nonlinear behavior, which is an important source of uncertainty. Since uncertainties must be taken into account in some step of the design to avoid unexpected system instability in closed-loop, they are a prominent issue for the design of control of second-order systems.

Some methods used to express second-order differential equations in an equivalent set of first-order equations require the inversion operation of a matrix (Datta 2003). However, it is important to note that matrix inversion is not always a trivial task, especially when dealing with complex systems or large sets of equations. Matrix inversion can be computationally intensive and require significant processing resources. Additionally, in certain cases, the matrix may be singular or ill-conditioned, making inversion impossible or inaccurate. Hence, considering the second-order system in controller design is of utmost relevance.

Besides that, acceleration feedback can be a requirement for systems with considerable mass imbalance (Acevedo et al. 2020) or even in the case of a singular mass matrix (Abdelaziz 2015a). Then, regularizing the mass matrix via acceleration feedback is often a need.

Second-order systems are also subject to time delay, due to several reasons, such as detection and actuation in the feedback of states, physical separation between sensors and measurement points, delay in communication in systems, online data acquisition, filtering, signal transmission from a computer to the actuator which can degrade control performance and destabilize a system (Araújo and Santos 2018; Zhang et al. 2020).

In this context, delays can be constant or time-varying. Delay variation can be applied to second-order systems, its resolution being more complex than constant delays, since the notion of poles and eigenvalues cannot be applied to time-varying systems. Given this, the assumption of constant time delay is reasonable for most second-order control systems, however, delay variation can be an important problem when, for example, the delay is network induced, which motivates the study of time-varying second-order systems (Santos et al. 2018; Seguy et al. 2010; Yu et al. 2015).

A number of requirements such as pole allocation, saturation prevention, disturbance rejection and time delay, can be met in systems in second-order control systems. In view of

this, linear matrix inequalities (Boyd et al. 1994; Chilali and Gahinet 1996) can be successfully applied in control problems that involve multiple requirements, such as robustness, guaranteed cost disturbance attenuation, regional pole placement, among others (Almeida and Araújo 2019; Li et al. 2013; Richiedei and Tamellin 2021).

Due to the convex nature of the formulation, several control challenges can be combined such as regional pole placement, robust stability and guaranteed robust performance for uncertain or time-varying systems, null tracking error in the presence of constant disturbance, and saturation avoidance, among other relevant issues.

Motivated by this problem of control of second-order systems that combines several requirements, this work presents a robust framework to design multivariable PID or, when necessary, PIDA controllers for parametric uncertain second-order systems. In contrast to related works based only on proportional and derivative feedback, the integral action is used to achieve null set-point tracking error. The acceleration action may be used to deal with the regularization problem, which is one of the contributions of this work. The design methodology is based on regional pole placement also known as D-stability, H_∞ performance, stabilization of asymmetric systems, regularization problem, actuator saturation avoidance, and set-point tracking, which are jointly handled within the linear matrix inequality (LMI) framework. Then, the robust framework presented for designing PID controllers is extended to second-order systems subject to time-varying delay at the control input, handled through LMI formulations. Furthermore, a design of PID/PD controllers based on Linear Quadratic Regulator (LQR) control is proposed. Finally, an observer-based controller framework is presented, together with a design methodology via LMI.

Next, a brief review of the literature is presented, listing some of the main works dedicated to the control problems of second-order systems.

1.3 Related Works

In the control of second-order systems, there are several topics to be addressed, ranging from system modeling to controller design, rejecting disturbances, avoiding control effort saturation, considering the nonlinearity of the systems, and including time-varying delay.

For both of the more used modeling approaches, namely, finite-element models (FEM) (Zhang and Li 2013) and the receptance approach (Mottershead et al. 2008; Ram and Mottershead 2013; Zhu et al. 2009), the modeling errors are unavoidable, given the approximate nature of the former and the experimental appeal on the latter. Motivated by the relevance of modeling error, some studies on the robustness analysis and design of the controlled system have been delivered in recent times. The robust control of systems described by second-order models using FEM or receptance models can be addressed by different approaches (Abdelaziz 2013; Adamson et al. 2020; Franklin et al. 2021; Henrion et al. 2005; Nichols 2000; Qian and Xu 2005).The partial eigenstructure assignment with guaranteed robustness is described in early

and more recent works as Araújo et al. 2018; Cai et al. 2010; Xie 2021. Since uncertainties must be taken into account in some step of the design to avoid unexpected system instability in closed-loop, they are a prominent issue for the design of second-order control systems.

The disturbance rejection problem in the context of control is another relevant issue in applications as structural control. In Gudarzi 2015 the aforesaid problem is dealt with estimating unknown disturbances in the context of seismic alleviation in buildings. Applications of piezoelectric actuators for disturbance rejection in the control of thin-walled and other smart structures are addressed in Li and Chen 2013; Zhang et al. 2014; Zhang et al. 2021; Zhang et al. 2019b. An alternative approach to dealing with the presence of disturbances is the active disturbance rejection control (ADRC) (Li et al. 2016; Ramirez-Neria et al. 2020; Ramírez-Neria et al. 2021; Safiullah et al. 2022; Zheng et al. 2008), which is a robust control method that uses an extended state observer (ESO) to estimate the disturbance input beyond the system states. The H_∞ control is also a method discussed in the literature that can guarantee stability and optimized performance despite insufficient or inaccurate knowledge of the structural system parameters (Chen et al. 2010; Du and Zhang 2008).

In addition, actuator saturation can occur in the closed-loop system under study, causing performance degradation and instability, often appearing in engineering systems and is a focus of study and application in the industry (Sun et al. 2014). Control approaches are most often proposed to manage compensation between conflicting requirements, such as disturbance clearance and actuator saturation, a large number of different arrangements have been investigated. Adaptive control is constantly applied while considering the necessary performance constraints and actuator saturation, application of anti-windup blocks to preserve stability and performance in the presence of saturation is also studied (Sun et al. 2014, 2012).

Another problem that directly affects the performance of the system is the singularity of the mass matrix, a way to deal with this problem is to regularize the matrix using acceleration feedback (Abdelaziz 2015b). In Yang et al. 2017, a negative acceleration feedback control algorithm is proposed to shift the active mass. In Abdelaziz 2014b an unstructured problem in the mass matrix is addressed, the combination of acceleration and velocity feedback is proposed.

Finally, another approach that is constantly studied is the time delay. In general, these systems can be stable in open-loop and become unstable in closed-loop, if delays are not properly considered at some stage of the project. The literature discusses the constant and time-varying delay (Araújo and Santos 2018; Santos et al. 2018; Shustin et al. 2008). In Araújo and Santos 2018 a method based on receptance and the Smith predictor is proposed to handle the constant delay, however, the proposal only deals with stable and marginally stable systems, not guaranteeing the internal stability of unstable systems in open-loop. Araujo and Santos 2020 propose a sample data strategy to apply a Smith predictor-based approach to address these unstable systems.

Regarding constant delays, Natori et al. 2008 investigate a dedicated control scheme for time delay compensation based on the concept of network disturbance and communication

disturbance observer. Belotti and Richiedei 2020 propose a numerical method for partial pole placement in time-delayed systems, which guarantees the a priori verification of the stability of the primary and secondary roots through the reception method, combined with an LMI, which guarantees asymptotic stability for a limited time delay.

More recent studies have focused on treating systems subject to variable delays, using robust control techniques. The use of LMI and the Lyapunov-Krasovskii theory is an effective methodology to investigate the stability of systems with a time-varying delay (Kwon et al. 2016; Mozelli and Souza 2016; Tognetti and Oliveira 2022).

Design techniques based on Linear Quadratic Regulator (LQR) are well known in modern control theory and have been widely used in many applications (Alavinasab et al. 2006; He et al. 2000; Kumar and Jerome 2013). There are several studies that prove the effectiveness of the PID controller design based on the LQR controller (Argentim et al. 2013; Heidari et al. 2018; Nasir et al. 2008).

The LQR controller can be used in conjunction with an estimator. The general procedure to obtain the Linear Quadratic Estimator (LQE) is very similar to that used for the LQR (Simoes et al. 2007). State estimators for dynamical systems have been the focus of many works, mainly for first-order systems (Demetriou 2004; Nguyen et al. 2020; Zheng et al. 2021).

In the next section, the objectives addressed in this work will be specified.

1.4 Objectives

- To present a robust framework for designing Proportional-Integral-Derivative (PID) multivariate controllers for uncertain parametric second-order systems.
- To present a robust framework for designing Proportional-Integral-Derivative-Acceleration (PIDA) multivariate controllers for uncertain parametric second-order systems with non-singularities in the mass matrix.
- To propose a methodology through Linear Matrix Inequalities (LMI), based on regional pole allocation, H_∞ performance, stabilization of asymmetric systems, regularization problem, actuator saturation prevention, setpoint tracking, LQR cost function, and observer-based controllers.
- Provide a robust framework for designing multivariable PID controllers for second-order systems with time-varying input delay.
- To present a robust framework for the design of observer-based controller for uncertain parametric second-order systems.

1.5 Outline of the chapters

The remaining of this document is organized as follows:

- Chapter 2 introduces a PID control structure for delayed second-order systems and a PID/PIDA structure for free delay second-order systems subject to uncertainty and constraints, both frameworks formulated through LMIs. Subsequently, a design methodology is presented for PD/PID controllers based on LQR control. Finally, it presents a robust framework for designing observer-based controllers for second-order systems subject to uncertainty.
- Chapter 3 presents numerical examples to validate the first method proposed in Chapter 2, which is the PID/PIDA controller for delay-free and delay systems.
- Chapter 4 a practical example of a mobile inverted pendulum (MIP) is presented, and the results obtained in Chapter 2, from the PD/PID controller based on the LQR and the observer-based control, are implemented and validated.
- Chapter 5 points out conclusions.

2 Problem Formulation

In this chapter, we present some fundamental aspects of the formulation of the control problem studied in this work. In the first section, we present the proposed methodology to represent second-order systems as descriptor systems. In the second section, we rewrite PID/PIDA as a state feedback control. In the third section, the control action project A is presented. And finally, the LMIs formulated to obtain the PID/PIDA controller and deal with the constraints are displayed.

2.1 Representation of second order linear systems as linear descriptor systems

Consider the second-order linear model:

$$M\ddot{z}(t) + D\dot{z}(t) + Sz(t) = Bu(t - d(t)) + Fw(t) \tag{2.1}$$

where $z(t) \in \mathbb{R}^n$ is the state vector and $w(t) \in \mathbb{R}^p$ is the exogenous disturbance vector, the delay is considered through the control signal $u(t - d(t))$. The delay is modeled as $d(t) = \tau + \mu(t)$, representing a time-varying delay, with τ being the nominal delay value and $\mu(t)$ a time-varying scalar function, which satisfies $\mu(t) \leq |\mu(t)| \leq \tau$. M, D, $S \in \mathbb{R}^{n\times n}$ are, respectively, the mass, damping and stiffness matrices, and $B \in \mathbb{R}^{n\times m}$, $F \in \mathbb{R}^{n\times p}$ are, respectively, the control and disturbance matrices.

In order to rewrite the second-order system (2.1) as a descriptor system we define the following state variables: $x_1(t) = z(t)$ and $x_2(t) = \dot{z}(t)$. So, we get the following descriptor system:

$$\begin{cases} E\dot{x}(t) = Ax(t) + B_u u(t - d(t)) + B_w w(t) & (2.2.1) \\ y(t) = Cx(t) & (2.2.2) \end{cases}$$

where:

$$x^T(t) = [x_1^T(t) \;\; x_2^T(t)],$$
$$A = \begin{bmatrix} 0_n & I_n \\ -S & -D \end{bmatrix}, \;\; B_u = \begin{bmatrix} 0_{n\times m} \\ B \end{bmatrix}, \;\; B_w = \begin{bmatrix} 0_{n\times p} \\ F \end{bmatrix},$$
$$E = \text{diag}\{I_n, M\}, C = \begin{bmatrix} I_n & 0_n \end{bmatrix}.$$

Now we define the descriptor system matrix as:

$$\mathcal{S} \triangleq \begin{bmatrix} E & A \\ B_u & B_w \end{bmatrix}. \tag{2.3}$$

In addition, assume that the S is uncertain and belongs to the polytopic set Δ. Thus, Δ is defined by all matrices obtained by the combination of its vertices:

$$\Delta \triangleq \text{cov}\{S_1, S_2, \ldots, S_N\} = \left\{ S(\alpha) \;:\; S(\alpha) = \sum_{i=1}^{N} \alpha_i S_i, \;\; \alpha \in \Omega \right\} \tag{2.4}$$

where the polytope vertices are

$$\mathcal{S}_i \triangleq \begin{bmatrix} E_i & A_i \\ B_{u,i} & B_{w,i} \end{bmatrix},$$

and the its coordinate vector $\alpha = [\alpha_1 \; \alpha_2 \; \ldots \; \alpha_N]^T$ belongs to the set

$$\Omega \triangleq \left\{ \alpha : \alpha_i \geq 0, \sum_{i=1}^{N} \alpha_i = 1 \right\}. \tag{2.5}$$

2.2 Rewriting PID/PIDA controller as state-feedback controller

In this section we define the control signal $u(t)$ which is an extension of the single-variable PIDA controller to the multivariable case, so the proportional control action (P) is proportional to the current error. The integral action (I) can eliminate the steady-state offset and the derivative action (D) is specially related with shaping the damping behavior of the closed-loop system. Finally, we use the acceleration action (A) to avoid impulsive behavior in the closed-loop system, see Example 3 for illustration of this point. Thus the multivariable PIDA controller is defined by

$$u(t) = K_P e(t) + K_I \int_0^t e_a(\tau) d\tau + K_D \dot{e}(t) + K_A \ddot{e}(t), \tag{2.6}$$

with $e(t) = z(t) - r(t)$ where $r(t) \in \mathbb{R}^n$ is the desired set-point vector, and $e_a(t)$ denotes the error signal on the states; $e_a(t) = Ue(t) \in \mathbb{R}^a$, for an appropriated binary matrix $U \in \mathbb{R}^{a\times n}$, chosen according to the controllability of the system.

In addition $K_P, K_D, K_A \in \mathbb{R}^{m\times n}$ and $K_I \in \mathbb{R}^{m\times a}$. $e_a(t)$, guarantees the tracking of the trajectory.

In order to enjoy from the LMI framework to design the robust controller we rewrite the system (2.1) such that the PID part of the controller (2.6) becomes a static state feedback controller. In view of that we define the following state variable:

$$x_3(t) = -\int_0^t e_a(\tau)d\tau \tag{2.7}$$

The free of time delay and with time delay closed-loop descriptor systems are presented below, respectively.

- **Descriptor system in closed-loop free of time delay:**

$$\begin{cases} E\dot{x}(t) = Ax(t) + B_u u(t) + B_w w(t) & (2.8.1)\\ \qquad +([0_n \;\; 0_n \;\; -U]^T)r(t) + (BK_A)\ddot{r}(t) & \\ u(t) = Kx(t) - K[r^T(t) \;\; \dot{r}^T(t) \;\; 0_{1\times a}]^T & (2.8.2)\\ y(t) = Cx(t) & (2.8.3) \end{cases}$$

- **Descriptor system in closed-loop subject to time delay:**

$$\begin{cases} E\dot{x}(t) = Ax(t) + B_u u(t-d(t)) & (2.9.1)\\ \qquad +B_w w(t) + ([0 \;\; 0 \;\; -U]^T)r(t) & \\ u(t-d(t)) = Kx(t-d(t)) - K[r^T(t-d(t)) \;\; \dot{r}^T(t-d(t)) \;\; 0_{1\times a}]^T & (2.9.2)\\ y(t) = Cx(t) & (2.9.3) \end{cases}$$

replacing (2.9.2) in (2.9.1), and considering $A_d = B_u K$, we get:

$$\begin{cases} E\dot{x}(t) = Ax(t) + A_d x(t-d(t)) + & (2.10.1)\\ \qquad +B_u K([r^T(t-d(t)) \;\; \dot{r}^T(t-d(t)) \; 0]^T) & \\ \qquad +B_w w(t) + ([0 \;\; 0 \;\; -U]^T)r(t) & \\ y(t) = Cx(t) & (2.10.2) \end{cases}$$

For (2.8) and (2.9) is given:

$$x^T(t) = [x_1^T(t) \;\; x_2^T(t) \;\; x_3^T(t)],$$

$$A = \begin{bmatrix} 0_n & I_n & 0_{n\times a} \\ -S & -D & 0_{n\times a} \\ U & 0_{a\times n} & 0_a \end{bmatrix}, \; B_u = \begin{bmatrix} 0_{n\times m} \\ B \\ 0_{a\times m} \end{bmatrix}, \; B_w = \begin{bmatrix} 0_{n\times p} \\ F \\ 0_{a\times p} \end{bmatrix},$$

$$E = \text{diag}\{I_n,\ (M - BK_A),\ I_a\},\ \ K = \begin{bmatrix} K_{Pm\times n} & K_{Dm\times n} & K_{Im\times a} \end{bmatrix},$$
$$C = \begin{bmatrix} I_n & 0_n & 0_{n\times a} \end{bmatrix}.$$

Note that if we want to rewrite the closed-loop descriptor system so that the PID controller part becomes a PD controller, we just need to remove the last $x_3(t)$ state from the (2.8) system.

- **Reduced descriptor system in closed-loop free of time delay:**

$$\begin{cases} E\dot{x}(t) = Ax(t) + B_u u(t) + B_w w(t) & (2.11.1) \\ u(t) = Kx(t) & (2.11.2) \\ y(t) = Cx(t) & (2.11.3) \end{cases}$$

Where:

$$x^T(t) = [x_1^T(t) \ \ x_2^T(t)],$$
$$A = \begin{bmatrix} 0_n & I_n \\ -S & -D \end{bmatrix},\ B_u = \begin{bmatrix} 0_{n\times m} \\ B \end{bmatrix},\ B_w = \begin{bmatrix} 0_{n\times p} \\ F \end{bmatrix},$$
$$E = \text{diag}\{I_n,\ (M - BK_A)\},\ \ K = \begin{bmatrix} K_{Pm\times n} & K_{Dm\times n} \end{bmatrix},$$
$$C = \begin{bmatrix} I_n & 0_n \end{bmatrix}.$$

Thus, in the case of uncertainty, the representation of uncertainties in (2.3) and (2.4) is considered. For simplification purposes, whenever there are uncertainties in the matrices, the index "i" will be added.

The proposed PIDA controller for free of time delay systems is defined by a linear time-invariant control law. Hence, standard tools for robustness analysis with respect to unstructured uncertainties and delays can be applied *a posteriori* (Franklin et al. 2021). Moreover, due to the generality of the polytopic description, polytopic difference inclusions can be used to formally represent time-varying delay effect (Gielen et al. 2010) and some types of nonlinearities (Boyd et al. 1994; Hu et al. 2006) *a priori*. In this last case, the robustness against the polytopic uncertainty is handled directly during design stage. In the next section, we will discuss the singularity of the mass matrix M.

2.3 Singulary on mass matrix, M, design the A control action

In this work we will consider two cases according with the mass matrix M singularity:

Case 1) M is nonsingular: we tune a standard PID controller setting $K_A = 0$ in (2.6);

Case 2) M is singular: we design K_A such that $(M - BK_A)$ is nonsingular, which is possible whenever $\big(M,\, B\big)$ has full row rank (Bender and Laub 1987).

Therefore, in both cases we have that $(M - BK_A)$ is nonsingular and the descriptor model above reduces to a standard state-space description left multiplying (2.8) by E^{-1}. This explain the reason why the proposed controller (2.6) has term $K_A\ddot{e}(t)$, which can be removed from the control law when the system mass matrix M is nonsingular.

In order to guarantee that E in (2.8) is nonsingular, in the case when the mass matrix M is singular, we present the next lemma.

Lemma 2.1

The matrix $(M - BK_A)$ *is nonsingular if there exist a nonzero scalar* β *and a matrix* $K_A \in \mathbb{R}^{m\times n}$ *such that*

$$\begin{bmatrix} \frac{1}{2}(M_i + M_i^T - B_iK_A - K_A^TB_i^T) & \beta I \\ \beta I & I \end{bmatrix} > 0, \tag{2.12}$$

for $i = 1, 2, \ldots, V$, *where* V *is the number of vertices of the polytopic set* Δ *in* (2.4) *keeping the matrices* M_i *and* B_i *and removing the others. Furthermore if* (2.12) *holds then the minimum eigenvalue of* $sm\Big\{\frac{1}{2}(M - BK_A)\Big\}$ *is greater than* β^2.

Proof. The lemma follows from the application of Theorem A.1, Appendix A that yields

$$\begin{bmatrix} \frac{1}{2}(A_F + A_F^T) & \hat{\beta} I \\ \hat{\beta} I & I \end{bmatrix} > 0$$

assuming that $A_F = (M - BK_A)$. Therefore the conditions in the Lemma are obtained by recalling that to ensure an LMI condition over an entire polytopic uncertain domain, it suffices to check the LMI at the vertices of the convex polytope. □ □

In the case system (2.1) is free of parametric uncertainties and E in (2.8) is nonsingular a myriad of LMI conditions from the literature can be applied directly in the system (2.8). However, in the presence of uncertainties the space-state description of the model (2.8) may require inversion of uncertain matrices which is a hard problem in general. Therefore, in the following we present tractable LMI conditions, which do not require inverses of uncertain matrices. The control problems considered are listed throughout the next section for second-order systems, and the respective LMI formulations for obtaining the controller.

2.4 PID/PIDA controller for second order linear systems

In this section, the control problems addressed are described, and in the subsections the respective LMI formulations, are followed by a step-by-step procedure for designing controllers.

Problem 1. Design a PID or PIDA controller for the second-order linear system in (2.1) free of time delay, such that the closed-loop system model can be written as a standard state space description; guaranteeing the existence and uniqueness of state responses and avoiding impulsive behavior that may cause degradation in performance; and for any combination of the following requirements:

1. the closed-loop poles belong to a prescribed stable region (D-region) on the complex plane as depicted in Fig. 2.1;

2. the H_∞ performance condition is satisfied for a given disturbance attenuation level $\gamma > 0$,

$$\sup_{\|w(t)\|_2 \neq 0} \frac{\|y(t)\|_2}{\|w(t)\|_2} < \gamma; \tag{2.13}$$

3. the control signal is bounded in amplitude by a given scalar $u_{\max} > 0$ and a set of initial conditions,

$$\max_{t \geq 0} \|u(t)\| \leq u_{\max}. \tag{2.14}$$

The design requirements listed in the above problem are linked to the system closed-loop behavior and performance. The item 1) is related to the desired closed-loop time response that often can be achieved by assigning the closed-loop poles into a suitable subregion of the complex left-half plane. The H_∞ performance in item 2) characterizes the worst case ratio, γ, of the energies contained in the output and the exogenous disturbance input of the system. In contrast, item 3) is concerned in maintaining the linear behavior of the closed-loop system avoiding control-signal saturation and eventual loss of stability by guaranteeing an upper bound on the norm of the control input $u_{\max}$.

It is important to mention that the main shortcoming of the proposed strategy is the full-state knowledge assumption. This requirement can be relaxed by using state observers. Also notice that displacement derivative may be directly measured or estimated from the direct displacement information. In the case when M is nonsingular, *Case 1)*, acceleration feedback is not used, but otherwise the accelaration state may be estimated or entirely measured due to the interesting properties of accelerometers (Abdelaziz 2015a). The following are LMI conditions for solving Problem 1.

2.4.1 H_∞ performance

The next theorem presents LMI conditions to design a controller PID/PIDA with prescribed closed-loop H_∞ performance.

Theorem 2.1

Let $\gamma > 0$ be a prescribed closed-loop H_∞ performance and K_A be a given matrix such that $E = (M - BK_A)$ is nonsingular, see Lemma 2.1. The system (2.1) *in closed-loop with the*

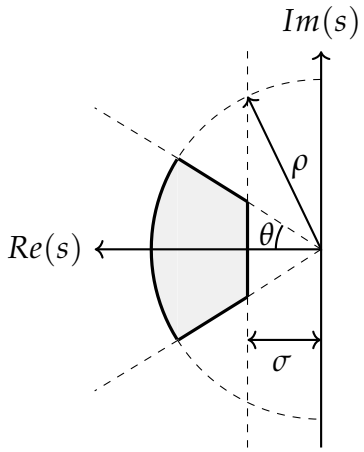

Figure 2.1: D-region for pole placement where s is a complex number.

controller (2.6) *is robustly stable with disturbance attenuation* γ *if there exist a symmetric matrix* $P \in \mathbb{R}^{2n+a\times 2n+a}$ *and a matrix* $Y \in \mathbb{R}^{m\times 2n+a}$ *such that* $P > 0$ *and*

$$\begin{bmatrix} sm\{A_iPE_i^T + B_{u,i}YE_i^T\} & E_iPC^T & B_{w,i} \\ CPE_i^T & -\gamma^2 I & 0 \\ B_{w,i}^T & 0 & -I \end{bmatrix} < 0, \tag{2.15}$$

for $i = 1,\ldots,N$, *where* N *is the number of vertices of the polytopic set* Δ *in* (2.4). *In affirmative case, the controller gains are given by* $K = YP^{-1}$.

Proof. As established in the previous section the theorem statement is equivalent to designing a controller of the form $u(t) = Kx(t)$ such that the descriptor model (2.8) in closed-loop is robustly stable with H_∞ disturbance attenuation level γ. Moreover, assuming that E is nonsingular, consider the state-space description obtained from system (2.8) left-multiplying the equation (2.8) by E^{-1}. Then such design problem can be formulated as the following matrix inequalities Boyd et al. 1994, Sec. 6.3.2:

$$P > 0,$$

$$\begin{bmatrix} sm\{P(E_i^{-1}(A_i+B_{u,i}K))^T\}+E_i^{-1}B_{w,i}(E_i^{-1}B_{w,i})^T & PC^T \\ CP & -\gamma^2 I \end{bmatrix} < 0, \tag{2.16}$$

for $i = 1,\ldots,N$ and $j = 1,\ldots,L$, vertices of the polytopic uncertain domain. Now defining the linearizing variable $Y = KP$ and applying Schur complement the last inequality is equivalent to

$$\begin{bmatrix} sm\{E_i^{-1}(A_iP + B_{u,i}Y)\} & PC^T & E_i^{-1}B_{w,i} \\ CP & -\gamma^2 I & 0 \\ B_{w,i}^T(E_i^{-1})^T & 0 & -I \end{bmatrix} < 0, \tag{2.17}$$

then pre-and post-multiplying it by $\mathsf{diag}\{E_i, I, I\}$ and its transpose, respectively, the conditions in the theorem are obtained. □ □

The next theorem considers the standard D-region given by the intersection of regions: 1) half-plane $Re(s) < -\sigma$, 2) conic sector with apex at the origin and inner angle 2θ, and 3) disk with radius ρ and center at the origin, as depicted in Fig. 2.1.

2.4.2 PID control via pole placement

The following theorem details how the pole placement in a given D-region can be done via PID/PIDA design.

Theorem 2.2

Let be given a D-region specified by the positive scalars σ, ρ, θ and a matrix K_A such that $E = M - BK_A$ is nonsingular, see Lemma 2.1. The system (2.1) is D-stable in closed-loop with the controller in (2.6), i.e. the poles of the closed-loop system belong to the D-region depicted in Fig. 2.1 , if and only if there exist a symmetric positive matrix $P \in \mathbb{R}^{2n+a\times 2n+a}$ and a matrix $Y \in \mathbb{R}^{m\times 2n+a}$ such that

$$2\sigma E_i P E_i^T + A_i P E_i^T + E_i P A_i^T + B_{u,i} Y E_i^T + E_i Y^T B_{u,i}^T < 0, \tag{2.18}$$

$$\begin{bmatrix} -\rho E_i P E_i^T & A_i P E_i^T + B_{u,i} Y E_i^T \\ E_i P A_i^T + E_i Y^T B_{u,i}^T & -\rho E_i P E_i^T \end{bmatrix} < 0, \tag{2.19}$$

$$\begin{bmatrix} \sin\theta(\Theta_i + \Theta_i^T) & \cos\theta(\Theta_i - \Theta_i^T) \\ \cos\theta(\Theta_i^T - \Theta_i) & \sin\theta(\Theta_i + \Theta_i^T) \end{bmatrix} < 0, \tag{2.20}$$

with $\Theta_i = A_i P E_i^T + B_{u,i} Y E_i^T$, for $i = 1, 2, \ldots, N$, where N is the number of vertices of the polytopic set Δ in (2.4) removing $B_{w,i}$. In affirmative case, the controller gains are given in $K = YP^{-1}$.

Proof. Based on the problem formulation in previous section, and assuming that E is non-singular, consider the state-space description obtained from system (2.8) left-multiplying the equation (2.8) by E^{-1}. Then by an application of Theorem A.2, Appendix A in the closed-loop matrix $E^{-1}(A + B_u K)$ we have that

$$2\sigma P + \Gamma + \Gamma^T < 0, \quad \begin{bmatrix} -\rho P & \Gamma \\ \Gamma^T & -\rho P \end{bmatrix} < 0,$$

$$\begin{bmatrix} \sin\theta(\Gamma + \Gamma^T) & \cos\theta(\Gamma - \Gamma(t)^T) \\ \cos\theta(\Gamma^T - \Gamma) & \sin\theta(\Gamma + \Gamma^T) \end{bmatrix} < 0,$$

with $\Gamma = E^{-1}(A + B_u K)P$. Therefore the conditions in the theorem are obtained defining the linearizing variable $Y = KP$, pre- and post- multiplying the first LMI by E and E^T, respectively, and the other ones by $\mathrm{diag}\{E, E\}$ and its transpose, and recalling that to ensure the resulting

LMI conditions over the entire polytopic uncertain domain, it suffices to check the LMIs at the vertices of the convex polytope. □ □

2.4.3 Saturation on the control input

The following LMI condition considers the physical limitation on the maximum amplitude of the control signal.

Lemma 2.2

(Boyd et al. 1994, Sec. 7.2.3) Assume the control signal $u(t) = Kx(t) = YP^{-1}x(t)$ *and the initial condition* $x(0)$*. Then* $\max_{t\geq 0} \|u(t)\| \leq u_{\max}$*, if*

$$\begin{bmatrix} 1 & x(0)^T \\ x(0) & P \end{bmatrix} \geq 0 \quad \textit{and} \quad \begin{bmatrix} P & Y^T \\ Y & u_{\max}^2 I_m \end{bmatrix} \geq 0. \tag{2.21}$$

Finally, taking into account the above development, the robust PID/PIDA controller design procedure is summarized next.

Procedure 2.1

PID/PIDA controller design for solving Problem 1:

Step 1: Rewrite the linear second-order system (2.1) as the augmented descriptor model (2.8);

Step 2: Set the H_∞ performance γ, the control input constraint $u_{\max}$ (if any), and the desired D-region for the closed-loop pole placement defined by the triplet (σ,θ,ρ) accordingly with Fig. 2.1;

Step 3: If the matrix M is singular determine the gain K_A by solving the LMIs presented in Lemma 2.1, otherwise set $K_A = 0$ and go to the next step;

Step 4: Find the solution (P,Y) that solves simultaneously the LMI conditions presented in Theorems 2.1, 2.2, and Lemma 2.2;

Step 5: The PID controller parameters are given in $K = [K_P \;\; K_D \;\; K_I]$ where $K = YP^{-1}$.

Next, we present the second control problem, whose control signal is subject to delay, and the respective LMI formulations to obtain the controller.

2.4.4 Delayed control input

Problem 2. Design a PID controller for time-delayed second-order linear system in (2.1) such that the closed-loop system model can be written as a standard state space description, ensuring

the stability of the system for a given exponential decay rate.

Theorem 2.3

Let $\tau > 0, \tau \geq \mu \geq 0$,such that $d(t) \in [\tau - \mu, \tau + \mu]$, $\delta > 0$ and $\alpha \neq 0$ a scalar fit parameter. Then, the system (2.10) *is exponentially stabilized with exponential convergence rate δ by the PID controller with gains given in the matrix $K = X\overline{F}^{-T}$, if there exist matrices of appropriate dimensions: $\overline{F}$, $\overline{P} = \overline{P}^T$, $\overline{S} = \overline{S}^T$, $\overline{Q}$, $\overline{R}_1 = \overline{R}_1^T$, $\overline{R}_2$, $\overline{R}_3 = \overline{R}_3^T$, $\overline{Z} = \overline{Z}^T$ and X such that the following LMIs are satisfied*

$$\begin{bmatrix} \overline{P} & \star \\ \overline{Q}^T & \varepsilon_1 \overline{S} \end{bmatrix} > 0, \tag{2.22}$$

where $\varepsilon_1 = e^{-2\delta\tau}/\tau$,

$$\overline{R} = \begin{bmatrix} \overline{R}_1 & \star \\ \overline{R}_2 & \overline{R}_3 \end{bmatrix} > 0, \tag{2.23}$$

and

$$\left[\begin{array}{c|c} \overline{\overline{\Xi}} & \star \\ \hline \overline{\Gamma}^T & \varepsilon_2^{-1}\mu\overline{Z} \end{array}\right] < 0, \tag{2.24}$$

where $\varepsilon_2 = e^{-2\delta(\tau+\mu)}$, $\overline{\Gamma}^T = \mu[X^T B^T \;\; \alpha X^T B^T \;\; 0 \;\; 0]$ and $\overline{\overline{\Xi}}$ given in (2.25).

$$\overline{\overline{\Xi}} = \begin{bmatrix} \overline{\mathcal{F}} & \star & \star & \star \\ E(\overline{P} + \tau\overline{R}_2)E^T - \varepsilon_2(E\overline{F}E^T - \alpha A\overline{F}^T E^T) & E\mathcal{G}E^T & \star & \star \\ \varepsilon_1\overline{R}_3^T E^T - \overline{Q}^T E^T + \varepsilon_2 X^T B^T & \varepsilon_2\alpha X^T B^T & -\varepsilon_1(\overline{R}_3 + \tau\overline{S}) & \star \\ 2\delta\overline{Q}^T E^T - \varepsilon_1\overline{R}_2^T E^T & \overline{Q}^T E^T & \varepsilon_1\overline{R}_2^T & -\varepsilon_1\overline{R}_1 \end{bmatrix}. \tag{2.25}$$

where $\overline{\mathcal{F}} = E(2\delta\overline{P} + \overline{Q} + \overline{Q}^T + \tau\overline{R}_1 - \epsilon_1\overline{R}_3 + \overline{S})E^T + \varepsilon_2(A\overline{F}^T E^T + E\overline{F}A^T)$ and $\mathcal{G} = \tau R_3 + 2\mu\overline{Z} - \epsilon_2(\overline{G} + \overline{G}^T)$.

Proof. This proof follows the Theorem A.3, Appendix A, for the state-space description obtained from system (2.10), assuming that E is nonsingular, left-multiplying the equation (2.10.1) for PID controller by E^{-1}. Then, in the closed-loop matrix $E^{-1}(A(t)x(t) + A_d x(t - d(t)) + B_u(t)K)$.

Define the variables: $\overline{F} \triangleq F^{-1}$ and

$$[\overline{P} \;\; \overline{Q} \;\; \overline{R}_1 \;\; \overline{R}_2 \;\; \overline{R}_3 \;\; \overline{Z}] \triangleq \overline{F}[P \;\; Q \;\; R_1 \;\; R_2 \;\; R_3 \;\; Z]\overline{F}^T$$

The LMI in (2.22) and (2.23) are obtained by pre and post multiplying the LMIs (A.18) and (A.19), respectively, by $diag\{\overline{F}, \ldots, \overline{F}\}$ and $diag\{\overline{F}, \ldots, \overline{F}\}^T$.

Furthermore, the LMI in (2.24) is obtained through the LMI in (A.20). The following substitutions are performed: $A_d = E^{-1}BK$, $A = E^{-1}A$ and $G = \alpha F$ in (2.24), and pre-and post-multiplying the LMI (2.24) by $diag\{\overline{F},\ldots,\overline{F}\}$ and $diag\{\overline{F},\ldots,\overline{F}\}^T$. Finally, considering the new linearizing variable $X = K\overline{F}^T$ and pre-and post-multiplying the LMI (2.24) by $diag\ \{E, E, I, I\}$ and its transpose, respectively, the conditions in the Theorem 2.3 are obtained.

□

Procedure 2.2

PID controller design for solving Problem 2.4.4

Step 1: Rewrite the time-delayed second-order linear system (2.1) as the augmented descriptor model (2.10.1);

Step 2: Define the decay rate of the system response, $\delta > 0$, and α, a free tuning parameter, defining the variation in the value of the delay, μ.

Step 3: Find the solution $(X, \overline{F})$ that solves the LMI conditions presented in Theorem 2.3.

Step 4: The PID controller parameters are given in $K = [K_P \ \ K_D \ \ K_I]$, where $K = X\overline{F}^{-T}$.

Next, we present the third control problem, followed by an analysis of the influence of the disturbance on the response of a system, and finally the LMI formulations for obtaining the controller.

2.4.5 PD/PID via LQR cost function

Problem 3. Design a PID/PD controller based on the linear quadratic regulator (LQR) controller for the second-order linear system in (2.1), that stabilizes the system and minimizes a quadratic cost function that relates the states of the system and the control signal. Establishing a compromise between the settling time of the system states and the used control energy.

Disturbance Response

The influence of disturbances on the system response is analyzed, and the findings from this analysis serve as the foundation for deriving LMIs conditions for designing controllers and filters. The focus lies on a linear and time-invariant system described by the following equations:

$$\dot{x}(t) = \Lambda(\alpha)x(t) + \Omega(\alpha)w(t) \tag{2.26}$$

where α represents a vector of uncertain parameters invariant in the time. The perturbation being $w(t)$ white noise, that is, a stochastic variable with zero means, uncorrelated in time and with a covariance matrix $W > 0$:

$$\mathcal{E}\{w(t)\} = 0 \quad \text{e} \quad \mathcal{E}\{w(t)w^T(\tau)\} = W\delta(t-\tau).$$

In addition, the cost function is defined

$$\lim_{t\to\infty} \mathcal{E}[x^T(t)\Theta x(t)] \tag{2.27}$$

where $\Theta \geq 0$ is a known matrix.

The result is presented below.

Lemma 2.3

Consider the system (2.26) *with zero initial condition,* $x(0) = 0$*, and the cost function* (2.27)*. Suppose that* $J \geq 0$ *and* $\Psi > 0$ *are the solution to the following optimization problem:*

$$\min tr(J) \quad \textit{subject to:}$$

$$J - \Omega(\alpha)^T \Psi \Omega(\alpha) \geq 0 \tag{2.28}$$

$$\Lambda(\alpha)^T\Psi + \Psi\Lambda(\alpha) + \Theta \leq 0. \tag{2.29}$$

Then the cost function (2.27) *satisfies*

$$\lim_{t\to\infty} \mathcal{E}[x^T(t)\Theta x(t)] \leq |W| tr\left(\Omega(\alpha)^T\Psi\Omega(\alpha)\right).$$

Proof. Initially, note that with zero initial condition, the state vector of the system (2.26) is given by

$$x(t) = \int_0^t e^{\Lambda(\alpha)(t-\tau)}\Omega(\alpha)w(\tau)d\tau$$

and that

$$\begin{aligned}
\lim_{t\to\infty} \mathcal{E}\left[tr(x^T(t)\Theta x(t))\right] &= \lim_{t\to\infty} \mathcal{E}\left[tr(\Theta x(t)x^T(t))\right] \\
&= \lim_{t\to\infty} \mathcal{E}\left[tr\left(\Theta \int_0^t e^{\Lambda(\alpha)(t-\tau)}\Omega(\alpha)w(\tau)d\tau \int_0^t w^T(\sigma)\Omega(\alpha)^T e^{\Lambda(\alpha)^T(t-\sigma)}d\sigma\right)\right] \\
&= \lim_{t\to\infty} tr\left(\Theta \int_0^t e^{\Lambda(\alpha)(t-\tau)}\Omega(\alpha) \int_0^t \mathcal{E}[w(\tau)w^T(\sigma)]\Omega(\alpha)^T e^{\Lambda(\alpha)^T(t-\sigma)}d\sigma d\tau\right) \\
&= \lim_{t\to\infty} tr\left(\Theta \int_0^t e^{\Lambda(\alpha)(t-\tau)}\Omega(\alpha) \int_0^t W\delta(\tau-\sigma)\Omega(\alpha)^T e^{\Lambda(\alpha)^T(t-\sigma)}d\sigma d\tau\right) \\
&= \lim_{t\to\infty} tr\left(\Theta \int_0^t e^{\Lambda(\alpha)(t-\tau)}\Omega(\alpha)W\Omega(\alpha)^T e^{\Lambda(\alpha)^T(t-\tau)}d\tau\right) \\
&= \lim_{t\to\infty} tr\left(\int_0^t \Theta e^{\Lambda(\alpha)\eta}\Omega(\alpha)W\Omega(\alpha)^T e^{\Lambda(\alpha)^T\eta}d\eta\right) \\
&= tr\left(W\Omega(\alpha)^T\left[\int_0^\infty e^{\Lambda(\alpha)^T\eta}\Theta e^{\Lambda(\alpha)\eta}d\eta\right]\Omega(\alpha)\right)
\end{aligned} \tag{2.30}$$

where $P(\alpha)$ is the solution of the equation

$$\Lambda(\alpha)^T P(\alpha) + P(\alpha)\Lambda(\alpha) + \Theta = 0. \tag{2.31}$$

Now, note that if there exists a positive symmetric definite matrix Ψ such that the inequality in (2.29) is satisfied, then $\Lambda(\alpha)$ is Hurwitz. Furthermore, relating (2.31) from (2.29) we have that

$$\Lambda(\alpha)(\Psi - P(\alpha)) + (\Psi - P(\alpha))\Lambda(\alpha)^T + \Theta \leq 0$$

and therefore if $\Lambda(\alpha)$ is Hurwitz then, $\Psi - P(\alpha) \geq 0$. Therefore, assuming that $\Psi \geq P(\alpha)$, we have the upper bound for (2.30)

$$tr\left(W\Omega(\alpha)^T P(\alpha)\Omega(\alpha)\right) \leq tr\left(W\Omega(\alpha)^T \Psi \Omega(\alpha)\right) \leq |W| tr\left(\Omega(\alpha)^T \Psi \Omega(\alpha)\right) \leq |W| tr(J),$$

where J is a positive definite symmetric matrix, which implies the inequality in (2.28). □

Assuming that E_i is non-singular, then the closed-loop descriptor system (2.8)/(2.11) with a state feedback control law $u(t) = Kx(t)$, can be rewritten as

$$\dot{x}(t) = E_i^{-1}(A_i + B_{u,i}K)x(t) + E_i^{-1}B_{w,i}w(t) \tag{2.32}$$

where the disturbance $w(t)$ is white noise as defined in (2.26). Furthermore, consider the quadratic cost function

$$\lim_{t\to\infty} \mathcal{E}[x(t)^T Q x(t) + u(t)^T R u(t)] = \lim_{t\to\infty} \mathcal{E}[x(t)^T (Q + K^T R K)x(t)] \tag{2.33}$$

in which the constant matrices $Q \geq 0$ and $R > 0$ are specified by the designer and the gain matrix K must be determined in order to reduce the cost function.

Therefore, noting that the dynamics of the system in (2.32) and the cost function (2.33) have the same form as the system in (2.26) and the function (2.27), respectively. A solution to the present problem can be obtained using the result in Lemma 2.3, as presented below.

Theorem 2.4

Let given symmetric matrices $Q \in \mathcal{R}^{n\times n}$ and $R \in \mathcal{R}^{m\times m}$. Consider the system (2.8)/(2.11) with E_i non-singular. If there exist matrices $P > 0 \in \mathcal{R}^{n\times n}$, $Y \in \mathcal{R}^{m\times n}$ and $J \geq 0 \in \mathcal{R}^{p\times p}$, solution of the optimization problem

$$\min_{P,Y,J} Tr(J) \tag{2.34}$$

$$\begin{bmatrix} J & B_{w,i}^T \\ B_{w,i} & E_i P E_i^T \end{bmatrix} \geq 0 \tag{2.35}$$

$$\begin{bmatrix} sm\{A_iPE_i^T + B_{u,i}YE_i^T\} & E_iPQ_F & E_iY^TR_F \\ Q_F^TPE_i^T & -I & 0 \\ R_F^TYE_i^T & 0 & -I \end{bmatrix} \leq 0, \tag{2.36}$$

for all $i = 1,2,\ldots,N$*, where* N *is the number of vertices of the polytopic set* Δ *in* (2.4)*. With* Q_F *and* R_F *defined such that* $Q = Q_FQ_F^T$ *and* $R = R_FR_F^T$*. Then, the closed-loop system* (2.8) *is robustly stable with* $K = YP^{-1}$ *and* $\sqrt{tr(J)}$ *is an upper bound for the LQR cost function* (2.33)*.*

Proof. Consider the system in (2.32) and the cost function (2.33), making the substitutions: $\Lambda(\alpha) \leftarrow E_i^{-1}(A_i + B_{u,i}K)$, $\Omega(\alpha) \leftarrow E_i^{-1}B_{w,i}$, $\Theta \leftarrow Q + K^TRK$ and $\Psi \leftarrow P^{-1}$ in Lemma 2.3 we have, from (2.28), that

$$J - B_{w,i}^TE_i^{-1}P^{-1}E_i^{-1}B_{w,i} \geq 0 \tag{2.37}$$

and applying Schur's complement we have

$$\begin{bmatrix} J & B_{w,i}^T \\ B_{w,i} & E_iPE_i^T \end{bmatrix} \geq 0. \tag{2.38}$$

Now, the second inequality resulting from Lemma 2.3 is

$$(A_i^T + K^TB_{u,i}^T)(PE_i^T)^{-1} + (E_iP)^{-1}(A_i + B_{u,i}K) + Q + K^TRK \leq 0$$

which pre and post multiplied by E_iP and PE_i^T, respectively, and defining the variable $Y = KP$, results in

$$E_i(PA_i^T + Y^TB_{u,i}^T) + (A_iP + B_{u,i}Y)E_i^T + E_i(PQP + Y^TRY)E_i^T \leq 0$$

then considering the factorials $Q = Q_FQ_F^T$ and $R = R_FR_F^T$ and applying Schur's complement we have

$$\begin{bmatrix} sm\{A_iPE_i^T + B_{u,i}YE_i^T\} & E_iPQ_F & E_iY^TR_F \\ Q_F^TPE_i^T & -I & 0 \\ R_F^TYE_i^T & 0 & -I \end{bmatrix} \leq 0.$$

Therefore, the LMIs in the theorem follow directly from the last inequality and from (2.38), by the fact that to guarantee an LMI in a polytope domain, it is sufficient to check the LMI on its vertices of the polytope. Finally, considering the aforementioned progress, the procedure for summarizing the design of a robust PID controller based on LQR control is outlined below. □

Procedure 2.3

PID controller design for solving Problem 3.

Step 1: Rewrite the second-order system (2.1) as the augmented descriptor model (2.8);

Step 2: If the matrix M is singular find the gain K_A by solving the LMIs presented in Lemma 2.1, otherwise set $K_A = 0$ and go to the next step;

Step 3: Define the weighting matrices Q and R;

Step 4: Find the solution (P,Y) that solves the LMI conditions presented in Theorem 2.4.

Step 5: The controller parameters are given in $K = [K_P \;\; K_D \;\; K_I]$, where $K = YP^{-1}$.

Similar to the PID controller, the procedure for designing PD controllers is described below:

Procedure 2.4

PD controller design for solving Problem 3.

Step 1: Rewrite the second-order system (2.1) as the augmented descriptor model (2.11);

Step 2: If the matrix M is singular find the gain K_A by solving the LMIs presented in Lemma 2.1, otherwise set $K_A = 0$ and go to the next step;

Step 3: Define the weighting matrices Q and R;

Step 4: Find the solution (P,Y) that solves the LMI conditions presented in Theorem 2.4;

Step 5: The controller parameters are given in $K = [K_P \;\; K_D]$, where $K = YP^{-1}$.

Next, we present a framework for designing observer-based controllers, and the last control problem addressed is described, followed by the LMIs formulations for obtaining the controller.

2.4.6 Observer control design

Consider the system in (2.11) and the observer-based controller

$$\begin{aligned} \hat{E}\dot{\hat{x}}(t) &= \hat{A}\hat{x}(t) + \hat{B}_u u(t) + \hat{E}L(\hat{y}(t) - y(t)) \\ \hat{y}(t) &= C\hat{x}(t) \\ u(t) &= K\hat{x}(t). \end{aligned} \tag{2.39}$$

in which the matrices with the $\wedge$ symbol overwritten are predefined matrices that can be chosen as the mean value of the respective matrix functions of the system, the K matrix is

assumed known and can be projected assuming full feedback of the system states (2.11) and finally, the L matrix must be determined.

Combining (2.11) and (2.39) we have

$$\begin{bmatrix} \hat{E} & 0 \\ 0 & E_i \end{bmatrix} \begin{pmatrix} \dot{\hat{x}} \\ \dot{x} \end{pmatrix} = \begin{bmatrix} \hat{A} + \hat{B}_u K & 0 \\ B_{u,i} K & A_i \end{bmatrix} \begin{pmatrix} \hat{x} \\ x \end{pmatrix} + \begin{bmatrix} \hat{E}L \\ 0 \end{bmatrix} \begin{bmatrix} C & -C \end{bmatrix} \begin{pmatrix} \hat{x} \\ x \end{pmatrix} + \begin{bmatrix} 0 \\ B_{w,i} \end{bmatrix} w$$

and defining $e(t) = x(t) - \hat{x}(t)$, we have that

$$\begin{bmatrix} -I & I \\ 0 & I \end{bmatrix} \begin{pmatrix} \hat{x} \\ x \end{pmatrix} = \begin{pmatrix} e \\ x \end{pmatrix} \quad \text{e} \quad \begin{bmatrix} -I & I \\ 0 & I \end{bmatrix} \begin{pmatrix} e \\ x \end{pmatrix} = \begin{pmatrix} \hat{x} \\ x \end{pmatrix},$$

which allows us to obtain the dynamics of the estimation error and the closed-loop system

$$\begin{aligned} \begin{bmatrix} \hat{E} & E_i - \hat{E} \\ 0 & E_i \end{bmatrix} \begin{pmatrix} \dot{e} \\ \dot{x} \end{pmatrix} = & \begin{bmatrix} \hat{A} + (\hat{B} - B_{u,i})K & A_i - \hat{A} + (B_{u,i} - \hat{B})K \\ -B_{u,i}K & A_i + B_{u,i}K \end{bmatrix} \begin{pmatrix} e \\ x \end{pmatrix} \\ & + \begin{bmatrix} \hat{E}L \\ 0 \end{bmatrix} \begin{bmatrix} C & 0 \end{bmatrix} \begin{pmatrix} e \\ x \end{pmatrix} + \begin{bmatrix} B_{w,i} \\ B_{w,i} \end{bmatrix} w \end{aligned} \tag{2.40}$$

which, assuming $\bar{E}_i$ not singular, is rewritten as

$$\begin{pmatrix} \dot{e} \\ \dot{x} \end{pmatrix} = \bar{E}_i^{-1} (\tilde{A}_i + \bar{E}_i \tilde{L} \tilde{C}) \begin{pmatrix} e \\ x \end{pmatrix} + \bar{E}_i^{-1} \tilde{B}_{w,i} w \tag{2.41}$$

whose matrices are obtained from (2.40) by comparison.

Note that the stability of the closed-loop system (2.40) is determined by the eigenvalues

$$\begin{aligned} eig\{\bar{E}_i^{-1}[\tilde{A}_i + \bar{E}_i \tilde{L} \tilde{C}]\} &= eig\{\tilde{E}_i^{-1} \tilde{A}_i + \tilde{L} \tilde{C}\} \\ &= eig\{\tilde{A}_i^T \bar{E}_i^{-T} + \tilde{C}^T \tilde{L}^T\} \end{aligned}$$

which reveals that the stability of the system (2.41) is equivalent to the stability of the dual system

$$\begin{aligned} \dot{\bar{x}}(t) =& \tilde{A}_i^T \bar{E}_i^{-T} \bar{x}(t) + \tilde{C}^T \bar{u}(t) + \bar{E}_i^{-1} \tilde{B}_{w,i} w \\ \bar{u}(t) =& \tilde{L}^T \bar{x}(t). \end{aligned} \tag{2.42}$$

Problem 4. Design an observer based on the LQR controller for the dual descriptor system in (2.42).

Theorem 2.5

Let given symmetric matrices $Q \in \mathcal{R}^{2n\times 2n}$ and $R \in \mathcal{R}^{q\times q}$. Consider the system (2.8) with non-singular E_i. If there are symmetric matrices $P_1 \in \mathcal{R}^{n\times n}$ and $P_2 \in \mathcal{R}^{n\times n}$, such that $P = \text{diag}\{P_1, P_2\} > 0$, $Y \in \mathcal{R}^{q\times n}$ and $J \geq 0 \in \mathcal{R}^{p\times p}$, solution of optimization problem

$$\min_{P,Y,J} Tr(J) \tag{2.43}$$

$$\begin{bmatrix} J & B_{w,i}^T \\ B_{w,i} & E_i P_1 E_i^T \end{bmatrix} \geq 0 \tag{2.44}$$

$$\begin{bmatrix} sm\{(\bar{E}_i^{-1}\tilde{A}_i)^T P + \tilde{C}^T Y[I \;\; 0]\} & PQ_F & [I \;\; 0]^T Y^T R_F \\ Q_F^T P & -I & 0 \\ R_F^T Y[I \;\; 0] & 0 & -I \end{bmatrix} \leq 0, \tag{2.45}$$

for all $i = 1,2,\ldots,N$, where N is the number of vertices of the polytopic set Δ in (2.4). With Q_F and R_F defined such that $Q = Q_F Q_F^T$ and $R = R_F R_F^T$.

Then, the (2.39) closed-loop system is robustly stable with $L = P_1^{-1} Y^T$ and $\sqrt{tr(J)}$ is an upper bound for cost function in (2.33) by performing the substitutions: $x(t) \leftarrow \bar{x}(t)$ and $K \leftarrow \tilde{L}^T$.

Proof. The result is obtained by applying Theorem 2.4 to the (2.42) system by making the substitutions:

$E_i \leftarrow I$, $A_i \leftarrow (\tilde{E}_i^{-1}\tilde{A}_i)^T$, $B_{w,i} \leftarrow \bar{E}_i^{-1}\tilde{B}_{w,i}$ and $B_{u,i} \leftarrow \tilde{C}^T$.

In addition, note that

$$\begin{bmatrix} P_1 & P_2 \\ P_2^T & P_3 \end{bmatrix} \begin{bmatrix} L \\ 0 \end{bmatrix} = \begin{bmatrix} P_1 L \\ P_2^T L \end{bmatrix}.$$

Therefore, for the solution of the LMI return to result in only one matrix L the substitution $P \leftarrow \text{diag}\{P_1, P_2\}$, and the multiplication of Y by $[I \;\; 0]$ is also performed, thus obtaining the LMI (2.45).

Finally, so that the cost function takes into account only the estimation error, the substitutions are made in the inequality used to minimize the cost function:

$P \leftarrow P_1$, $\bar{E}_i \leftarrow E_i$ and $\bar{B}_{w,i} \leftarrow B_{w,i}$. Pre and post multiplied by $[0 \;\; E_i]$ and $[0 \;\; E_i]^T$, respectively, we get the LMI (2.44). □

Procedure 2.5

Observer-based controller project to solve Problem 4.

Step 1: Define the weighting matrices Q_F, R_F and K found in the Theorem 2.4;

Step 2: Calculate the average value matrices $\hat{E}$, $\hat{A}$ and $\hat{B}$ in (2.39), and find the matrices $\tilde{E}$, $\tilde{A}$ and $\tilde{C}$ in (2.42);

Step 3: Find the solution (P,Y) that solves the LMI conditions presented in Theorem 2.5.

Step 4: The observer parameter is given for L, where $L = P_1^{-1}Y^T$.

In this chapter, the representation of the second-order uncertain linear system as a descriptor system, the treatment of the singularity of the mass matrix, as well as the design of controllers involving multiple control requirements were presented. Next, the 2.1 and 2.2 procedures presented in this chapter will be applied to numerical examples in order to validate the presented methods.

3 Numerical Examples

In this chapter, are presented four numerical examples drawn from the literature to illustrate and validate the proposed robust PID/PIDA controller design method.The LMIs were programmed using LMI Lab (Gahinet et al. 1994) in the MATLAB platform. The first session presents three numerical examples of free time delay second order systems. In the first example is designed a PID controller for a grasping robot and in the second one a PID controller for an active suspension of a car seat, in which the driver-plus-seat mass is assumed uncertain. In the third example, a PIDA controller is designed for a mechanical system with four degrees of freedom and a singular mass matrix. In the last example, the proposed approach is applied in a setpoint tracking control for a non-linear system, a model of a flexible rotor coupled to an arm link. In the second section, two numerical examples taken from the literature are presented for illustrations and to validate the proposed method of designing a robust PID controller for systems with time delay.

3.1 Second order systems free of time delay

Example 1. Consider a second-order linearized model, as in (2.1), of a grasping robot (Shapiro 2005) with

$$M = diag\{10,11\},\ D = \begin{bmatrix} 4 & 1 \\ 1 & 5 \end{bmatrix},\ S = \begin{bmatrix} 8 & 4 \\ -4 & 9 \end{bmatrix},\ B = F = I_{2\times 2}. \tag{3.1}$$

This model can also be rewritten as the augmented descriptor representation in (2.8) by setting $U = I$.

The control specifications are: *i*) limitation on the control signal amplitude as in (2.14) with $u_{\max} = 150$ for initial condition $x(0) = [0.2\ 0.2\ 0.8\ 0.8\ 0.1\ 0.1]^T$, *ii*) H_∞ disturbance attenuation level $\gamma = 1.2570$ and *iii*) the system closed-loop pole placement in the D-region defined as the intersection of the half-plane $\mathrm{Re}(s) < 0.7$, a conic sector centered at the origin

Table 3.1: Open-loop and closed-loop system poles in the Example 1.

Open-loop	Closed-loop
$0.0039 \pm j0.9001$	$-0.9119 \pm j0.1141$
$-0.4312 \pm j0.8953$	$-2.0789 \pm j1.3140$
	$-2.3439 \pm j1.1754$

and with inner angle given by $\theta = \pi/4$, and a disk with radius $\rho = 5$ as shown in Fig. 2.1. Then following the steps in Procedure 2.1 yield the PID controller gains:

$$K_P = \begin{bmatrix} -101.9639 & 9.7931 \\ -1.8587 & -101.0996 \end{bmatrix}, \; K_D = \begin{bmatrix} -51.3961 & 2.6837 \\ 3.0071 & -51.4268 \end{bmatrix}, K_I = \begin{bmatrix} -62.1859 & 6.3242 \\ -5.9849 & -61.5149 \end{bmatrix}.$$

For illustration, the respective open-loop and closed-loop poles are summarized in Table 3.1, all closed-loop poles belong to the desired D-region as can be seen in the Fig. 3.1. Fig. 3.2 describes the displacement, $z(t)$ and its derivative $\dot{z}(t)$, to a unity set point and to an exogenous sinusoidal disturbance signal $w(t) = 5\sin(10t) + 5$ for $t \in [10, 20]$sec. The displacement error paths $e(t)$ and the input signal $u(t)$, can be seen in Fig. 3.3, where the boundary condition in (2.14) for the given $u_{\max}$ is respected for a given perturbation and the error paths reach zero in steady state for a constant reference.

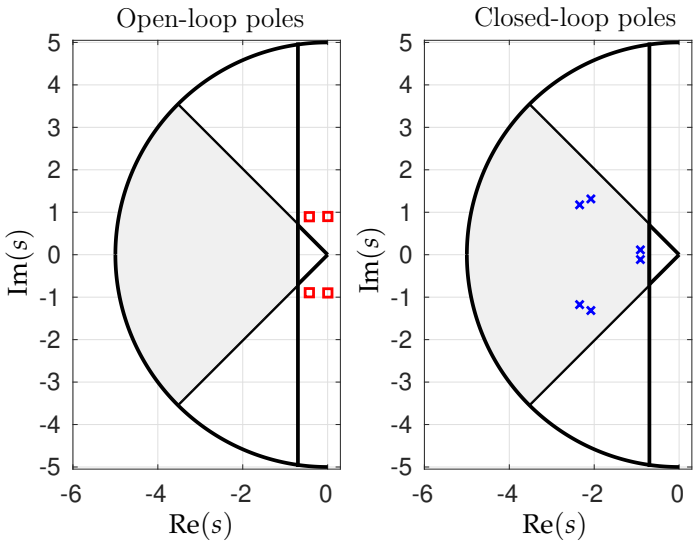

Figure 3.1: The left-hand figure shows the system finite open-loop poles and the right-hand one its closed-loop poles. The shaded area indicates the desired D-region for the system closed-loop pole placement. Example 1.

Example 2. Consider the active suspension of a car seat sketched in Fig. 3.4 drawn from Reithmeier and Leitmann 2003. This model has been successfully used to design controllers for vehicle active suspension (Pan and Sun 2019; Sun et al. 2015), vehicle driver seat (Alfadhli et al. 2018; Tu et al. 2021), or for a combination of them as in Reithmeier and Leitmann 2003. The model consists of the car mass (m_c) and driver-plus-seat mass (m_s). The vibrations are

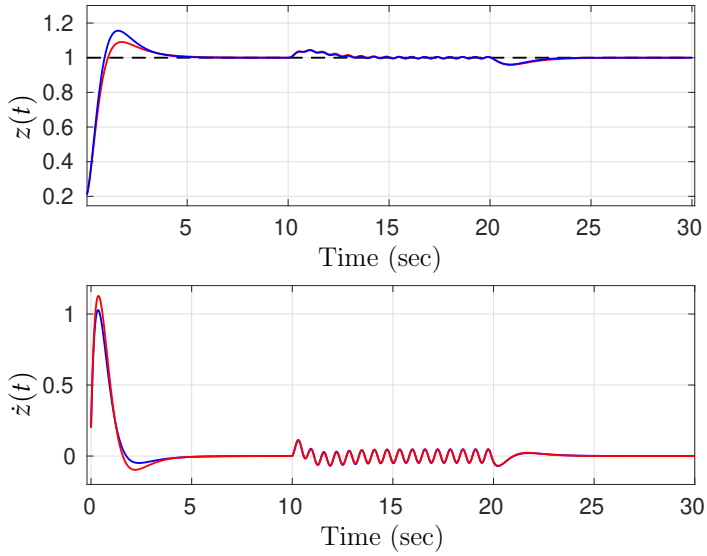

Figure 3.2: The system closed-loop response to a unity set point and to an exogenous sinusoidal disturbance signal $w(t) = 5\sin(10t) + 5$ for $t \in [10,\ 20]$sec. Example 1.

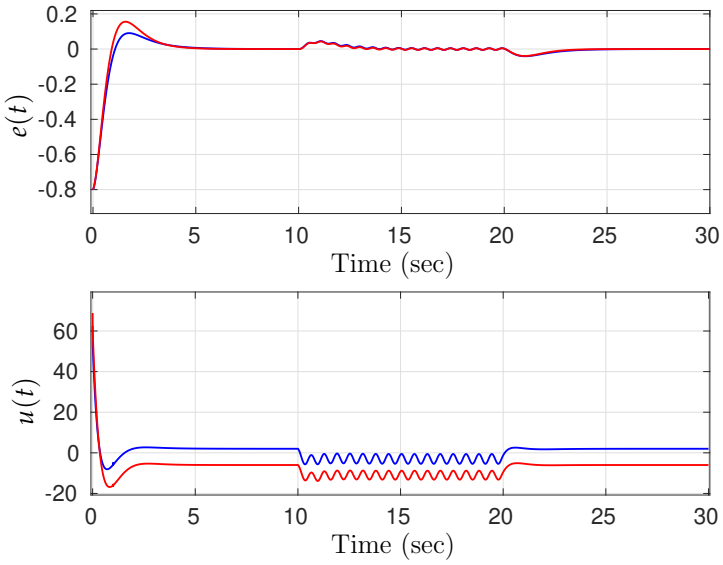

Figure 3.3: Closed-loop response error vector $e(t)$ and control signal $u(t)$ to a unity set point and to an exogenous sinusoidal disturbance signal $w(t) = 5\sin(10t) + 5$ for $t \in [10,\ 20]$sec. Example 1.

partially mitigated by the shock absorbers at the car and at the seat whose stiffness (k_1 and k_2) and damping (b_1 and b_2) that can be adjusted by $u_1(t)$ and $u_2(t)$, respectively. The system model is given by (2.1) with data:

$$M = \text{diag}\{m_s, m_c\},\ B = I_{2\times 2}, F = \text{diag}\{0, 1\}, D = \begin{bmatrix} b_2 & -b_2 \\ -b_2 & b_1 + b_2 \end{bmatrix}, \text{ and } S = \begin{bmatrix} k_2 & -k_2 \\ -k_2 & k_1 + b_2 \end{bmatrix}$$

where $m_c = 1500$kg and $m_s \in [70,\ 120]$kg (according to the driver's weight), $k_1 = 4\times 10^4$N/m, $k_2 = 5000$N/m, $b_1 = 4000$N-sec/m and $b_2 = 500$N-sec/m. Further, this system can be modeled as (2.8) by setting $U = B^T$.

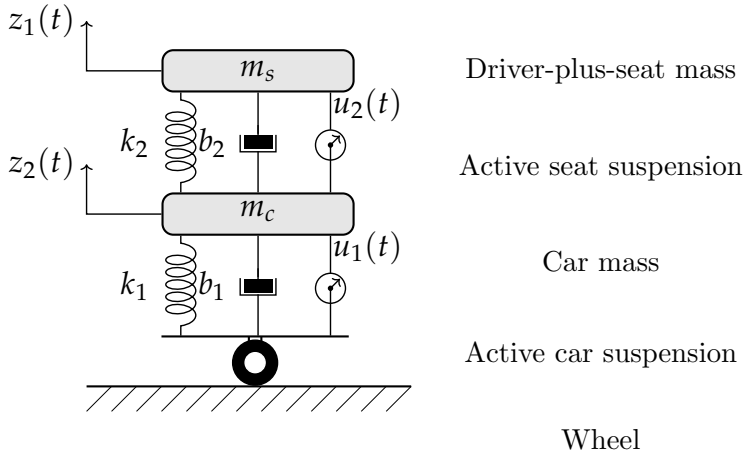

Figure 3.4: The quarter–vehicle model of active suspension system. Example 2.

In this example the control specifications are: *i*) limitation on the control signal amplitude as in (2.14) with $u_{\max} = 40000$ for initial condition $x(0) = [-0.1\ -0.1\ 0.09\ 0.09\ 0.05\ 0.05]^T$, *ii*) H_∞ disturbance attenuation level $\gamma = 0.1732$ and *ii*) the system closed-loop pole placement in the D-region defined as the intersection of the half-plane $\mathbf{Re}(s) < -0.9$, a conic sector centered at the origin and with inner angle given by $\theta = \pi/3$, and a disk with radius $\rho = 15$ as shown in Fig. 2.1. Then following Procedure 2.1 yields the PID controller gains:

$$K_P = \begin{bmatrix} -5748 & -3723 \\ -4844 & -7029 \end{bmatrix}, K_D = \begin{bmatrix} -1090 & -567 \\ -485 & -9837 \end{bmatrix}, K_I = \begin{bmatrix} -11803 & 1676 \\ -4838 & -46515 \end{bmatrix}.$$

For the results analysis Fig. 3.5 shows the open and closed-loop system poles for all integer admissible values of m_s where the shaded area indicates the desired D-region for the system closed-loop pole placement. Moreover, for $m_s = 100$, Fig. 3.6 shows the response evolution of the closed-loop system state vector $z(t)$ and its derivative to a unity set point and to an exogenous sinusoidal disturbance signal $w(t) = 1000\sin(5t) + 1000$ for $t \in [7,\ 12]$sec. It is important to mention that small impacts are observed on the dynamic response of the system for different values of the driver-plus-seat mass. Fig. 3.7 shows close views of the evolution of the displacement on the seat, $z_1(t)$, and its time-derivative, according to the value of $m_s \in [70,\ 120]$. Finally, Fig. 3.8 shows the control signal, where we can see that it does not exceed the limit $u_{\max}$ for a given perturbation and the error in the state reaches zero in steady state for a constant reference.

Example 3. Consider the singular mass four degrees-of-freedom mechanical system explored in Abdelaziz 2015a, sketched in Fig. 3.9, which dynamics model can be written as (2.1) with:

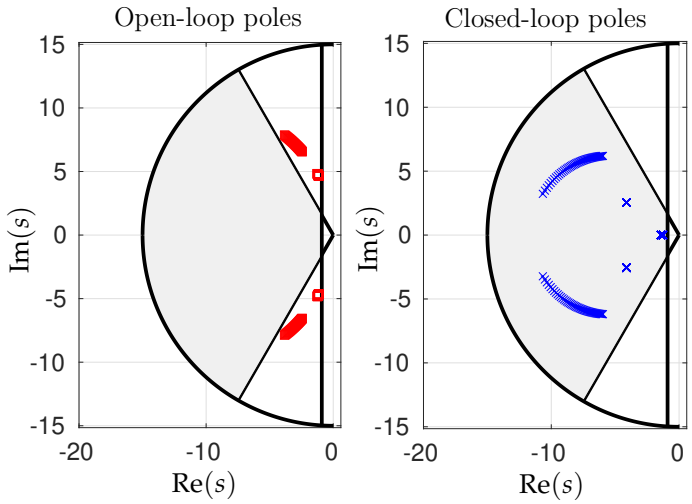

Figure 3.5: The left-hand figure shows the system open-loop poles and the right-hand one its closed-loop poles for all integer values of m_s. The shaded area indicates the desired D-region for the system closed-loop pole placement. Example 2.

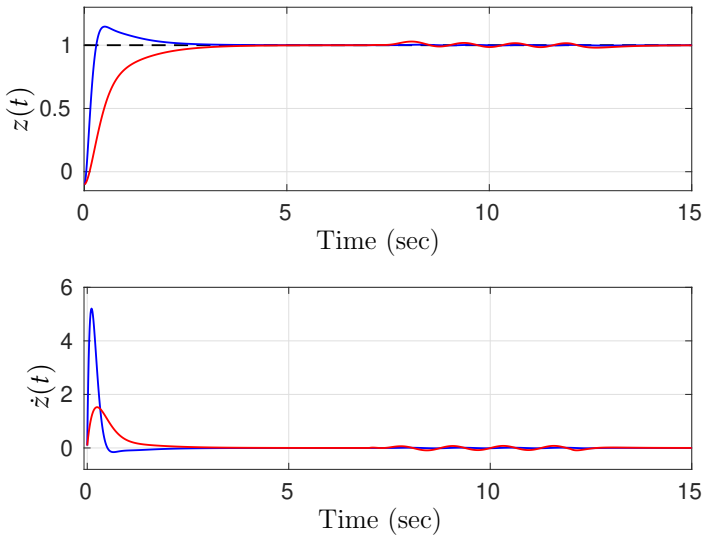

Figure 3.6: The system closed-loop response to a unity set point and to an exogenous sinusoidal disturbance signal $w(t) = 1000\sin(5t)$ +1000 for $t \in [7, 12]$sec. Example 2.

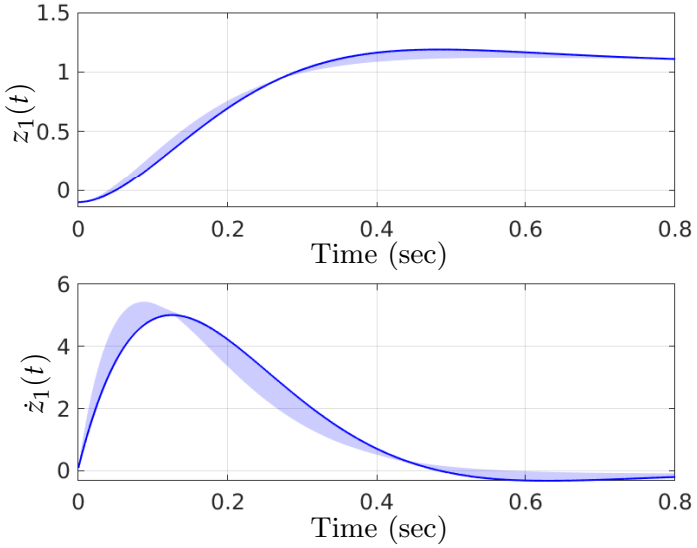

Figure 3.7: Close views of the closed-loop system states, $z_1(t)$ and $\dot{z}_1(t)$, where the shaded area indicates where the signal may takes place for integer values of m_s. Example 2.

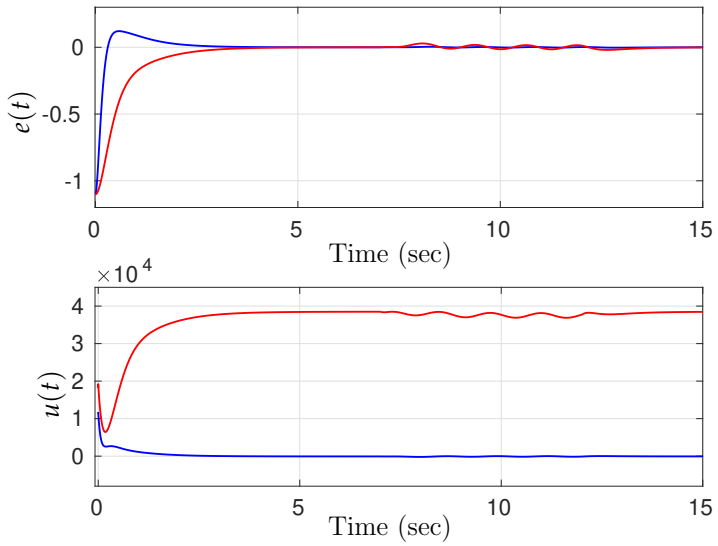

Figure 3.8: Closed-loop error response on the state $e(t)$ and control signal $u(t)$ to a unity set point and to an exogenous sinusoidal disturbance signal $w(t) = 1000\sin(5t) + 1000$ for $t \in [7,\ 12]$sec, for $m_s = 100$kg. Example 2.

$M = \text{diag}\{m_1,m_2,m_3,0\}$,

$$D = \begin{bmatrix} b_1+b_2 & -b_2 & 0 & 0 \\ -b_2 & b_2+b_3 & -b_3 & 0 \\ 0 & -b_3 & b_3+b_4 & -b_4 \\ 0 & 0 & -b_4 & b_4 \end{bmatrix}, \; S = \begin{bmatrix} k_1+k_2 & -k_2 & 0 & 0 \\ -k_2 & k_2+k_3 & -k_3 & 0 \\ 0 & -k_3 & k_3+k_4 & -k_4 \\ 0 & 0 & -k_4 & k_4 \end{bmatrix},$$

$$B = \begin{bmatrix} 1 & 0 & 0 & 0 \\ 0 & 0 & 0 & 1 \end{bmatrix}^T \quad \text{and} \quad F = \text{diag}\{1,0,0,1\},$$

where are assumed the physical system parameters values: $m_1 = 3$kg, $m_2 = 2$kg, $m_3 = 1$kg, $b_1 = 5$N-sec/m, $b_2 = 10$N-sec/m, $b_3 = 15$N-sec/m, $b_4 = 20$N-sec/m, $k_1 = 5$N/m, $k_2 = 15$N/m, $k_3 = 15$N/m, $k_4 = 20$N/m. Note that this system can be represented by (2.8) setting $U = B^T$.

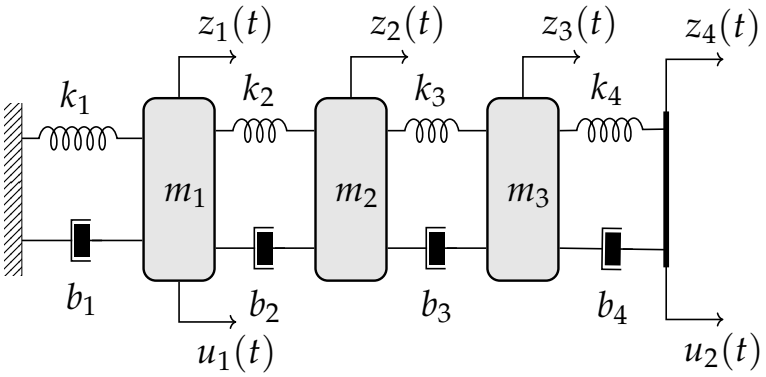

Figure 3.9: Mechanical system. Example 3.

Before proceeding to the controller design, note that this system presents an impulsive behavior due to an open-loop pole at infinite, see Table 3.2, which can result in possible harmful unwanted dynamic behaviors. Physically, the $4th$ degree of freedom is stressed to a jump in velocity due to its negligible mass, resulting in a mechanical shock in the connected dashpot and spring. Acceleration feedback brings the benefit of eliminating this issue. Thus, the objective of the PIDA controller proposed is to eliminate the impulsive behavior with acceleration feedback, generated by the infinite open-loop pole, and to assign for the system desired dynamic behaviors by the closed-loop pole placement.

Thus for the controller design the specifications are: i) limitation on the control signal amplitude as in (2.14) with $u_{\max} = 120$ for the initial condition $x(0) = [0.4\ 0.4\ 0.4\ 0.4\ \ -0.02\ \ -0.02\ \ -0.02\ \ -0.02\ \ 0.001\ \ 0.001]^T$, ii) H_∞ disturbance attenuation level $\gamma = 0.9010$ and iii) the system closed-loop pole placement in the D-region defined as the intersection of the half-plane defined by $\text{Re}(s) < -0.9$, a conic sector centered at the origin and with inner angle given by $\theta = \pi/4$, and a disk with radius $\rho = 20$ as shown in Fig. 2.1. Then following the steps in Procedure 2.1, we set $\beta = 0.1$ in Lemma 2.1, that yields the PIDA controller gains,

Table 3.2: Open-loop and closed-loop system poles in the Example 3.

Open-loop	Closed-loop
$-\infty$, -23.698,	$-14.2587 \pm j6.2459$,
$-0.3680 \pm j0.7923$,	-4.0065, -3.2294,
-1.9284, -5.0792,	-1.4582, -1.3700,
-1.0585, $-1.$	-7.2055, -5.8602,
	-1.2489, $-1.0232.$

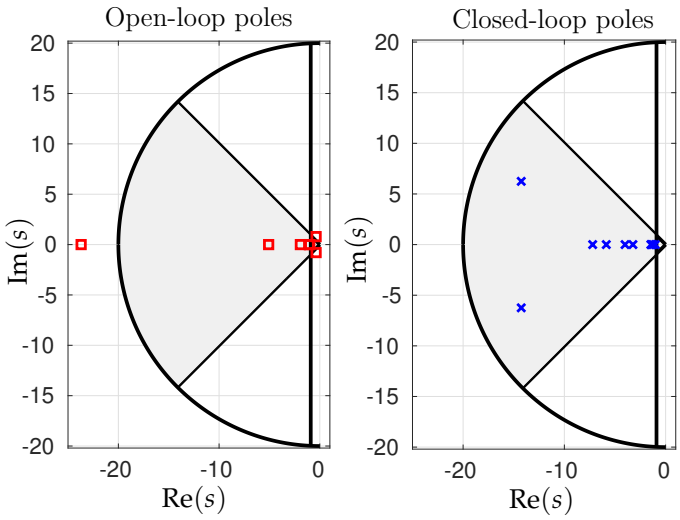

Figure 3.10: The left-hand figure shows the system finite open-loop poles and the right-hand one its closed-loop poles. The shaded area indicates the desired D-region for the system closed-loop pole placement. Example 3.

$$K_A = \begin{bmatrix} 1.2655 & 0 \\ 0 & 0 \\ 0 & 0 \\ 0 & -1.7345 \end{bmatrix}^T, \; K_P = \begin{bmatrix} -61.819 & -16.591 \\ -27.325 & 31.7718 \\ 14.2869 & -71.324 \\ -20.834 & 2.8653 \end{bmatrix}^T$$

$$K_D = \begin{bmatrix} -7.9785 & -16.5291 & 10.9827 & -10.6981 \\ -6.8143 & 29.4912 & -71.0446 & 31.8443 \end{bmatrix}, \; K_I = \begin{bmatrix} -75.4615 & -4.2255 \\ -9.7808 & -33.2117 \end{bmatrix}.$$

For illustration, the respective open-loop and closed-loop poles are summarized in Table 3.2, all closed-loop poles belong to the desired D-region as can be seen in the Fig. 3.10. Fig. 3.11 describes the displacement, $z(t)$ and its derivative $\dot{z}(t)$, to a unity set point and to an exogenous sinusoidal disturbance signal $w(t) = \sin(5t) + 1$ for $t \in [10, 20]$sec. The displacement error paths $e_a(t)$ and the input signal $u(t)$, can be seen in Fig. 3.12, where the maximum limit value $u_{\max}$ is respected for a given perturbation.

Example 4. In this example the proposed approach is applied to a set-point tracking control for a nonlinear system. We borrowed from Lipták et al. 2017 the model of a flexible rotor coupled to an arm link, sketched in Fig. 3.13. The system consists of a rotor actuated by the torque generated with a motor, where the degrees of freedom are the angles in the two extreme

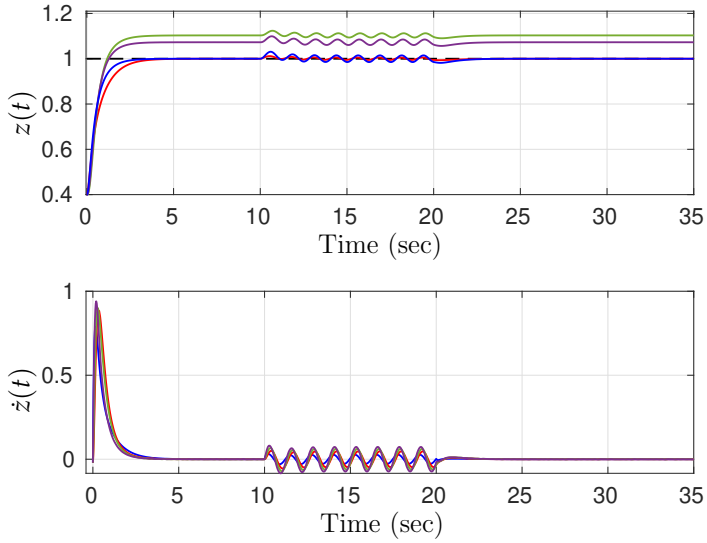

Figure 3.11: The system closed-loop response to a unity set point and to an exogenous sinusoidal disturbance signal $w(t) = \sin(5t) + 1$ for $t \in [10, 20]$sec. Example 3.

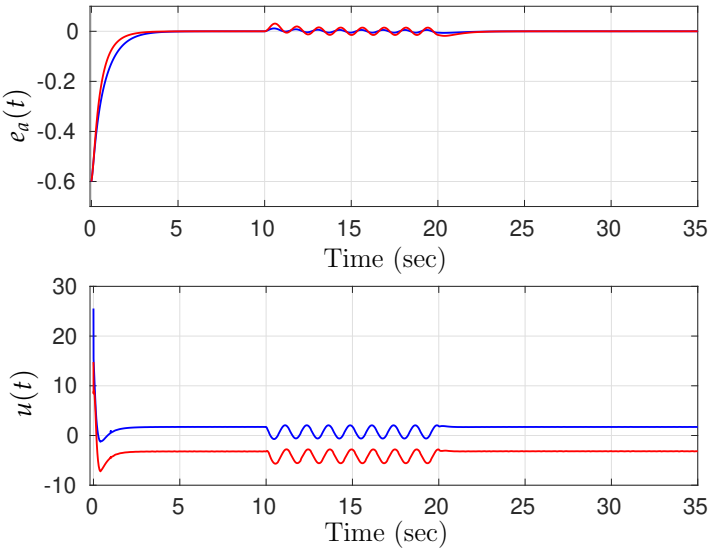

Figure 3.12: Closed-loop error response, and control signal $u(t)$ to a unity set point and to an exogenous sinusoidal disturbance signal $w(t) = \sin(5t) + 1$ for $t \in [10, 20]$sec. Example 3.

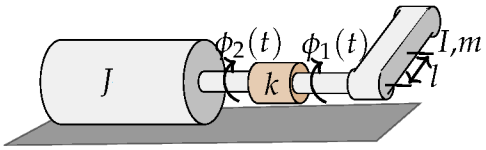

Figure 3.13: Flexible rotor coupled to an arm link. Example 4.

points of the rotor: $\varphi_1(t)$ in the side coupled to the link and $\varphi_2(t)$ in the side driven by the motor. A non-linearity of sweep-pendulum type can be noticed in the dynamical equations of the system derived by the Euler-Lagrange formulation:

$$\begin{aligned} I\ddot{\varphi}_1(t) + mgl\sin(\varphi_1(t)) + k[\varphi_1(t) - \varphi_2(t)] &= 0 \\ J\ddot{\varphi}_2 + k[\varphi_2(t) - \varphi_1(t)] &= u(t) \end{aligned} \tag{3.2}$$

Denoting the nonlinear term as

$$\sin(\varphi_1(t)) = \varphi_1(t)\ \text{sinc}\ (\varphi_1(t)), \tag{3.3}$$

the system time-varying stiffness matrix is given by:

$$S(t) = \begin{bmatrix} k + mgl\ \text{sinc}\ (\varphi_1(t)) & -k \\ -k & k \end{bmatrix}. \tag{3.4}$$

Now assuming that the swing angle of the link belongs in the interval $\varphi_1(t) \in [-\frac{\pi}{2}, \frac{\pi}{2}]$ such that $\text{sinc}(\varphi_1(t)) \in [\frac{2}{\pi}, 1]$, considering the nonlinear term in $\varphi_1(t)$ as the source of uncertainty for the system dynamics and setting values for the system parameters: $l = 0.1$, $m = 1$, $I = 0.05$, $J = 0.1$, $g = 10$, $k = 50$. This setup allow us to describe the system dynamics by an uncertain second-order linear model whose matrices belong to the polytopic set in (**??**) with vertices:

$$M_1 = M_2 = \begin{bmatrix} 0.05 & 0 \\ 0 & 0.1 \end{bmatrix}, D_1 = D_2 = \begin{bmatrix} 0 & 0 \\ 0 & 0 \end{bmatrix}, S_1 = \begin{bmatrix} 51 & -50 \\ -50 & 50 \end{bmatrix}, S_2 = \begin{bmatrix} 50.64 & -50 \\ -50 & 50 \end{bmatrix},$$

$$B_1 = B_2 = \begin{bmatrix} 0 & 1 \end{bmatrix}^T.$$

Thus with the controller design specifications: system closed-loop pole placement in the D-region defined as the intersection of the half-plane defined by $\text{Re}(s) < -5$, a conic sector centered at the origin and with inner angle given by $\theta = \pi/3$, and a disk with radius $\rho = 15$ as shown in Fig. 2.1. The Procedure 2.1 yields the PID controller gains:

$$K_P = \begin{bmatrix} -75.7438 & 69.9357 \end{bmatrix}, K_D = \begin{bmatrix} 3.2975 & -4.1265 \end{bmatrix}, K_I = -13.9027.$$

Table 3.3: Open-loop and closed-loop system poles at its vertices, Example 4.

$\varphi_1(t)$	Open-loop	Closed-loop
$-\frac{\pi}{2}$	$\pm 38.9023j$, $\pm 2.5705j$	$-8.0620 \pm 11.9675j$, -13.5952, $-5.7727. \pm 4.0952j$.
$\frac{\pi}{2}$	$\pm 38.8396j$, $\pm 2.0543j$	$-6.8103 \pm 9.9304j$, -5.9872, $-10.8284 \pm 6.7034j$.

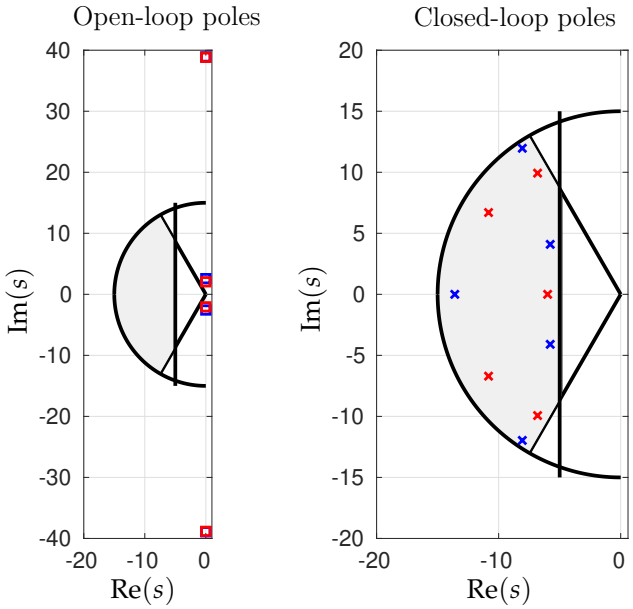

Figure 3.14: The left-hand figure shows the system finite open-loop poles and the right-hand one its closed-loop poles. The shaded area indicates the desired D-region for the system closed-loop pole placement. Example 4.

For the results analysis purposes, the open and closed-loop system poles at its vertices are summarized in Table 3.3. All closed-loop poles belong to the desired D-region as can be seen in the Fig. 3.14. Fig. 3.15 shows the response evolution of the closed-loop system state vector $z(t)$ and its derivative $\dot{z}(t)$ to a piece-wise constant set-point (dashed line). The displacement error paths $e_a(t)$ and the input signal $u(t)$, can be seen in Fig. 3.16. One can notice that the reference tracking depicts the expected response despite the nonlinear effect induced by the significant excursion range beyond the original rest positioning.

3.2 Second order systems subject to time delay

Example 1. In this example a standard benchmark is considered, the 3-DoF model for a wing in an airflow studied in Araujo and Santos 2020, the system matrices are given by:

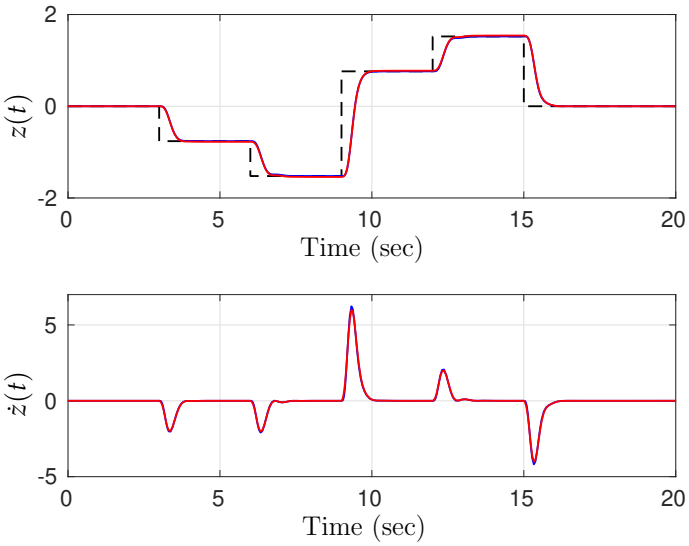

Figure 3.15: The system closed-loop response to a piece-wise constant set-point. Example 4.

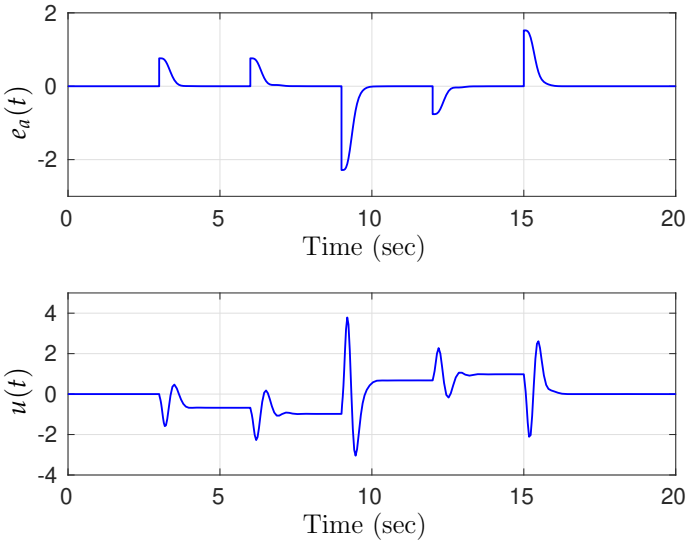

Figure 3.16: Closed-loop error response, and control signal $u(t)$. Example 4.

$$M = \begin{bmatrix} 17.6 & 1.28 & 2.89 \\ 1.28 & 0.824 & 0.413 \\ 2.89 & 0.413 & 0.725 \end{bmatrix}, \quad D = \begin{bmatrix} 7.66 & 2.5 & 2.1 \\ 0.23 & 1.04 & 0.223 \\ 0.6 & 0.756 & 0.658 \end{bmatrix}, \quad S = \begin{bmatrix} 121 & 18.9 & 15.9 \\ 0 & 27 & 0.145 \\ 11.9 & 3.64 & 15.5 \end{bmatrix},$$

$$B = \begin{bmatrix} 1 \\ 0 \\ 0 \end{bmatrix}, \quad U = B^T. \tag{3.5}$$

The delay value considered was $\tau = 0.2$, $\mu = 0.5\tau$, the decay rate of the system's response is $\delta = 0.6$, and parameter of the free matrix $\bar{F}$, $\alpha = 0.6$. The Procedure 2.2 yields the PID controller gains:

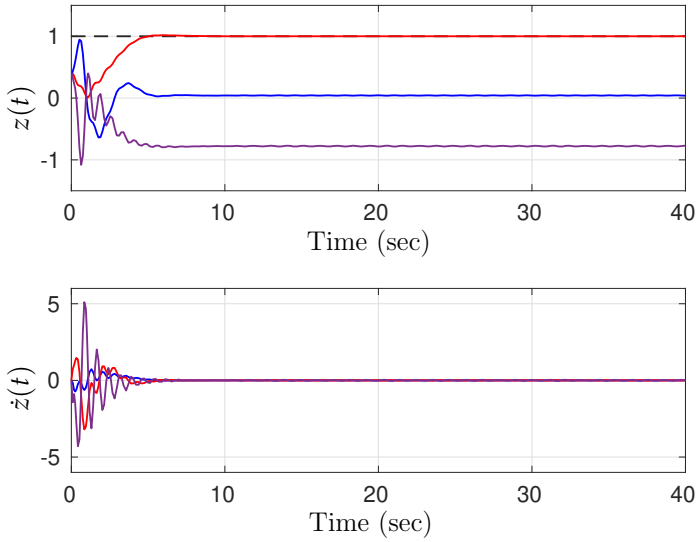

Figure 3.17: The system closed-loop response. Example 1.

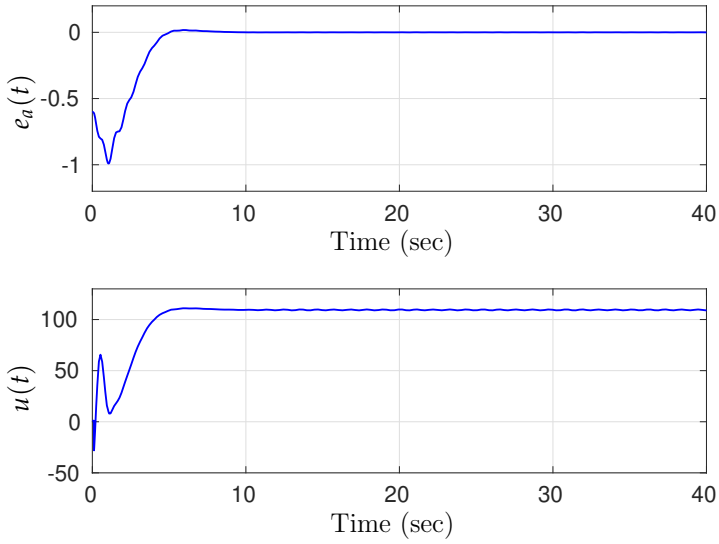

Figure 3.18: Closed-loop error response, and control signal $u(t)$. Example 1.

$$K_P = [-7.7475 \quad 15.5212 \quad 0.9003],\ K_D = [-75.0955 \quad -4.6038 \quad -12.3270],\ K_I = -66.2748.$$

For the results analysis, the Fig. 3.17 shows the evolution of the closed-loop system state vector, $z(t)$ and its derivative $\dot{z}(t)$ for a unity set-point. The displacement error paths $e_a(t)$ and the input signal $u(t)$, can be seen in Fig. 3.18.

Example 2. Consider the system studied in Ram et al. 2011, represented by matrices:

$$M = \begin{bmatrix} 1 & 0 \\ 0 & 1 \end{bmatrix},\ D = \begin{bmatrix} 1 & -1 \\ -1 & 1 \end{bmatrix},\ S = \begin{bmatrix} 3 & -2 \\ -2 & 3 \end{bmatrix}, B = \begin{bmatrix} 1 \\ 0 \end{bmatrix},\quad U = B^T. \tag{3.6}$$

For this example we considered a delay of $\tau = 0.4$, $\mu = 0.5\tau$, with a decay rate equal to $\delta = 0.1$, and the free matrix parameter $\bar{F}$, $\alpha = 0.8$. The PID controller gains obtained through the procedure 2.2 are

$$K_P = [0.2727 \quad -0.0513],\ K_D = [-1.1878 \quad -1.0302],\ K_I = -0.3308.$$

For the results analysis purposes, the Fig. 3.19 shows the response evolution of the closed-loop system state vector $z(t)$ and its derivative $\dot{z}(t)$ to a constant set-point (dashed line). The displacement error paths $e_a(t)$ and the input signal $u(t)$, can be seen in Fig. 3.20.

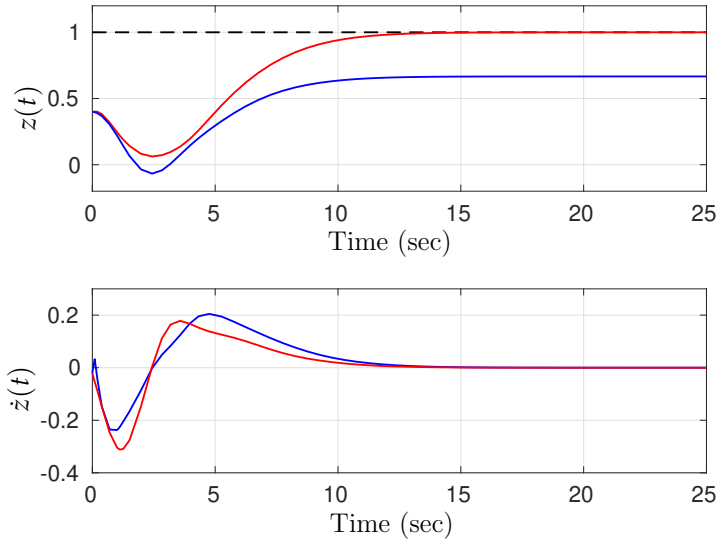

Figure 3.19: The system closed-loop response. Example 2.

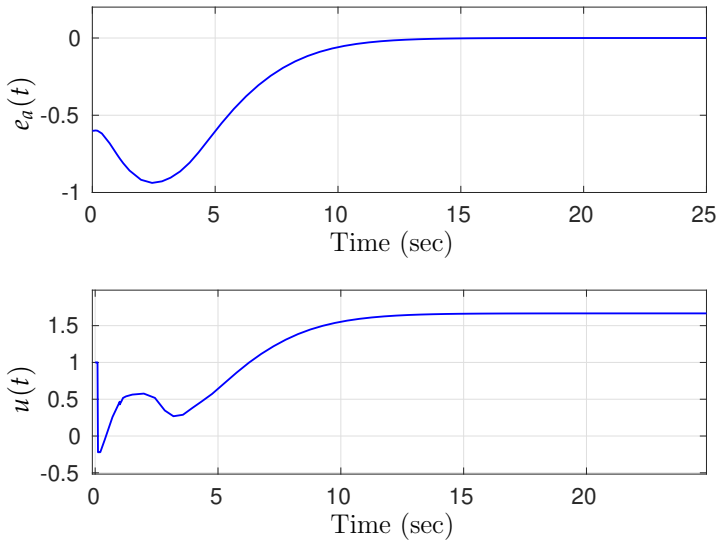

Figure 3.20: Closed-loop error response, and control signal $u(t)$. Example 2.

In the section 3.1, the results obtained through the procedure 2.1 were applied to four numerical examples, each one with its peculiarity, validating the proposed PID/PIDA controller for time-delay-free systems. In section 3.2 the PID controller obtained through the procedure 2.2 for systems subject to time delay in the control input was validated through two numerical examples. In the next Chapter, the PD/PID-LQR controller, and the observer-based controller from Chapter 2, are applied to a practical experiment of a mobile inverted pendulum.

4 Practical Experiment: Mobile Inverted Pendulum

In this chapter, a mobile inverted pendulum (MIP) is studied. The initial section is dedicated to obtaining a model for the inverted pendulum system based on the Lagrange equations. Subsequently, the second section provides an exposition of the experimental methods used to estimate some model parameters. Next, the third section covers the design of PID/PD-LQR and observer-based control, taking advantage of the techniques proposed in Chapter 2, and the results of the application of the controllers in the MIP, showing their effectiveness and performance.

The mobile inverted pendulum (MIP) is a robotic platform, similar to an autonomous vehicle with two independently driven wheels, highly extensible, and compatible with open standards. The existing development board in the MIP is the BeagleBone Black, based on Linux (BeagleBoard.org 2023). This board offers several functionalities, and allows the addition of sensors and hardware, according to the needs of the project to be executed. EduMIP, Fig.4.1, is a prototype of MIP, used in this thesis, which can be purchased at Hackster.io 2023.

Figure 4.1: EduMIP

The MIP is studied to illustrate and validate the design of PID/PD controllers based on the LQR control, and the design of the observer-based control. To implement the controllers, the `pyctrl` library, available at GitHub 2018, was used. The following section presents a model for the inverted pendulum system based on the Lagrange equations.

4.1 Modeling

Obtaining a model that characterizes the system will allow us to design a suitable controller for the MIP. To idealize the model, we will consider that the body and the wheels are rigid bodies and the friction between the wheels and the ground is zero. Consider the model for the MIP represented by Fig. 4.2.

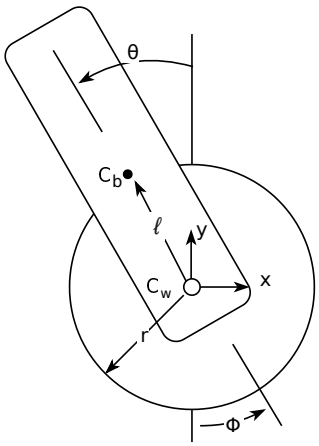

Figure 4.2: MIP system sketch

where x and y are the coordinates, the body angle (θ) and the wheel angle (ϕ), r represents the radius of the wheels, and ℓ is the distance between the center of mass of the wheels (C_w) and the center of mass of the body (C_b).

The model is obtained using the Lagrangian formalism, which allows us to obtain the equations of motion of a system systematically. The Lagrangian equations of motion for a system are written as:

$$\frac{d}{dt}\left(\frac{\partial L}{\partial \dot{q}_i}\right) - \frac{\partial L}{\partial q_i} = F_i \tag{4.1}$$

where:

q_i - represents one of the generalized coordinates;

$\dot{q}_i$ - represents the first time derivative of q_i;

L - the Lagrangian function;

F_i - non-conservative forces acting;

The Lagrangian function can be defined by:

$$L = T - U \tag{4.2}$$

where T is the kinetic energy, and P is the potential energy of the system. The kinetic energy of the system is given by the translational kinetic energy plus the rotational kinetic energy:

$$T = \frac{M_b}{2}V_B^2 + 2M_w V_w^2 + \frac{I_B}{2}\dot{\theta}^2 + 2\frac{I_w}{2}\dot{\phi}^2 \tag{4.3}$$

where:
M_b - mass of the body;
M_w - mass of a wheel;
V_b - translational velocity of the body;
V_w - translational speed of the wheels;
I_b - body inertia;
I_w - wheel inertia with gearbox;

The translational speed of the wheels can be easily obtained by first writing the position of M_w in cartesian coordinates (x_w, y_w). Given by $x_w(t) = -r\phi(t)$ and $y_w(t) = 0$. Then the center of mass of the wheels is:

$$C_w = (-r\phi(t), 0)$$

and the translational speed of the wheels is defined as

$$V_w = \dot{C}_w = (-r\dot{\phi}(t) + 0) \tag{4.4}$$

For body mass M_b, the position in cartesian coordinates are written as $x_b(t) = -r\phi(t) + \ell\ sin\ \theta(t)$ and $y_b(t) = \ell\ cos\ \theta(t)$. Then the center of mass of the body is given by:

$$C_b = (-r\phi(t) + \ell\ sin\ \theta(t), \ell\ cos\ \theta(t))$$

The translational speed of the body is:

$$V_b = \dot{C}_b = \big(-r\dot{\phi}(t) - \ell\dot{\theta}(t)cos\theta(t) - \ell\dot{\theta}(t)sin\theta(t)\big) \tag{4.5}$$

We define the inertia of the geared wheel as:

$$I_w = \frac{M_w r^2}{2} + R_g^2 I_a \tag{4.6}$$

where:
R_g− gearbox ratio;
I_a− inertia of the motor armature;

Substituting the equations (4.4), (4.5) and (4.6) in (4.3), we can describe the kinetic energy as:

$$T = \frac{M_b}{2}\left(\ell^2\dot{\theta}^2(t) + r^2\dot{\phi}^2(t) + 2\ell r\dot{\phi}(t)\dot{\theta}(t)\cos\theta\right) - M_w r^2\dot{\phi}^2(t) + \frac{I_b}{2}\dot{\theta}^2(t) + \frac{M_w}{2}r^2 + G_r^2 I_m \quad (4.7)$$

The potential energy of system is described as

$$U = M_b g y_b(t) = M_b g l cos\theta(t) \quad (4.8)$$

Subtracting the potential energy (4.8) from the kinetic energy (4.7) of the system that was determined, we find the value of the Lagrangian function L.

Now solving the Euler-Lagrange equations (4.1) in terms of the generalized coordinates θ and ϕ:

$$\begin{cases} \dfrac{d}{dt}\left(\dfrac{\partial L}{\partial \dot{\theta}}\right) - \dfrac{\partial L}{\partial \theta} = -F(t) & (4.9.1) \\ \dfrac{d}{dt}\left(\dfrac{\partial L}{\partial \dot{\phi}}\right) - \dfrac{\partial L}{\partial \phi} = F(t) & (4.9.2) \end{cases}$$

we find the following system of equations of motion

$$\begin{cases} I_b\ddot{\theta}(t) + M_b\ell^2\theta\ddot{(t)} - M_b\ell g\sin\theta(t) + M_b\ell r\ddot{\phi}(t)\cos\theta(t) = -F(t) & (4.10.1) \\ M_b r\ell\ddot{\theta}(t)\cos\theta(t) - M_b r\ell\dot{\theta}(t)^2\sin\theta(t) + \ddot{\phi}(t)2I_w + \ddot{\phi}r^2 M_B + \ddot{\phi}r^2 2M_w = F(t) & (4.10.2) \end{cases}$$

In this system $F(t)$ is the torque supplied by the motor, calculated as

$$F(t) = 2R_g(t_m n - C_m w_m) \quad (4.11)$$

where:

$n = V(t)/V_{max}$ - normalized motor duty cycle;

t_m - motor stall torque;

$V(t)$ - motor voltage;

V_{max} - maximum voltage of motor;

C_m - motor constant;

$w_m = R_g(\dot{\phi} - \dot{\theta})$ - motor armature speed.

Substituting (4.11) into (4.10), isolating the generalized variables, and setting the following substitution for simplicity:

$a = r^2(M_b + 2M_w) + 2I_w$

$b = M_b \ell r$

$c = I_b + M_b \ell^2$

$d = M_b \ell g$

$e = \frac{2R_g t_m}{V_{max}}$

$f = 2R_g^2 C_m$

Thus equation (4.10) is now:

$$\begin{cases} c\ddot{\theta}(t) - d\sin\theta(t) + b\cos\theta(t)\ddot{\phi}(t) = -eV(t) + f(\dot{\phi} - \dot{\theta}) & (4.12.1) \\ b\cos\theta(t)\ddot{\theta}(t) - b\sin\theta(t)\dot{\theta}(t)^2 + a\ddot{\phi}(t) = eV(t) - f(\dot{\phi} - \dot{\theta}) & (4.12.2) \end{cases}$$

Solving the equations for $\ddot{\theta}$ and $\ddot{\phi}$ in the equation (4.12), we have the nonlinear MIP model:

$$\begin{bmatrix} ac - b^2\cos^2\theta(t) & 0 \\ 0 & ac - b^2\cos^2\theta(t) \end{bmatrix} \begin{bmatrix} \ddot{\theta}(t) \\ \ddot{\phi}(t) \end{bmatrix} = \\ \begin{bmatrix} -bf\cos\theta(t) - af - b^2\sin\theta(t)\cos\theta(t)\dot{\theta}(t) & bf\cos\theta(t) + af \\ bf\cos\theta(t) + cf + bc\sin\theta(t)\dot{\theta}(t) & -bf\cos\theta(t) - cf \end{bmatrix} \begin{bmatrix} \dot{\theta}(t) \\ \dot{\phi}(t) \end{bmatrix} + \\ \begin{bmatrix} ad\sin\theta(t) \\ -bd\sin\theta(t)\cos\theta(t) \end{bmatrix} + \begin{bmatrix} -beV(t)\cos\theta(t) - ae \\ beV(t)\cos\theta(t) + ce \end{bmatrix} V(t) \qquad (4.13)$$

4.1.1 Linearization

Since the control design techniques we will employ in this example apply only to linear systems, the (4.13) equation set needs to be linearized. It is desired to linearize the system at an equilibrium point, approximating the non-linear behavior of the system by a linear model. Analyzing the differential equations, it turns out that equilibrium points are dependent on the value of θ and ϕ. There are two equilibrium points for the system, the equilibrium 1: $\theta(t) = \dot{\theta}(t) = \dot{\phi}(t) = V(t) = 0$, is an unstable equilibrium, where it is necessary to apply a control. And the equilibrium point 2, where $\theta(t) = \pi$, and the other variables are 0, is a stable equilibrium, which is reached without any control.

The (4.13) equations are linearized assuming that the system is close to the point of Equilibrium 1. Let θ_2 be a small deviation of the pendulum position from equilibrium, that is, $\theta = 0 + \theta_2$, we can use the following approximations of the nonlinear functions in our system equations:

$$\begin{gathered} \cos\theta = \cos(0 + \theta_2) \approx 1 \\ \sin\theta = \sin(0 + \theta_2) \approx \theta_2 = \theta \\ \dot{\theta}^2 = \dot{\theta_2}^2 \approx 0 \end{gathered} \qquad (4.14)$$

Substituting (4.14) in (4.13), we get the linearized model:

$$\begin{bmatrix} ac-b^2 & 0 \\ 0 & ac-b^2 \end{bmatrix} \begin{bmatrix} \ddot{\theta}(t) \\ \ddot{\phi}(t) \end{bmatrix} + \begin{bmatrix} f(a+b) & -f(a+b) \\ -f(b+c) & f(b+c) \end{bmatrix} \begin{bmatrix} \dot{\theta}(t) \\ \dot{\phi}(t) \end{bmatrix} + \begin{bmatrix} -ad & 0 \\ bd & 0 \end{bmatrix} \begin{bmatrix} \theta(t) \\ \phi(t) \end{bmatrix}$$
$$= \begin{bmatrix} e(a+b) \\ -e(b+c) \end{bmatrix} u(t) \tag{4.15}$$

Note that the obtained model is similar to the second-order model in (2.1), where the state vector is $z = [\theta \quad \phi]^T$.

4.2 System Identification

System identification is used to estimate the parameters of mathematical models of dynamical systems. In this context, the gray box modeling approach is used, which means that we have partial access to system information, both through experimental measurements and observations (Aguirre 2015; MathWorks n.d.; Zhuo 2017). The objective is to estimate the unknown parameters of the MIP mathematical model, represented by (4.15).

To perform the system identification, we conducted two experiments: the first was performed with the body angle θ, and the second with the wheel angle ϕ. During these experiments, we collected data from MIP input and output signal measurements. These measurements are used to infer the values of unknown parameters in the model.

Gray box modeling allows the combination of known information (theoretical modeling and known parameters) with information obtained from experimental data. In this way, we can improve the precision of the mathematical model of the MIP, making it closer to the real behavior of the system.

At the end of the identification process, we obtained the parameters of the MIP mathematical model, which is a more accurate representation of the real system, enabling the design of more efficient control strategies for the MIP. Next, we detail each of the experiments carried out.

4.2.1 Body angle θ experiment

In the first experiment, we collected data on the angular velocity of the MIP body while constraining the movement of the wheels. This restriction was made by holding the MIP by the wheels upside down. We then analyze the body data and identify parameters I_b, C_m, and t_m that are relevant to the mathematical model of the system.

Since the movement of the wheels is restricted, we can state that $\phi(t) = 0$, $\dot{\phi}(t) = 0$, and $\ddot{\phi}(t) = 0$. Then the equation of motion (4.12.1) can be rewritten:

$$c\ddot{\theta}(t) - d\sin\theta(t) = -eV(t) - f\dot{\theta}(t) \tag{4.16}$$

The experiment is carried out at equilibrium point 2, where $\theta(t) = \pi$, and the other variables are 0, resulting in a stable system. Linearizing the model around this equilibrium point, we obtain the model in reduced state space, which describes the relationship between the voltage $V(t)$ and the angular velocity of the body $\dot{\theta}(t)$:

$$\begin{bmatrix} \dot{\theta}(t) \\ \ddot{\theta}(t) \end{bmatrix} = \begin{bmatrix} 0 & 1 \\ -\frac{d}{c} & -\frac{f}{c} \end{bmatrix} \begin{bmatrix} \theta(t) \\ \dot{\theta}(t) \end{bmatrix} + \begin{bmatrix} 0 \\ -\frac{e}{c} \end{bmatrix} u(t) \tag{4.17}$$

We get the transfer function from $V(t)$ to $\dot{\theta}(t)$:

$$H(s)_{\dot{\theta}} = \frac{-\frac{e}{c}s}{s^2 + \frac{f}{c}s + \frac{d}{c}} \tag{4.18}$$

The chirp signal applied to the MIP is 1.85 V, so the PWM duty cycle is 25%, varying the frequency, starting at 1 Hz, gradually increasing to 20 Hz in 30 seconds, and decreasing in 30 seconds to 1 Hz. The response is shown in Figure 4.3:

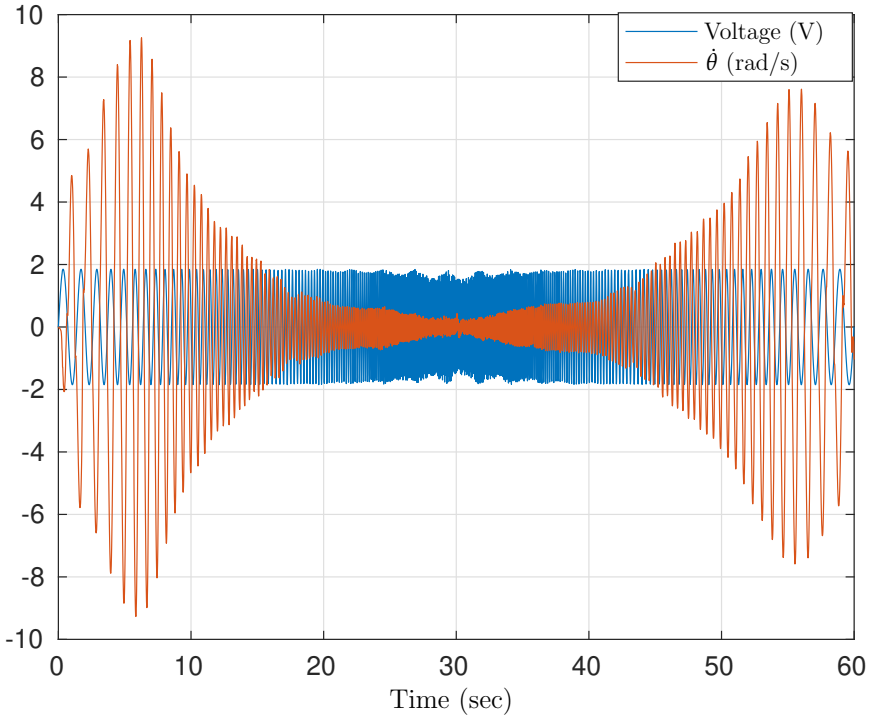

Figure 4.3: Experiment with body angle θ

From this experiment, we collect input (voltage V) and output (body angular velocity) data and then estimate the transfer function (4.19) using MatLab function `tfest`.

$$H(s)_{\dot{\theta}_{original}} = \frac{-30.11s - 52.49}{s^2 + 7.133s + 110.6} \tag{4.19}$$

It was necessary to move a zero from the estimated model (4.19) to obtain a transfer function in the same form as (4.18), to determine the parameters. We move a zero to the origin in MatLab as follows: for the obtained transfer function, we calculate the gain peak and the frequency where this peak occurs, using the `getPeakGain` function. We extract the numerical coefficients and denominators of the transfer function by applying `tfdata`. Subsequently, the peak gain is calculated for a transfer function with a zero at the origin, with the same denominator as the original function. With this, the ratio between the gain peaks of the two transfer functions, the original and the one with zero at the origin, is determined. Finally, the original new transfer function is obtained, inserting a new zero at the origin equal to the ratio of the two transfer functions and the unchanged denominator:

$$H(s)_{\dot{\theta}} = \frac{-30.52s}{s^2 + 7.133s + 110.6} \tag{4.20}$$

Note that the method used to obtain the transfer function allows us to obtain only an approximation. Given this, it is necessary to consider uncertainties in obtaining the transfer function, we consider an uncertainty of ±4%. In Fig. 4.4, we can analyze the Bode diagram of the transfer function in (4.20), with an uncertainty of ±4%. In Fig. 4.5 is a magnitude zoom, where we see the uncertainty better.

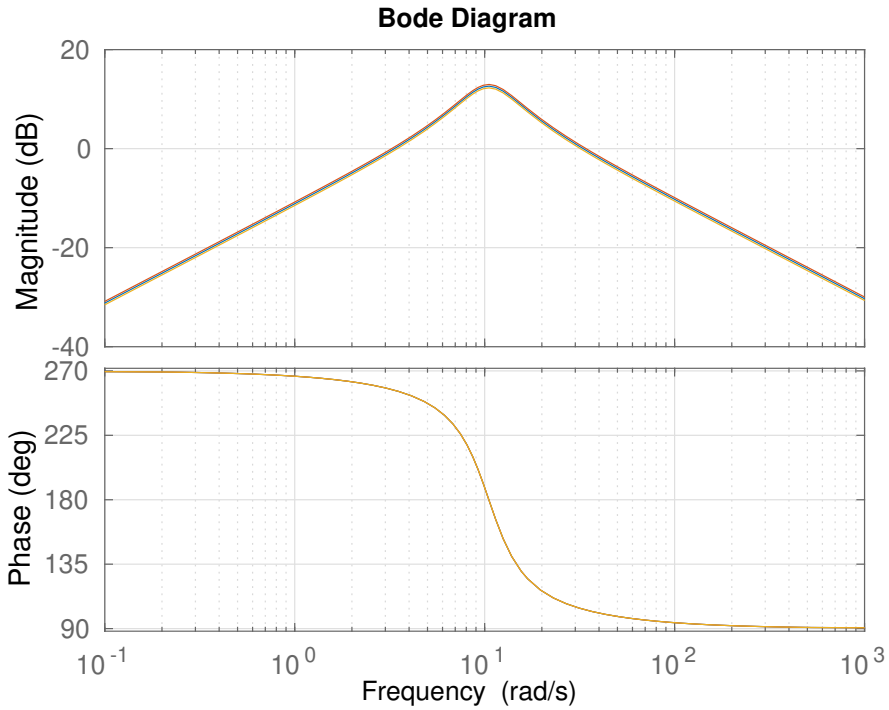

Figure 4.4: Bode diagram $H(s)_{\dot{\theta}}$

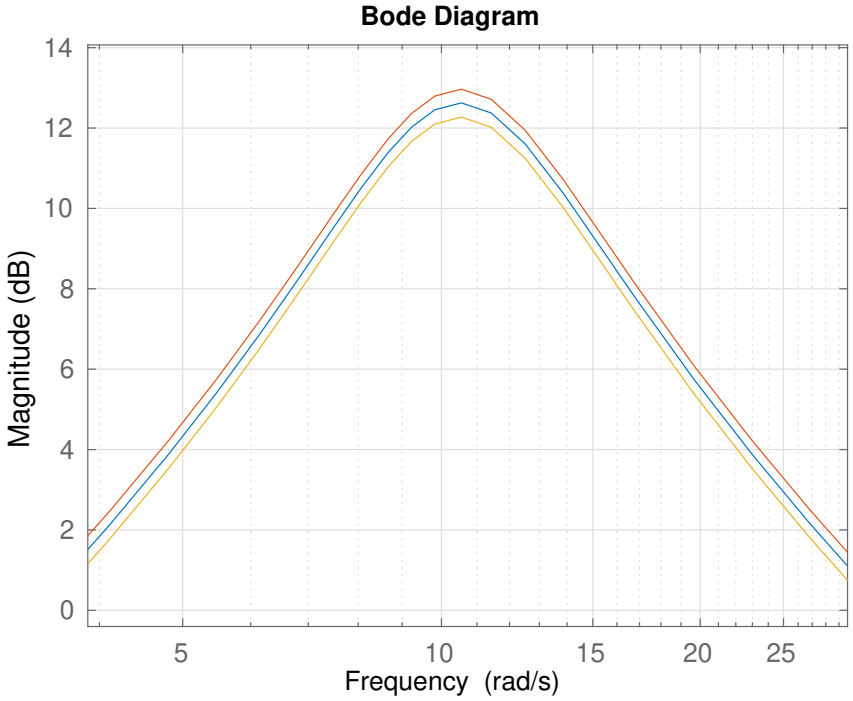

Figure 4.5: Close look at the Bode diagram, the blue line is the $H(s)_{\dot{\theta}}$, and the red and yellow lines are the transfer function with an uncertainty of ±4%.

4.2.2 Wheels angle ϕ experiment

The second experiment is carried out to observe the speed of the wheels, to identify the parameter I_w. The back of the MIP is placed on the table, as in Figure 4.6, and data regarding wheel speed is collected.

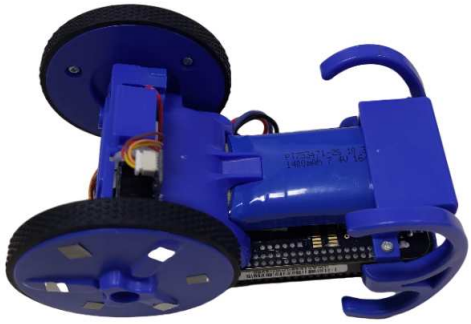

Figure 4.6: Experiment with wheels angle ϕ

As the body is not moving in this experiment and there is no speed of translation in the wheels, thus M_b and M_w terms. Then we rewrite:

$a = r^2(M_b + 2M_w) + 2I_w \Rightarrow a = 2I_w$

We can say that $\dot{\theta}(t) = 0$ and $\ddot{\theta}(t) = 0$, so there is only one equation of motion from (4.12):

$$\ddot{\phi}(t) = -\frac{f}{a}\dot{\phi}(t) + \frac{e}{a}u(t) \tag{4.21}$$

This model describes the relationship between the voltage V and angular velocity of wheels $\dot{\phi}(t)$. Convert the state-space model to a transfer function from $V(t)$ to $\dot{\phi}(t)$:

$$H(s)_{\dot{\phi}} = \frac{\frac{e}{a}}{s + \frac{f}{a}} \tag{4.22}$$

The chirp signal applied to the MIP is 1.85 V, that is, the PWM duty cycle is 25%, varying the frequency, starting at 0.3 Hz, gradually increasing to 30 Hz in 30 seconds, and gradually decreasing in 30 seconds to 0.3 Hz. The signal response is shown in Figure 4.7:

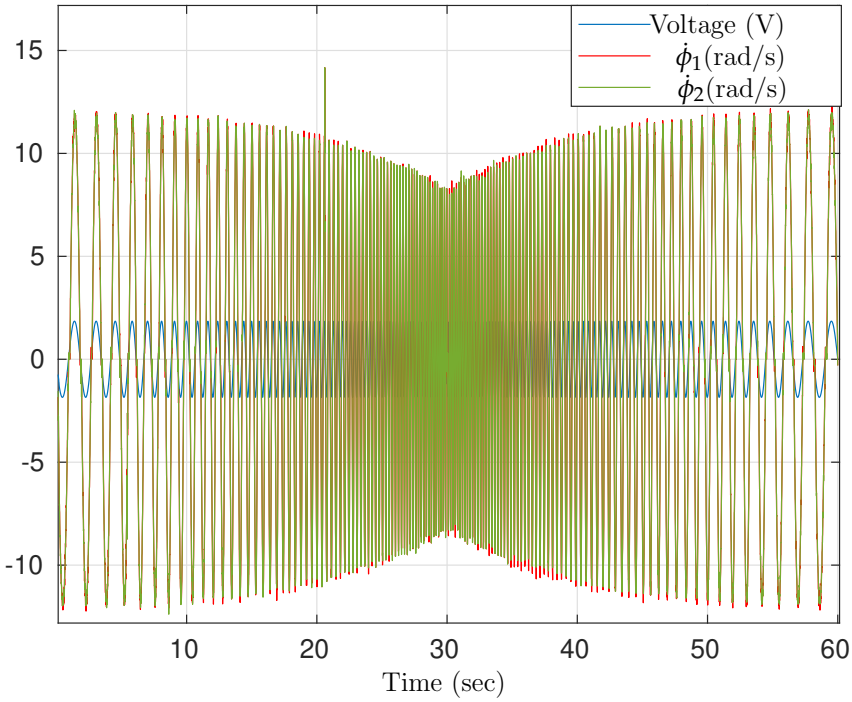

Figure 4.7: Wheel angle experiment ϕ, where the blue line is the input voltage and the red and green lines represent the speed of wheels 1 and 2, respectively. The red and green lines almost overlap as the speed data collected for both wheels was very close.

From this experiment, we collect input (voltage V) and output (angular velocity of wheels) data and then estimate the transfer function using MatLab function `tfest`. With the results of the experiment, we can estimate the transfer functions:

$$H(s)_{\dot{\phi}_1} = \frac{208.8}{s + 33.02} \tag{4.23}$$

$$H(s)_{\dot{\phi}_2} = \frac{208.5}{s + 33.32} \tag{4.24}$$

As in the body angle experiment, the transfer function obtained in this experiment is only an estimate, so there is uncertainty, considering a variation of $\pm 4\%$ in the transfer function of voltage (V) and angular speed of the wheels.

To identify the parameters of the experiments I_b, C_m, t_m, and I_w. We determine some values from the transfer functions (4.20), (4.23) and (4.24):

$$\frac{e}{c} = 30.52\Delta,\ \frac{f}{c} = 7.133,\ \frac{d}{c} = 110.6,\ \frac{e}{a} = 208.8\Delta,\ \frac{f}{a} = 33.02$$

where Δ represents an uncertainty of $\pm 4\%$ given by $\Delta = [0.96 \quad 1.04]$. Considering the above variables, and performing the necessary substitutions, we find the following parameters:

$$\begin{array}{rcccc} I_b & = & \frac{M_b g l - M_b l^2 (d/c)}{d/c} & = & 4.98 \times 10^{-4}\Delta \\ C_m & = & \frac{M_b g l (f/c)}{2R_g^2 (d/c)} & = & 2.39 \times 10^{-6}\Delta \\ t_m & = & \frac{M_b g l V_{max} (e/c)}{2R_g (d/c)} & = & 0.0027\Delta \\ I_w & = & \frac{M_b g l (e/c)}{2(d/c)(e/a)} & = & 6.1313 \times 10^{-5}\Delta \end{array}$$

After substituting these expressions, and the known parameters: $g = 9.8$, $V_{max} = 7.4$, $R_g = 35.37$, $M_b = 0.027$, $M_w = 0.263$ and $r = 0.034$, we get the linear model parameters (4.15): $a = 10^{-3} \times [0.4747 \quad 0.4639 \quad 0.4865]$, $b = 10^{-3} \times 0.3482$, $c = 10^{-3} \times 0.9641$, $d = 0.1066$, $e = [0.0282 \quad 0.0306]$ and $f = 0.0069$. Note that the parameters a and e, assume more than one value, due to Δ uncertainty. Substituting the parameters in (4.15), we obtain the matrices

$$M_1 = M_4 = 10^{-6} \times \text{diag}\{0.3365, 0.3365\},\ M_2 = 10^{-6} \times \text{diag}\{0.3260, 0.3260\},$$

$$M_3 = 10^{-6} \times \text{diag}\{0.3478, 0.3478\},$$

$$D_1 = D_4 = 10^{-5} \times \begin{bmatrix} -0.5659 & 0.5659 \\ 0.9024 & -0.9024 \end{bmatrix},\ D_2 = 10^{-5} \times \begin{bmatrix} -0.5584 & 0.5584 \\ 0.9024 & -0.9024 \end{bmatrix},$$

$$D_3 = 10^{-5} \times \begin{bmatrix} -0.5739 & 0.5739 \\ 0.9024 & -0.9024 \end{bmatrix},$$

$$S_1 = S_4 = 10^{-4} \times \begin{bmatrix} 0.5062 & 0 \\ -0.3712 & 0 \end{bmatrix},\ S_2 = 10^{-4} \times \begin{bmatrix} 0.4946 & 0 \\ -0.3712 & 0 \end{bmatrix},\ S_3 = 10^{-4} \times \begin{bmatrix} 0.5187 & 0 \\ -0.3712 & 0 \end{bmatrix},$$

$$B_1 = 10^{-4} \times \begin{bmatrix} -0.2324 & 0.3706 \end{bmatrix}^T,\ B_2 = 10^{-4} \times \begin{bmatrix} -0.2294 & 0.3706 \end{bmatrix}^T,$$

$$B_3 = 10^{-4} \times \begin{bmatrix} -0.2554 & 0.4015 \end{bmatrix}^T,\ B_4 = 10^{-4} \times \begin{bmatrix} -0.2518 & 0.4015 \end{bmatrix}^T,$$

$$F = \begin{bmatrix} 1 \\ 1 \end{bmatrix} \text{ and } C = \begin{bmatrix} 0 & 1 & 0 \\ 0 & 0 & 1 \end{bmatrix}. \tag{4.25}$$

where M_i, D_i, S_i and B_i of $i, \ldots, V$, where V is the number of vertices of o polytopic set P given in (**??**).

4.3 Controller Design

In this section, the designs and implementations of the PD/PID-LQR controllers and the observer-based controller in the MIP robot are carried out, whose control objective is to stabilize the MIP, that is, to keep it in a vertical position. Initially, the gains of the PD/PID-LQR controllers are obtained and the discretization process is presented, and the results are subsequently compared. Next, the observer-based controller gains are presented, along with the process of discretization and analysis of the results obtained.

4.3.1 Design of PD/PID-LQR controllers

Procedures 2.3 and 2.4 were carried out and the results were implemented in the acquired MIP system model. Initially, a Proportional-Derivative (PD) controller was obtained through the LQR approach. Then a Proportional-Integral-Derivative (PID) controller.

1. PD-LQR controller

   The second-order model obtained in (4.25) is rewritten as a representation of the reduced descriptor system in (2.11).

   The weighting matrices are: $Q = I_n$, and varying R: $R = 2$, $R = 3$ and $R = 5$. The choice of $Q = I$ is commonly used in LQR control, eliminating the need to adjust different weights for each state, each state is treated equally. By varying the values of R, it is possible to adjust the weight assigned to the control signals. Larger values of R increase the penalty associated with control effort, encouraging the controller to generate smoother control signals and reducing the effort required to control the system. On the other hand, smaller values of R reduce the penalty associated with control effort, allowing the controller to generate more aggressive control signals.

   Following the steps described in Procedure 2.4, the PD controller gains can be obtained. The resulting gains from the PD controller are summarized in Table 4.1.

   Table 4.1: PD controller gains, varying the weighting variable R.

R	K_P	K_D
1	[38.3431 1.0001]	[4.0221 1.5153]
2	[29.0634 0.7072]	[2.9553 1.1669]
5	[21.2689 0.4472]	[2.0587 0.8688]

2. PID-LQR controller

   The second-order model obtained in (4.25) is rewritten as a representation of the descriptor system in (2.8), defining $U = [0\ 1]$, among the ones we tested, the only matrix U that the LMIs of Theorem 2.4 return a feasible result, for other values of the matrix U

tested: $U = [0\ 1]$ and $U = I_2$, the system is not controllable, and LMIs are unfeasible. With $U = [0\ 1]$, the integral action acts only on the wheel speed ($\dot{\phi}$).

The weighting matrices are defined as $Q = I_n$, and varying R: $R = 2$, $R = 3$ and $R = 5$, to adjust the influence of the control signals on the control cost.

Following the steps described in Procedure 2.3, we obtain the resulting gains of the PID controller, summarized in Table 4.2.

Table 4.2: PID controller gains, varying the weighting variable R.

R	K_P	K_D	K_i
1	[41.0411 1.9873]	[4.3391 1.7000]	0.9997
2	[30.8834 1.4191]	[3.1781 1.2952]	0.7071
5	[22.2760 0.9197]	[2.1935 0.9469]	0.4472

For the results analysis purpose, the responses with the PD controllers gain, from Table 4.1, can be seen in Fig. 4.8, we can see that by varying R, noise and control effort decrease. In Fig. 4.9 we compare the MIP response to the PID controllers gain, in Table 4.2 considering the variation of parameter R, it is noted that for $R = 5$ the response is less noisy, for both controllers obtained the voltage does not exceed the maximum value of 7.4 V. Doing a more exhaustive search, and varying the weighting variables, the answer may improve. This is the advantage of designing controllers based on the LQR controller, you can adjust the weighting variables according to what project needs.

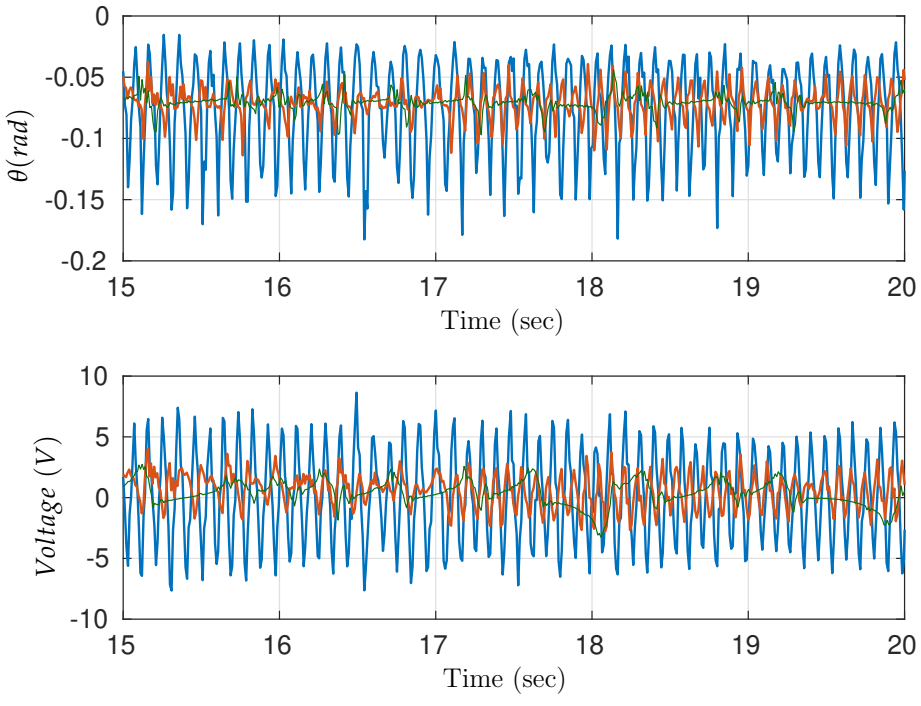

Figure 4.8: Response of body position (θ) and voltage, with PD controller, for $R = 1$, $R = 2$ and $R = 5$, blue, red and green line, respectively.

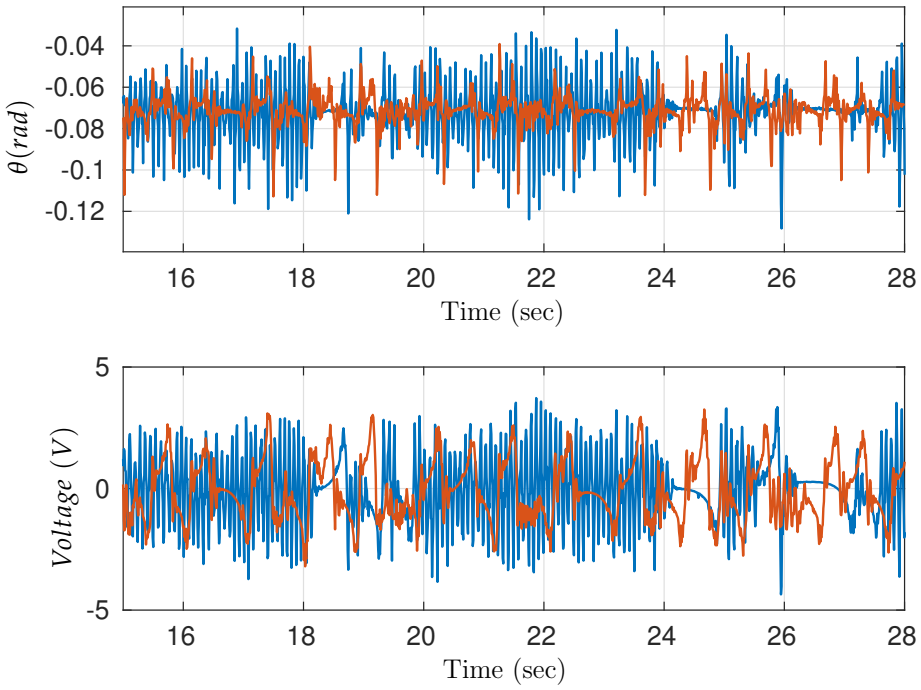

Figure 4.9: Response of body position (θ) and voltage, with PID controller, for $R = 2$ and $R = 5$, blue and red line, respectively.

Now, we compare the results of the PID controller with the PD. In Fig. 4.10, we analyze the position of the body. The MIP is initialized in a position close to the equilibrium point, and it can be observed that both controllers quickly stabilize the MIP. Fig. 4.11 shows that the position of the wheels for the PD controller varies a little, i.e., the MIP moves to keep the body in the balance position, unlike the PID, where the position of the wheels is maintained. This was expected since an integrator has been added. Regarding the control signal, neither exceeds the maximum voltage of 7.4 V.

The PD/PID-LQR controllers were discretized in state space to be implemented in the MIP system:

$$\begin{bmatrix} x_1(k+1) \\ x_2(k+1) \end{bmatrix} = \begin{bmatrix} 1 & 0 \\ T_s & 1 \end{bmatrix} \begin{bmatrix} x_1(k) \\ x_2(k) \end{bmatrix} + \begin{bmatrix} K_I \\ K_P \end{bmatrix} \begin{bmatrix} \dot{\theta} \\ \dot{\phi} \end{bmatrix}$$
$$y(k) = \begin{bmatrix} 0 & T_s \end{bmatrix} \begin{bmatrix} x_1(k) \\ x_2(k) \end{bmatrix} + K_d \begin{bmatrix} \dot{\theta} \\ \dot{\phi} \end{bmatrix} \tag{4.26}$$

The discretization step-by-step is in Appendix B.

4.3.2 Observer-based controller

In this section, we present observer-based controller applied in MIP. In order to simplify, we shall refer to the observer-based controller as PD/LQE controller. The second-order model obtained in (4.25) is rewritten as a representation of the reduced descriptor system in (2.11),

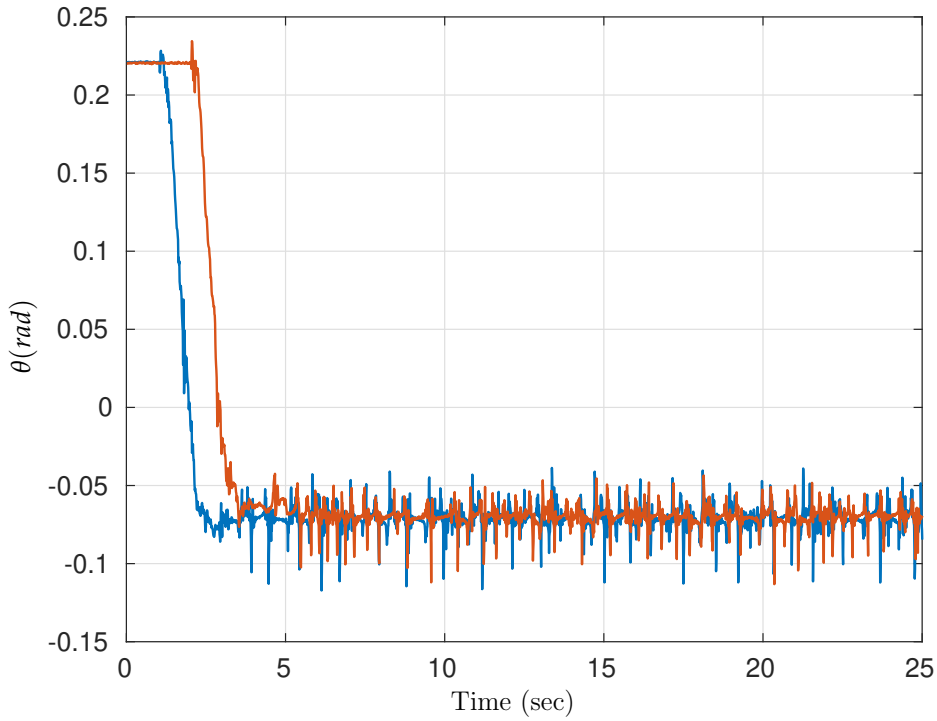

Figure 4.10: Response of body position (θ) and voltage, with PID controller (blue line), and PD controller (red line) for $R = 5$.

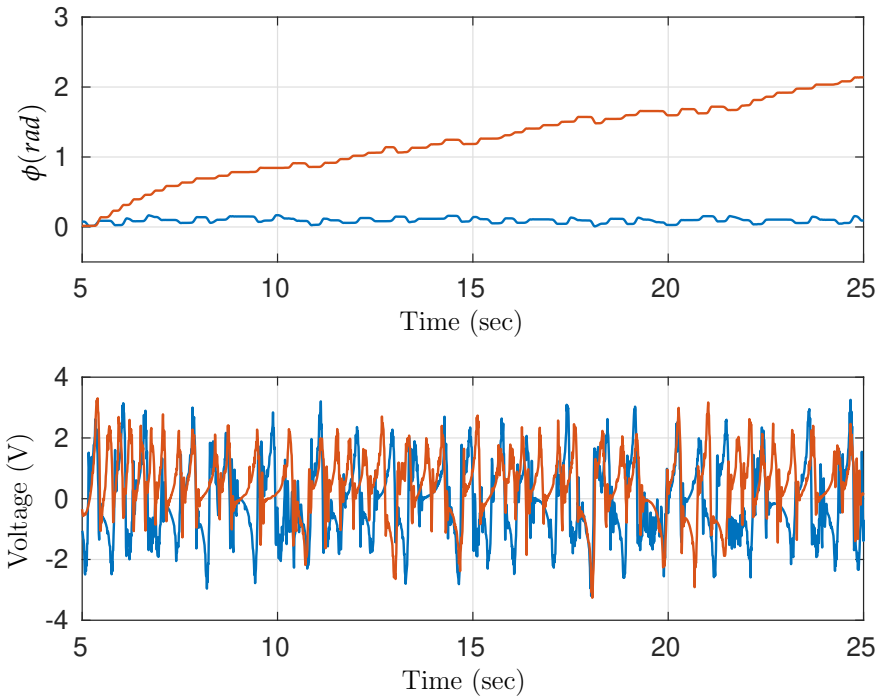

Figure 4.11: Response of wheel position and control signal V(t), with PID controller (blue line), and PD controller (red line) for $R = 5$.

the obtained descriptor system is not observable. Analyzing the obtained descriptor system, we can see that the state $\phi(t)$, has no impact on any other state. This is what happens in reality,

the MIP can balance if the body is vertical, no matter the position of the wheels, so it is a good option to reduce the state $\phi(t)$. After reduction, the system matrices are:

$$E_1 = \text{diag}\{1,\, 0.3365 \times 10^{-6},\, 0.3365 \times 10^{-6}\}, \ldots,\, E_4,$$

$$A_1 = \begin{bmatrix} 0 & 1 & 0 \\ 0.5062 \times 10^{-4} & -0.5659 \times 10^{-5} & 0.5659 \times 10^{-5} \\ -0.3712 \times 10^{-4} & 0.9024 \times 10^{-5} & -0.9024 \times 10^{-5} \end{bmatrix}, \ldots,\, A_4,$$

$$B_1 = 10^{-4} \times \begin{bmatrix} 0 & -0.2518 & 0.4015 \end{bmatrix}^T, \ldots,\, B_4,$$

$$C = \begin{bmatrix} 0 & 1 & 0 \\ 0 & 0 & 1 \end{bmatrix}, B_w = \begin{bmatrix} 0 & 1 & 1 \end{bmatrix}^T. \tag{4.27}$$

where E_i, A_i and B_i from $i, \ldots, 4$, the vertices of the polytopic set. And the states vector is $x^T(t) = [\theta \;\; \dot{\theta} \;\; \dot{\phi}]$. The descriptor system with these matrices is observable.

Considering the reduced MIP model matrices as given in (4.27), and defining the weight matrices for the LQE as $Q_F = \sqrt{\text{diag}\{0.01,\, 0.1\}}$ and $R_F = [2\hat{E}^{-1}\hat{B}_u \;\; 0]^T$, chosen using an iterative fitting process based on systematic experimentation. LQR weighting matrices are defined as $Q = I_n$, while R is varied. Following the steps described in Procedure 2.4, in step 1, we consider the matrices reduced in 4.27. Then, following the steps in Procedure 2.5, we obtain the gains for the reduced PD controller and the LQE estimator. The resulting gains are summarized in Table 4.3.

Table 4.3: PD/LQE gains, varying the weighting variable R.

R	K_P	K_D	L
1	[34.6136 3.6216]	1.2728	$10^3 \times \begin{bmatrix} -0.0019 & -0.0005 \\ -1.2599 & 0.1975 \\ 1.9754 & -0.3320 \end{bmatrix}$
2	[26.3376 2.6619]	0.9914	$10^3 \times \begin{bmatrix} -0.0018 & -0.0004 \\ -1.2580 & 0.1976 \\ 1.9763 & -0.3302 \end{bmatrix}$

Next, step by step discretization of the observer-based controller will be shown. As an illustrative example, we consider the PD/LQE controller with $R = 2$, according to Table 4.3. The controller transfer function is then specified:

$$H(s)_{PD/LQE\ (\dot{\theta})} = \frac{-1436.1(s + 9.031)(s + 88.33)}{(s + 1694)(s + 10.45)(s + 5.039)}$$

$$H(s)_{PD/LQE\ (\dot{\phi})} = \frac{188.18(s - 232.5)(s + 1.992)}{(s + 1694)(s + 10.45)(s + 5.039)} \tag{4.28}$$

In the transfer functions obtained, all poles of the controller have a negative real part, resulting in a stable controller. Next, we will discretize the controller at 100 Hz, which is the

frequency at which the MIP works. Although the controller is stable, we can notice in (4.28) that some poles and zeros have very high values. Since we are going to discretize the controller at 100 Hz, all poles and zeros above or close to this frequency can generate random results, disturbing the discretization of the system. To address this issue, we chose to remove the pole at 1694 and the zero at 232.5. The reduced controller is a second-order controller with the specified poles and zeros removed.

$$H(s)_{PD/LQE(\dot{\theta})\ reduced} = \frac{-0.8476(s+9.031)(s+88.33)}{(s+5.039)(s+10.45)}$$
$$H(s)_{PD/LQE(\dot{\phi})\ reduced} = \frac{-25.831(s+1.992)}{(s+5.039)(s+10.45)} \tag{4.29}$$

The bode diagram in Figure 4.12 shows the comparison between the obtained transfer functions. In red, $H(s)$ given in (4.28), and in blue, reduced $H(s)$, given in (4.29).

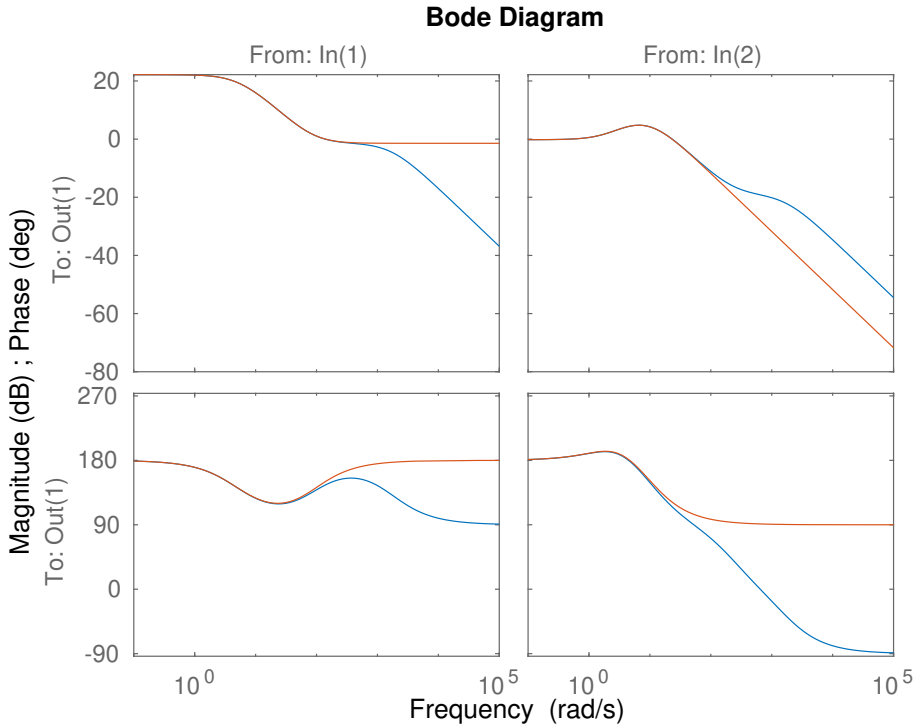

Figure 4.12: Bode Diagram: Controller Order Comparison

Next, we performed the discretization of the reduced order model at 100 Hz, adapting it for implementation in the MIP system. We used the zero-order hold method, generating an exact time-domain discretization for staircase inputs. The resulting discretized model in state space is:

$$PD/LQE_{discrete} = \left[\begin{array}{cc|cc} 0.9008 & 0.1481 & -0.08405 & -0.03019 \\ 0 & 0.9509 & -0.02148 & 0.00599 \\ \hline 8 & 0 & -0.8477 & 0 \end{array}\right] \tag{4.30}$$

All PD/LQE controllers obtained in Table 4.3 were discretized before being applied in the MIP. Fig. 4.13 shows the position of the body for $R = 1$ and $R = 3$. There was not a significant effect on noise suppression with the variation of R, which can be attributed to the chosen values of R.

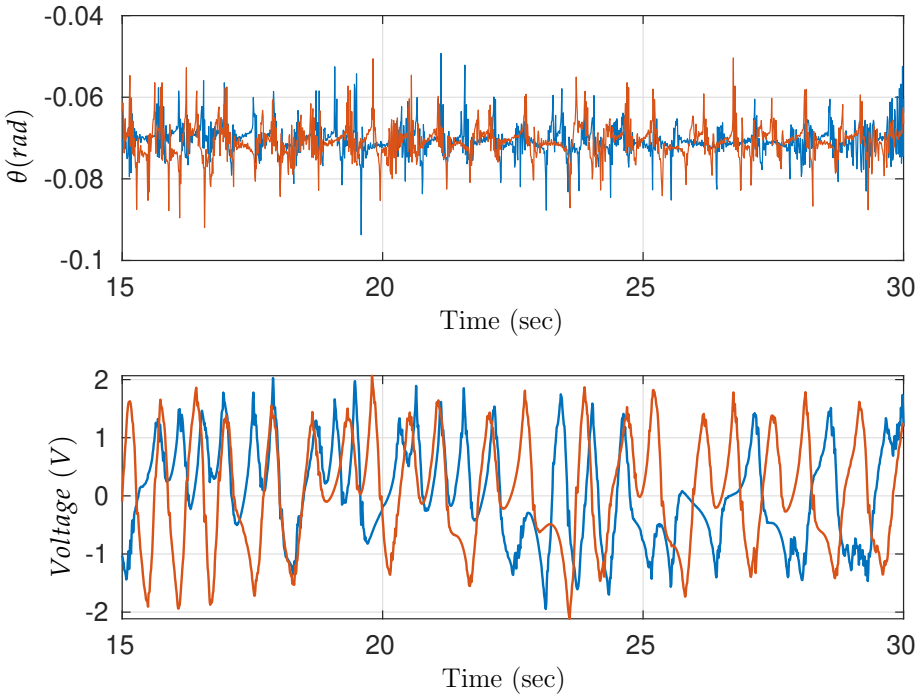

Figure 4.13: Response of body position (θ) and voltage, with PD/LQE controller, for $R = 1$ and $R = 2$, blue and red line, respectively.

Next, the MIP results with the PID controller are compared with the PD/LQE controller. In Fig. 4.14, it is possible to compare the position of the body, both quickly converge to the equilibrium point, with body position in the closest range, we can observe that the response is similar. Regarding the motor voltage response in Fig. 4.15, both controllers limit the applied voltage to 3V, which is far from the 7.4V limit. This shows that both controllers are effective in controlling the MIP within the desired voltage range. In Fig. 4.16, the position of the wheels for the PID controller remains more constant compared to the PD/LQE control, which is an advantage of using PID control. This is because the PID controller is capable of integrating the position error and generating a control action proportional to the magnitude and duration of the error. This allows the control system to continuously adjust the position of the wheels to compensate for any deviation and maintain a more constant position. As for the speed of the wheels, according to our analysis, when the MIP tried to stay vertical from a certain angle, the wheels would shoot to the same side as the direction of the fall to achieve equilibrium.

Analyzing the obtained results, we see that the variation of the weighting matrices of the PD/PID-LQR controller is a flexible approach that allows to adjusting the performance and the characteristics of the system according to specific requirements. Increasing the value of the

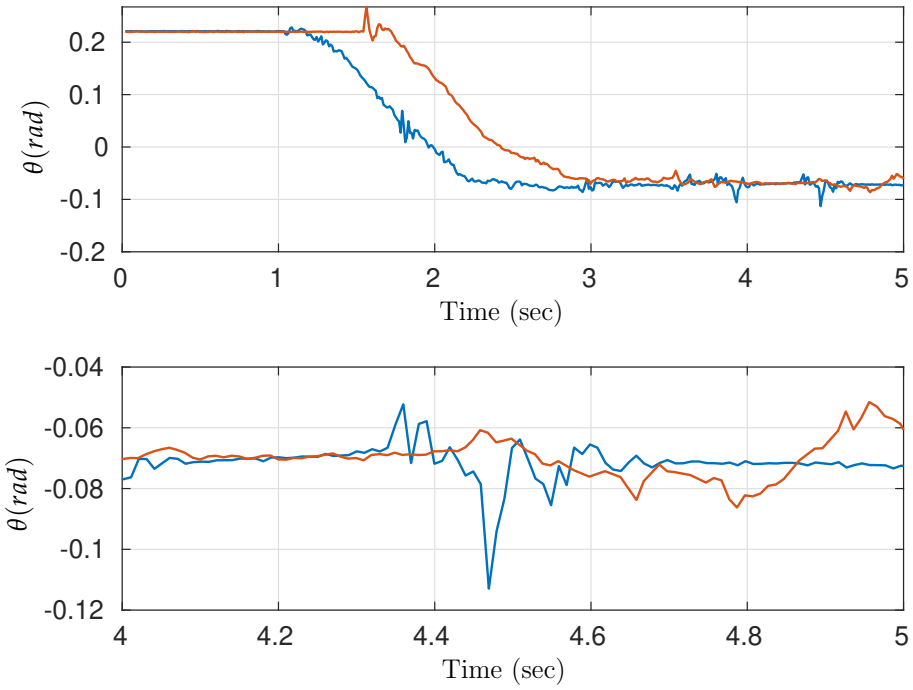

Figure 4.14: Response of body position (θ), with PID controller (blue line) for $R = 5$, and PD/LQE controller (red line) for $R = 2$.

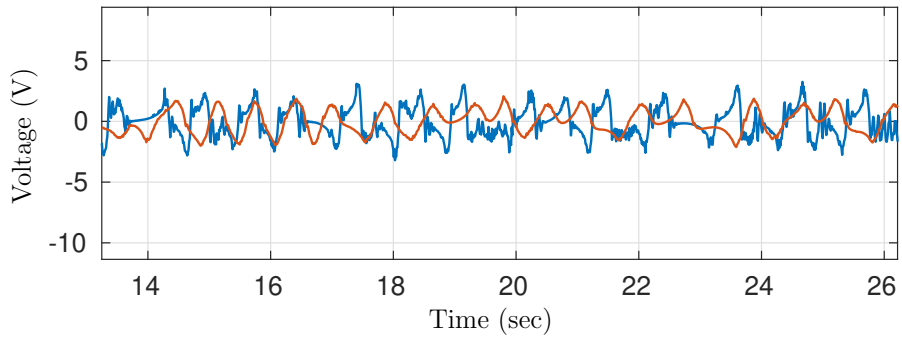

Figure 4.15: Control signal, with PID controller (blue line) for $R = 5$, and PD/LQE controller (red line) for $R = 2$.

weighting parameter R resulted in greater control input penalties, leading to smoother MIP control. When comparing the MIP displacement (ϕ), we noticed that the PID controller kept the MIP in a more constant position than the other PD and PD/LQE controllers, with the advantage of adding the integral of the error in the control. All proposed controllers were able to stabilize the MIP, each with its distinct characteristics.

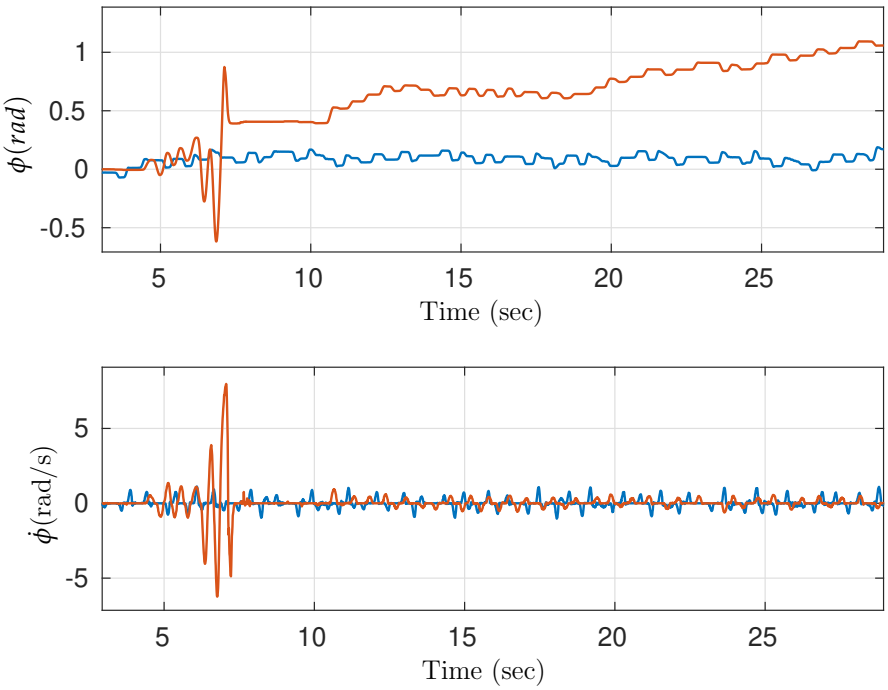

Figure 4.16: Response of wheel position and speed, with PID controller (blue line) for $R = 5$, and PD/LQE controller (red line) for $R = 2$.

5 Concluding Remarks

This work investigated the control of second-order systems with and without time delay and proposed new methods. The first contribution, presented in Chapter 2, proposes a robust framework to design multivariable Proportional-Integral-Derivative (PID) and Proportional-Integral-Derivative-Acceleration (PIDA) controllers to control systems modeled by second-order differential equations. The PID controller covers both free of time delay and with input time delay systems, while the PIDA only includes free of time delay systems.

The integral action of the controllers provides additional design flexibility, while acceleration action is proposed to solve the regularization problem. One of the main benefits of the proposed framework comes from the fact that the design approach is systematic. Hence, integral and acceleration gains bring no relevant drawback with respect to design complexity, despite the benefits with respect to performance improvement, and regularization effect. Relevant control challenges such as modeling error, regulatory performance optimization, regional pole allocation, saturation prevention, input delay, and LQR cost function are addressed within the design approach via linear matrix inequality (LMI). Furthermore, an observer-based controller design was developed for second-order systems.

In Chapter 3, simulation case studies are presented to illustrate the usefulness of the proposed methodology. A practical experiment using an inverted pendulum mobile (MIP) system is presented in Chapter 4; the state space model of the MIP was derived using the Lagrangian method. Subsequently, two system identification experiments were conducted to achieve a more accurate model. The obtained controllers were then implemented in the MIP robot, and the results were validated.

The choice of the U matrix in the examples in Chapter 3 and in the experiments in Chapter 4 was made randomly, taking into account only the controllability of the system. A proposal to continue the results presented is a more in-depth analysis, defining conditions for choosing the U matrix.

5.1 Publications

The publications related to the contributions of this thesis are listed below:

- Gontijo D. G., J. M. Araújo, T. L. Santos and F. O. Souza. "Proportional-Integral-Derivative-Acceleration Robust Controllers for Vibrating Systems". In *Journal of Vibration and Control*. 29.5-6 (2023): 1243-1253.

- Gontijo D. G., F. O. Souza, J. M. Araújo. "Robust PID Controller for Second-Order Systems plus Time Delay". In *XXIV Congresso Brasileiro de Automática* (2022), Fortaleza-CE, Brasil.

Bibliography

Abdelaziz, T. (2013). “Robust pole placement for second-order linear systems using velocity-plus-acceleration feedback”. In: *IET Control Theory and Applications* 7.14, pp. 1843–1856.

Abdelaziz, T. H. (2014a). “Parametric approach for eigenstructure assignment in descriptor second-order systems via velocity-plus-acceleration feedback”. In: *Journal of Dynamic Systems, Measurement, and Control* 136.4, p. 044505.

Abdelaziz, T. H. (2014b). “Parametric approach for eigenstructure assignment in descriptor second-order systems via velocity-plus-acceleration feedback”. In: *Journal of Dynamic Systems, Measurement, and Control* 136.4, p. 044505.

Abdelaziz, T. H. (2015a). “Robust pole assignment using velocity–acceleration feedback for second-order dynamical systems with singular mass matrix”. In: *ISA transactions* 57, pp. 71–84.

Abdelaziz, T. H. (2015b). “Robust pole assignment using velocity plus acceleration feedback for second-order dynamical systems with singular mass matrix”. In: {*ISA*} *Transactions* 57, pp. 71 –84.

Acevedo, M., M. T. Orvaãnos Guerrero, R. Velázquez, and V. Arakelian (2020). “An Alternative Method for Shaking Force Balancing of the 3RRR PPM through Acceleration Control of the Center of Mass”. In: *Applied Sciences* 10.4. ISSN: 2076-3417.

Adamson, L., S. Fichera, and J. Mottershead (2020). “Receptance-based robust eigenstructure assignment”. In: *Mechanical Systems and Signal Processing* 140, p. 106697. ISSN: 0888-3270.

Aguirre, L. A. (2015). *Introdução à Identificação de Sistemas–Técnicas Lineares e Não-Lineares Aplicadas a Sistemas Reais*. Editora UFMG. ISBN: 978-85-423-0079-6.

Alavinasab, A., H. Moharrami, and A. Khajepour (2006). “Active control of structures using energy-based LQR method”. In: *Computer-Aided Civil and Infrastructure Engineering* 21.8, pp. 605–611.

Alfadhli, A., J. Darling, and A. J. Hillis (2018). “The control of an active seat with vehicle suspension preview information”. In: *Journal of Vibration and Control* 24.8, pp. 1412–1426.

Almeida, M. O. de and J. M. Araújo (2019). “Partial Eigenvalue Assignment for LTI systems with D-stability and LMI”. In: *Journal of Control* 30, pp. 2195–3899.

Araújo, J. M., C. E. T. Dórea, L. M. G. Gonçalves, J. B. P. Carvalho, and B. N. Datta (2018). "Robustness of the Quadratic Partial Eigenvalue Assignment using Spectrum Sensitivities for State and Derivative Feedback Designs". In: *Journal of Low Frequency Noise, Vibration & Active Control* 37.2, pp. 253–268.

Araujo, J. M. and T. L. Santos (2020). "Control of second-order asymmetric systems with time delay: Smith predictor approach". In: *Mechanical Systems and Signal Processing* 137, p. 106355.

Araújo, J. M. and T. L. M. Santos (2018). "Control of a class of second-order linear vibrating systems with time-delay: Smith predictor approach". In: *Mechanical Systems and Signal Processing* 108, pp. 173–187.

Argentim, L. M., W. C. Rezende, P. E. Santos, and R. A. Aguiar (2013). "PID, LQR and LQR-PID on a quadcopter platform". In: *2013 International Conference on Informatics, Electronics and Vision (ICIEV)*. IEEE, pp. 1–6.

BeagleBoard.org (2023). urlhttps://beagleboard.org/p/edumip/edumip-13a29c. accessed on July 13, 2023.

Belotti, R. and D. Richiedei (Mar. 2020). "Pole assignment in vibrating systems with time delay: An approach embedding an a-priori stability condition based on Linear Matrix Inequality". In: *Mechanical Systems and Signal Processing* 137, p. 106396.

Bender, D. and A. Laub (1987). "The linear-quadratic optimal regulator for descriptor systems". In: *IEEE Transactions on Automatic Control* 32.8, pp. 672–688.

Boyd, S., L. E. Ghaoui, E. Feron, and V. Balakrishnan (1994). *Linear Matrix Inequalities in System and Control Theory*. Society for Industrial and Applied Mathematics.

Cai, Y.-F., J. Qian, and S.-F. Xu (2010). "The formulation and numerical method for partial quadratic eigenvalue assignment problems". In: *Numerical Linear Algebra with Applications* 18.4, pp. 637–652.

Chen, Y., W. Zhang, and H. Gao (2010). "Finite frequency H_∞ control for building under earthquake excitation". In: *Mechatronics* 20.1, pp. 128–142.

Chilali, M. and P. Gahinet (1996). "H_∞ design with pole placement constraints: an LMI approach". In: *IEEE Transactions on Automatic Control* 41.3, pp. 358–367.

Chu, E. and B. Datta (1996). "Numerically robust pole assignment for second-order systems". In: *International Journal of Control* 64.6, pp. 1113–1127.

Datta, B. (2003). *Numerical Methods for Linear Control Systems*. Academic Press.

Datta, S. (2017). "Feedback Controller Norm Optimization for Linear Time Invariant Descriptor Systems With Pole Region Constraint". In: *IEEE Transactions on Automatic Control* 62.6, pp. 2794–2806.

Demetriou, M. A. (2004). "Natural second-order observers for second-order distributed parameter systems". In: *Systems & control letters* 51.3-4, pp. 225–234.

Du, H. and N. Zhang (2008). "H_∞ control for buildings with time delay in control via linear matrix inequalities and genetic algorithms". In: *Engineering Structures* 30.1, pp. 81–92.

Fenili, E. P., F. O. Souza, and L. A. Mozelli (2014). "Sintonia de PID via LMIs: imposiçao de tempo de acomodaçao em sistemas com retardo no tempo incerto". In: *Anais do XX Congresso Brasileiro de Automática*, pp. 1127–1134.

Franklin, T. S., J. M. Araújo, and T. L. Santos (2021). "Receptance-based robust stability criteria for second-order linear systems with time-varying delay and unstructured uncertainties". In: *Mechanical Systems and Signal Processing* 149, p. 107191. ISSN: 0888-3270.

Gahinet, P., A. Nemirovskii, A. J. Laub, and M. Chilali (1994). "The LMI control toolbox". In: *Proceedings of 1994 33rd IEEE Conference on Decision and Control*. Vol. 3. IEEE, pp. 2038–2041.

Gielen, R., S. Olaru, M. Lazar, W. Heemels, N. van de Wouw, and S.-I. Niculescu (2010). "On polytopic inclusions as a modeling framework for systems with time-varying delays". In: *Automatica* 46.3, pp. 615–619. ISSN: 0005-1098.

GitHub (2018). *pyctrl: a Python Suite for Systems and Control*. urlhttps://github.com/mcdeoliveira/pyctrl. accessed on July 13, 2023.

Gudarzi, M. (2015). "μ-Synthesis controller design for seismic alleviation of structures with parametric uncertainties". In: *Journal of Low Frequency Noise, Vibration and Active Control* 34.4, pp. 491–511.

Hackster.io (2023). urlhttps://www.hackster.io/renaissance-robotics/products/edumip?ref=project-13a29c. accessed on July 13, 2023.

Hayati, H., D. Eager, A.-M. Pendrill, and H. Alberg (2020). "Jerk within the Context of Science and Engineering—A Systematic Review". In: *Vibration* 3.4, pp. 371–409. ISSN: 2571-631X.

He, J.-B., Q.-G. Wang, and T.-H. Lee (2000). "PI/PID controller tuning via LQR approach". In: *Chemical Engineering Science* 55.13, pp. 2429–2439.

Heidari, A. H., S. Etedali, and M. R. Javaheri-Tafti (2018). "A hybrid LQR-PID control design for seismic control of buildings equipped with ATMD". In: *Frontiers of Structural and Civil Engineering* 12, pp. 44–57.

Henrion, D., M. Sebek, and V. Kucera (2005). "Robust pole placement for second-order systems: an LMI approach". In: *Kybermetika* 41.1, pp. 1–14.

Hu, T., A. R. Teel, and L. Zaccarian (2006). "Stability and Performance for Saturated Systems via Quadratic and Nonquadratic Lyapunov Functions". In: *IEEE Transactions on Automatic Control* 51.11, pp. 1770–1786.

Kumar, E. V. and J. Jerome (2013). "Robust LQR controller design for stabilizing and trajectory tracking of inverted pendulum". In: *Procedia Engineering* 64, pp. 169–178.

Kwon, O., M.-J. Park, J. H. Park, and S.-M. Lee (2016). "Stability and stabilization of TS fuzzy systems with time-varying delays via augmented Lyapunov-Krasovskii functionals". In: *Information Sciences* 372, pp. 1–15.

Li, H., H. Liu, C. Hilton, and S. Hand (2013). "Non-fragile H_∞ control for half-vehicle active suspension systems with actuator uncertainties". In: *Journal of Vibration and Control* 19.4, pp. 560–575.

Li, W., B Luo, and H Huang (2016). "Active vibration control of flexible joint manipulator using input shaping and adaptive parameter auto disturbance rejection controller". In: *Journal of Sound and Vibration* 363, pp. 97–125.

Li, W. and X. Chen (2013). "Compensation of hysteresis in piezoelectric actuators without dynamics modeling". In: *Sensors and Actuators A: Physical* 199, pp. 89–97.

Lipták, T., M. Kelemen, A. Gmiterko, I. Virgala, and D. Hroncová (2017). "Input-state Linearization of Mechanical System". In: *American Journal of Mechanical Engineering* 5.6, pp. 298–302. ISSN: 2328-4110.

MathWorks (n.d.). *System Identification Overview*. urlhttps://www.mathworks.com/help/ident/gs/about-system-identification. accessed on July 14, 2023.

Mottershead, J. E., M. G. Tehrani, S. James, and Y. M. Ram (2008). "Active vibration suppression by pole-zero placement using measured receptances". In: *Journal of Sound and Vibration* 311.3, pp. 1391 –1408.

Mozelli, L. A. and F. d. O. Souza (2016). "PID design via LMIs: Improved transient response with robustness to uncertain time-delay". In: *Recent results on time-delay systems: analysis and control*, pp. 267–286.

Nasir, A. N. K., M. A. Ahmad, and M. F. Rahmat (2008). "Performance comparison between LQR and PID controllers for an inverted pendulum system". In: *AIP conference proceedings*. Vol. 1052. 1. American Institute of Physics, pp. 124–128.

Natori, K., R. Oboe, and K. Ohnishi (2008). "Stability analysis and practical design procedure of time delayed control systems with communication disturbance observer". In: *IEEE Transactions on Industrial Informatics* 4.3, pp. 185–197.

Nguyen, Q., T. Li, R. Yu, Q. Shan, Y. Wu, and J. Ning (2020). "An LQG Optimal Linear Controller for Fin Stabilizer System of Marine Vessels". In: *2020 International Conference on System Science and Engineering (ICSSE)*. IEEE, pp. 1–6.

Nichols, N. (2000). "Robust eigenstructure assignment in second-order control systems". In: *MTNS2000: the Fourteenth International Symposium on the Mathematical Theory of Networks and Systems*, pp. 1–6.

Pan, H. and W. Sun (2019). "Nonlinear Output Feedback Finite-Time Control for Vehicle Active Suspension Systems". In: *IEEE Transactions on Industrial Informatics* 15.4, pp. 2073–2082.

Patel, K. and A. Mehta (2017). "Second order sliding mode control of active suspension system with supertwisting algorithm and disturbance observer". In: *IECON 2017-43rd Annual Conference of the IEEE Industrial Electronics Society*. IEEE, pp. 6526–6531.

Pratt, J., K. Singh, and B. Datta (2009). "Quadratic partial eigenvalue assignment problem with time delay for active vibration control". In: *Journal of Physics: Conference Series* 181.1.

Qian, J. and S. Xu (2005). "Robust partial eigenvalue assignment problem for the second-order system". In: *Journal of Sound and Vibration* 282.3–5, pp. 937 –948.

Ram, Y. and J. Mottershead (Nov. 2013). "Multiple-input active vibration control by partial pole placement using the method of receptances". In: *Mechanical Systems and Signal Processing* 40.2, pp. 727–735.

Ram, Y., J. Mottershead, and M. Tehrani (2011). "Partial pole placement with time delay in structures using the receptance and the system matrices". In: *Linear Algebra and Its Applications* 434.7, pp. 1689–1696.

Ramirez-Neria, M., R. Madonski, A. Luviano-Juárez, Z. Gao, and H. Sira-Ramírez (2020). "Design of ADRC for second-order mechanical systems without time-derivatives in the tracking controller". In: *2020 American control conference (ACC)*. IEEE, pp. 2623–2628.

Ramírez-Neria, M., J. Morales-Valdez, and W. Yu (2021). "Active vibration control of building structure using active disturbance rejection control". In: *Journal of Vibration and Control*, p. 10775463211009377.

Reithmeier, E and G Leitmann (2003). "Robust vibration control of dynamical systems based on the derivative of the state". In: *Archive of Applied Mechanics* 72.11, pp. 856–864.

Richiedei, D. and I. Tamellin (2021). "Active control of linear vibrating systems for antiresonance assignment with regional pole placement". In: *Journal of Sound and Vibration* 494, p. 115858.

Safiullah, S., A. Rahman, and S. A. Lone (2022). "A second-order ADRC for synchronized frequency-voltage mitigation of EV integrated power system". In: *IETE Journal of Research*, pp. 1–16.

Santos, T. L., J. M. Araújo, and T. S. Franklin (2018). "Receptance-based stability criterion for second-order linear systems with time-varying delay". In: *Mechanical Systems and Signal Processing* 110, pp. 428–441.

Seguy, S., T. Insperger, L. Arnaud, G. Dessein, and G. Peigné (2010). "On the stability of high-speed milling with spindle speed variation". In: *The International Journal of Advanced Manufacturing Technology* 48.9, pp. 883–895.

Shapiro, A. (Mar. 2005). "Stability of Second-Order Asymmetric Linear Mechanical Systems With Application to Robot Grasping". In: *Journal of Applied Mechanics* 72.6, pp. 966–968.

Shustin, E., L. Fridman, E. Fridman, and F. Castanos (2008). "Robust semiglobal stabilization of the second order system by relay feedback with an uncertain variable time delay". In: *SIAM Journal on Control and Optimization* 47.1, pp. 196–217.

Simoes, R. C., V. Steffen Jr, J. Der Hagopian, and J. Mahfoud (2007). "Modal active vibration control of a rotor using piezoelectric stack actuators". In: *Journal of Vibration and Control* 13.1, pp. 45–64.

Singh, K. V., C. Black, and R. Kolonay (2019). "Active aeroelastic output feedback control with partial measurements by the method of receptances". In: *Aerospace Science and Technology* 86, pp. 47–63. ISSN: 1270-9638.

Sun, W., H. Gao, and O. Kaynak (2014). “Vibration isolation for active suspensions with performance constraints and actuator saturation”. In: *IEEE/ASME transactions on mechatronics* 20.2, pp. 675–683.

Sun, W., H. Gao, and O. Kaynak (2015). “Vibration Isolation for Active Suspensions With Performance Constraints and Actuator Saturation”. In: *IEEE/ASME Transactions on Mechatronics* 20.2, pp. 675–683.

Sun, W., Z. Zhao, and H. Gao (2012). “Saturated adaptive robust control for active suspension systems”. In: *IEEE Transactions on industrial electronics* 60.9, pp. 3889–3896.

Tognetti, E. S. and G. A. de Oliveira (2022). “Robust state feedback-based design of PID controllers for high-order systems with time-delay and parametric uncertainties”. In: *Journal of Control, Automation and Electrical Systems* 33.2, pp. 382–392.

Tu, L., H. Du, M. Dong, D. Ning, Y. Wu, W. Li, and H. Huang (2021). “Semiactively Controllable Vehicle Seat Suspension System With Negative Stiffness Magnetic Spring”. In: *IEEE/ASME Transactions on Mechatronics* 26.1, pp. 156–167.

Wei, L., Z. Mengde, W. Zhengquan, Y. Zhuang, L. Yu, W. Shihong, C. Xiaochun, L. Xiao, B. Liang, and J. Zhenyuan (2019). “An active damping vibration control system for wind tunnel models”. In: *Chinese Journal of Aeronautics* 32.9, pp. 2109–2120.

Xie, H. (2021). “A receptance method for robust and minimum norm partial quadratic eigenvalue assignment”. In: *Mechanical Systems and Signal Processing* 160, p. 107838. ISSN: 0888-3270.

Yang, D.-H., J.-H. Shin, H. Lee, S.-K. Kim, and M. K. Kwak (2017). “Active vibration control of structure by active mass damper and multi-modal negative acceleration feedback control algorithm”. In: *Journal of Sound and Vibration* 392, pp. 18–30.

Yu, Y., J. Guo, L. Li, G. Song, P. Li, and J. Ou (2015). “Experimental study of wireless structural vibration control considering different time delays”. In: *Smart Materials and Structures* 24.4, p. 045005.

Zhang, G. and P. Yu (2018). “Lyapunov method for stability of descriptor second-order and high-order systems”. In: *Journal of Industrial & Management Optimization* 14.2, pp. 673–686.

Zhang, J.-F., H. Ouyang, K.-W. Zhang, and H.-M. Liu (2020). “Stability test and dominant eigenvalues computation for second-order linear systems with multiple time-delays using receptance method”. In: *Mechanical Systems and Signal Processing* 137, p. 106180.

Zhang, L., G. Zhang, and W. Liu (2019a). “Optimal control of second-order and high-order descriptor systems”. In: *Optimal Control Applications and Methods* 40.4, pp. 791–806.

Zhang, S., H. Li, R. Schmidt, and P. Müller (2014). “Disturbance rejection control for vibration suppression of piezoelectric laminated thin-walled structures”. In: *Journal of Sound and Vibration* 333.5, pp. 1209–1223. ISSN: 0022-460X.

Zhang, S.-Q., X.-Y. Zhang, H.-L. Ji, S.-S. Ying, and R. Schmidt (2021). "A refined disturbance rejection control for vibration suppression of smart structures under unknown disturbances". In: *Journal of Low Frequency Noise, Vibration and Active Control* 40.1, pp. 427–441.

Zhang, T. and H. G. Li (2013). "Adaptive pole placement control for vibration control of a smart cantilevered beam in thermal environment". In: *Journal of Vibration and Control* 19.10, pp. 1460–1470.

Zhang, X.-Y., S.-Q. Zhang, Z.-X. Wang, X.-S. Qin, R.-X. Wang, and R. Schmidt (2019b). "Disturbance rejection control with H_∞ optimized observer for vibration suppression of piezoelectric smart structures". In: *Mechanics & Industry* 20.2, p. 202.

Zhao, L., F.-Q. Sun, J.-C. Ren, and B.-W. Li (2016). "Optimal preview control for a class of continuous time-invariant descriptor systems". In: *Optimal Control Applications and Methods* 37.2, pp. 279–289.

Zheng, Q., L. Dong, D. H. Lee, and Z. Gao (2008). "Active disturbance rejection control for MEMS gyroscopes". In: *2008 American control conference*. IEEE, pp. 4425–4430.

Zheng, Y., L. Furieri, M. Kamgarpour, and N. Li (2021). "Sample complexity of linear quadratic gaussian (LQG) control for output feedback systems". In: *Learning for dynamics and control*. PMLR, pp. 559–570.

Zhu, J., J. E. Mottershead, and A. Kyprianou (2009). "An inverse method to assign receptances by using classical vibration absorbers". In: *Journal of Vibration and Control* 15.1, pp. 53–84.

Zhuo, Z. (2017). *LQG Controller Design of the Mobile Inverted Pendulum*. University of California, San Diego.

A Appendix

This appendix presents some useful matrix theorems used to construct the main results in the Chapter 2.

Consider the descriptor system represented by the following equation:

$$E\dot{x} = Ax + Bu \tag{A.1}$$

where $E \in \mathbb{R}^{n\times n}$ is singular, $A \in \mathbb{R}^{n\times n}$, $B \in \mathbb{R}^{n\times m}$. Considering a linear state feedback control $u = Fx$ where $F \in \mathbb{R}^{m\times n}$. In order to compute the feedback gain matrix F, consider $u = \hat{F}x + \tilde{u}$, where $\hat{F} \in \mathbb{R}^{m\times n}$, which yields an impulse-free descriptor system

$$E\dot{x} = (A + B\hat{F})x + B\tilde{u} \tag{A.2}$$

Since E is singular, there exist orthogonal matrices $Z \in \mathbb{R}^{n\times n}$ and $W \in \mathbb{R}^{n\times n}$ such that (Datta 2017):

$$ZEW = \begin{bmatrix} \sum_e & 0 \\ 0 & 0 \end{bmatrix}, ZAW = \begin{bmatrix} A_{11} & A_{12} \\ A_{21} & A_{22} \end{bmatrix}, ZB = \begin{bmatrix} B_1 \\ B_2 \end{bmatrix} \tag{A.3}$$

where $\sum_e \in \mathbb{R}^{d\times d}$ is a diagonal matrix with positive diagonal entries. By defining the feedback gain matrix $\hat{F}$ as

$$\hat{F} := [0 \;\; \hat{F}_2]W^T, \tag{A.4}$$

where $\hat{F}_2 \in \mathbb{R}^{m\times(n-d)}$, we have

$$Z(A + B\hat{F})W = \begin{bmatrix} A_{11} & A_{12} + B_1\hat{F}_2 \\ A_{21} & A_{22} + B_2\hat{F}_2 \end{bmatrix} \tag{A.5}$$

Considering the matrices in (A.3) and (A.5), the system in (A.2) is impulse-free if and only if $det(A_{22} + B_2\hat{F}_2) \neq 0$.

Theorem A.1: (Theorem 1, (Datta 2017))

Let $A_F := A_{22} + B_2\hat{F}_2$. *If* $\hat{F}_2$ *satisfies following condition:*

$$\begin{bmatrix} \frac{1}{2}(A_F + A_F^T) & \hat{\beta}I \\ \hat{\beta}I & I \end{bmatrix} > 0 \tag{A.6}$$

for some positive β *then* A_F *is non singular.*

Definition 2.1 (LMI Regions) (Chilali and Gahinet 1996): A subset D of the complex plane is called an LMI region if there exist a symmetric matrix $\alpha = [\alpha_{kl}] \in \mathbb{R}^{m\times m}$ and a matrix $\beta = [\beta_{kl}] \in \mathbb{R}^{m\times m}$ such that

$$D = \{z \in C : f_D(z) < 0\} \tag{A.7}$$

with

$$f_D(z) :\approx \alpha + z\beta + \bar{z}\beta^T = [\alpha_{kl} + \beta_{kl}z + \beta lk\bar{z}]_{1\le k,\ l\le m}. \tag{A.8}$$

Note that the characteristic function f_D takes values in the space of $m \times m$ Hermitian matrices and that $'' < 0''$ stands for negative definite. In other words, an LMI region is a subset of the complex plane that is representable by an LMI in z and $\bar{z}$, or equivalently, an LMI in $x = Re(z)$ and $y = Im(z)$. As a result, LMI regions are convex. Moreover, LMI regions are symmetric with respect to the real axis since for any $z \in D$, $f_D(\bar{z}) = \overline{f_D(z)} < 0$.

Interestingly, there is a complete counterpart of Gutman's theorem for LMI regions. Specifically, pole location in a given LMI region can be characterized in terms of the $m \times m$ block matrix

$$\begin{aligned} M_D(A,X) &:= \alpha \otimes X + \beta \otimes (AX) + \beta^T \otimes (AX)^T \\ &= [\alpha_{kl}X + \beta_{kl}AX + \beta_{lk}XA^T]_{1\le k,\ l\le m} \end{aligned} \tag{A.9}$$

Theorem A.2: (Theorem 2.2, (Chilali and Gahinet 1996))

The matrix A *is* $D-$*stable if and only if there exists a symmetric matrix* X *such that*

$$M_D(A,X) < 0, \quad X > 0 \tag{A.10}$$

Note that $M_D(A,\ X)$ in (A.9) and $f_D(z)$ in (A.8) are related by the substitution $(X,\ AX,\ XA^T) \leftrightarrow (1,\ z,\ \bar{z})$. As an example, the disk of radius r and center $(-q,\ 0)$ is an LMI region with characteristic function

$$f_D(z) = \begin{bmatrix} -r & q+z \\ q+\bar{z} & -r \end{bmatrix}. \tag{A.11}$$

In this case, (A.10) reads

$$\begin{bmatrix} -rX & qX + AX \\ qX + XA^T & -rX \end{bmatrix} < 0, \quad X > 0. \tag{A.12}$$

Consider now the region $S(\alpha, r, \theta)$ and take $\alpha = r = 0$. The sector $S(0, 0, \theta)$ if and only if there exists a positive definite matrix P such that

$$(W \otimes A)P + P(W \otimes A)^T < 0 \tag{A.13}$$

where

$$W = \begin{bmatrix} \sin\theta & \cos\theta \\ -\cos\theta & \sin\theta \end{bmatrix}. \tag{A.14}$$

On the other hand, $S(0, 0, \theta)$ is an LMI region with characteristic function

$$f_\theta(z) = \begin{bmatrix} \sin\theta(z+\overline{z}) & \cos\theta(z-\overline{z}) \\ -\cos\theta(\overline{z}-z) & \sin\theta(z+\overline{z}) \end{bmatrix}. \tag{A.15}$$

A has its poles in $S(0, 0, \theta)$ if and only if there exists $X > 0$ such that

$$\begin{bmatrix} \sin\theta(AX + XA^T) & \cos\theta(AX - XA^T) \\ -\cos\theta(XA^T - AX) & \sin\theta(AX + XA^T) \end{bmatrix} < 0. \tag{A.16}$$

or equivalently

$$(W \otimes A)Diag(X,X) + Diag(X,X)(W \otimes A)^T < 0. \tag{A.17}$$

Compared to (A.13), this last condition gives additional information on the structure of P. It is also better from an LMI optimization perspective since the number of optimization variables is divided by four when replacing P by $Diag(X, X)$.

Theorem A.3: (Theorem 1, (Fenili et al. 2014))

Consider the system $\dot{x}(t) = Ax(t) + A_d x(t - d(t))$. Let $\tau > 0$ and $0 \leq \mu \leq \tau$ be given , such that $d(t) \in [\tau - \mu, \tau + \mu]$, and $\delta > 0$, the exponential convergence rate. So the system with $d(t) \in [\tau - \mu, \tau + \mu]$ is exponentially stable, with exponential convergence rate δ, if there are matrices of appropriate dimensions: F, G, $P = P^T$, $S = S^T$, Q, $R_1 = R_1^T$, R_2, $R_3 = R_3^T$, $Z = Z^T$, such that the LMIs below are satisfied

$$\begin{bmatrix} P & \star \\ Q^T & \varepsilon_1 S \end{bmatrix} > 0, \tag{A.18}$$

where $\varepsilon_1 = e^{-2\delta\tau}/\tau$,

$$R = \begin{bmatrix} R_1 & \star \\ R_2 & R_3 \end{bmatrix} > 0, \tag{A.19}$$

and

$$\left[\begin{array}{c|c} \Xi & \star \\ \hline \Gamma^T & \varepsilon_2^{-1}\mu Z \end{array}\right] < 0, \tag{A.20}$$

where $\varepsilon_2 = e^{-2\delta(\tau+\mu)}$, $\Gamma^T = \mu[A_d^T F^T \;\; \alpha A_d^T G^T \;\; 0 \;\; 0]$ *and* Ξ *is give:*

$$\Xi = \begin{bmatrix} \mathcal{F} & * & * & * \\ P + \tau R_2 - \epsilon_2(F^T - GA) & \tau R_3 + 2\mu Z - \epsilon_2(G + G^T) & * & * \\ \epsilon_1 R_3^T - Q^T + \epsilon_2 A_d^T F^T & \epsilon_2 A_d^T G^T & -\epsilon_1(R_3 + \tau S)* & \\ 2\delta Q^T - \epsilon_1 R_2^T & Q^T & \epsilon_1 R_2^T & -\epsilon_1 R_1 \end{bmatrix}. \tag{A.21}$$

where $\mathcal{F} = 2\delta P + Q + Q^T + \tau R_1 - \epsilon_1 R_3 + S + \varepsilon_2(AF^T + FA^T)$.

B Appendix

This appendix presents the discretization of PD/PID-LQR controllers.

Consider the following PID controller diagram:

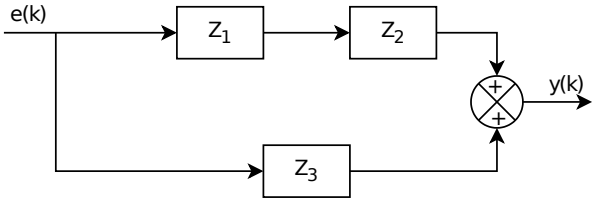

Figure B.1: Diagram: PID discretization

Z_1 represents the proportional integral (PI) control, described by the discrete time equations:

$$\begin{cases} x_1(k+1) = x_1(k) + K_I e(k) & \text{(B.1.1)} \\ y_1(k) = T_s x_1(k) + K_P e(k) & \text{(B.1.2)} \end{cases}$$

with $e(k) = [\dot{\theta} \quad \dot{\phi}]^T$. And Z_2 represents the integrator (I) represented by:

$$\begin{cases} x_2(k+1) = x_2(k) + u_1(k) & \text{(B.2.1)} \\ y_2(k) = T_s x_2(k) & \text{(B.2.2)} \end{cases}$$

Rewriting the equations (B.1) and (B.2) in state spaces, assuming that Z_3 is the derivative, given by $D = K_p e(k)$, based on the Fig. B.1, we get the PID discretized in state space:

$$\begin{bmatrix} x_1(k+1) \\ x_2(k+1) \end{bmatrix} = \begin{bmatrix} 1 & 0 \\ T_s & 1 \end{bmatrix} \begin{bmatrix} x_1(k) \\ x_2(k) \end{bmatrix} + \begin{bmatrix} K_I \\ K_P \end{bmatrix} \begin{bmatrix} \dot{\theta} \\ \dot{\phi} \end{bmatrix}$$

$$y(k) = \begin{bmatrix} 0 & T_s \end{bmatrix} \begin{bmatrix} x_1(k) \\ x_2(k) \end{bmatrix} + K_d \begin{bmatrix} \dot{\theta} \\ \dot{\phi} \end{bmatrix} \quad \text{(B.3)}$$

The controller has been discretized at 100Hz, which is also the frequency at which the MIP runs, then $T_s = 0.01$. In the case of the discretization of the PD controllers obtained in Table 4.1, we use the same process of discretization of the PID controller, assuming $K_i = 0$.